Supporting Information

Glycidyl Ethers from Acyclic Terpenes: A Versatile Toolbox for Multifunctional Poly(Ethylene Glycol)s with Modification Opportunities

Sandra Schüttner[1], Gregor M. Linden[1], Elena C. Hoffmann[1], Philipp Holzmüller, Holger Frey[1,*]

[1]Department of Chemistry, Johannes Gutenberg University Mainz, Duesbergweg 10-14, 55128 Mainz, Germany.

E-Mail: hfrey@uni-mainz.de

Table of Contents

1. Experimental Sections

Reagents

All chemicals and solvents were acquired from commercial suppliers (*Sigma-Aldrich, Fluka, Alfa Aesar, Acros, TCI*) and used without prior purification, unless otherwise stated. Deuterated solvents were purchased from *Deutero GmbH*. Ethylene oxide (EO) was obtained from *Air Liquide*. All terpenoids were purchased from *Sigma-Aldrich*. The long-chain terpenyl glycidyl ethers (TGEs), farnesyl glycidyl ether (FarGE) and hexahydrofarnesyl glycidyl ether (HHFarGE), were dried azeotropically with benzene overnight under reduced pressure. All other TGEs were dried by cryo-transfer after stirring over calcium hydride (CaH_2) for 2 h prior to polymerizaton. Tetrahydrofuran (THF) was dried over diphenylhexyllithium (adduct of sec-butyllithium and 1,1-diphenylethylene), degassed by three freeze-pump-thaw cycles and stored under vacuum until distilled into the polymerization flask. Anhydrous dimethyl sulfoxide (DMSO) stored over molecular sieves was used for the statistical copolymerizations. Prior to all *in situ* ^{1}H NMR kinetics, deuterated THF (THF-d_8) was cryo-transferred after stirring over CaH_2 overnight. For each kinetics study, a new bottle of deuterated DMSO (DMSO-d_6) was utilized to ensure the absence of water residues.

Instrumentation

Nuclear Magnetic Resonance (NMR) Spectroscopy.

Standard NMR spectra were recorded at 23 °C either on a *Bruker Avance II HD 400* spectrometer or on a *Bruker Advance III HD 300* spectrometer, referenced internally to residual proton signals of the deuterated solvent (^{1}H NMR spectra) and the deuterated solvent itself (^{13}C NMR spectra).

2D NMR analysis and *in situ* ^{1}H NMR copolymerization kinetics were investigated using a Bruker Avance III HD 400 spectrometer operated at 400 MHz (5 mm BBFO-SmartProbe (Z-gradient), an ATM and a SampleXPress 60 auto sampler). Diffusion-Ordered Spectroscopy (DOSY) spectra were collected using a *Bruker Avance III HD 400* spectrometer at 23 °C. Spectra were processed using *MestReNova* software 14.2.0. NMR spectroscopy data is reported as follows: chemical shift, multiplicity and integration. Spectra annotation uses lowercase letters for proton signals and capital letters for carbon signals.

Fourier-Transformations-Infrared Spectroscopy (FT-IR Spectroscopy).

FT-IR spectroscopy was performed on a *Nicolet* iS10 FT-IR spectrometer (Thermo Scientific, Waltham, MA, USA) equipped with a diamond ATR unit. Spectra were recorded in a frequency range of 650–3500 cm^{-1}.

Size Exclusion Chromatography (SEC).

SEC analysis was carried out with an Agilent 1100 series SEC system with a HEMA 300/100/40 Å column cascade, equipped with UV (254 nm) and RI detectors. Measurements were conducted with a flow rate of 1 $mL \cdot min^{-1}$ with DMF as eluent (with 1 $g \cdot mL^{-1}$ lithium bromide) at 50 °C. Toluene was used as a reference for the baseline. SEC calibration was carried out with poly(ethylene glycol) (PEG) standards provided from *Polymer Standard Service* (PSS). *PSS WinGPC UniChrom* software was used for all data recording and processing.

Matrix-assisted Laser Desorption Ionization Time-of-Flight (MALDI-ToF) Mass Spectrometry.

MALDI-ToF was conducted on a *Bruker autoflex maX MALDI-ToF-MS/MS* with multi target plate in linear mode. *Trans*-2-[3-(4-*tert*-butylphenyl)-2-methyl-2-propenylidene]malononitrile was used as a matrix (DCTB) and potassium trifluoroacetate (KTFA) as a salt additive.

Differential Scanning Calorimetry (DSC).

DSC measurements of the polymer samples were carried out on a *DSC 250*, *TA Instrument*, applying indium and *n*-octane as calibration standard. After drying all samples azeotropically, each sample was sealed in an aluminum pan and measured against an empty pan as reference under a nitrogen atmosphere. The DSC samples were cooled from 40 °C to -90 °C and then heated to 100 °C, followed by an additional cooling and heating cycle in the temperature range of -90 °C to 100 °C. Heating and cooling cylces were set to a rate of 10 °C/min. All melting temperatures (T_ms) and glass transition temperatures (T_gs) values were evaluated from the second heating cycle to ensure the removal of the thermal history.

Gas Chromatography (GC).

GC measurements were conducted using a Shimadzu GC-2010 (*Shimadzu*, Japan) with a *VWR Avantor™ Hichrom HI-5 MS* column (*VWR International GmbH*, Germany). Dimensions of the column: Length 30 m, inner diameter 0.25 mm, coating thickness 0.25 µm. Carrier gas hydrogen. Injector temperature 250 °C, start temperature 27 °C for 3 min. Heating rate 1 °C/min to 32 °C, heating rate 40 °C/min to 300 °C, hold for 4 min. Detector temperature 330 °C. Total time 18.7 min.

2. Monomer Synthesis

The phase transfer catalysis protocol reported by Mouzin et al. was modified subject to the terpenyl side chain targeted.[1,2] The synthesis for TGEs of hemiterpenoids has been slightly altered with respect to previously reported synthetic approaches.

Synthesis of TGEs from hemiterpenoids

The following synthesis protocol was used for the short-chain TGEs, namely prenyl glycidyl ether (PreGE), isoprenyl glycidyl ether (IsoPreGE) and dihydro glycidyl ether (DHPreGE).

An aqueous sodium hydroxide solution (33 % (*w*/*w*) solution, $V_{solution}$ = 150.5 mL; NaOH: 50.14 g, 1.25 mol, 12.7 equiv.), tetrabutylammonium hydrogen sulfate (TBAHS, 1.89 g, 0.006 mol, 0.04 equiv.) and epichlorohydrin (ECH, 57.9 mL, 68.32 g, 0.738 mol, 5.30 equiv.) were added to a three-necked flask, equipped with a dropping funnel and mechanical stirrer. The mixture was cooled to 0 °C using an ice bath and the prenol (3-methyl-2-buten-1-ol, 13.6 mL, 12.00 g, 0.139 mol, 1 equiv.) was added dropwise over 90 min whilst vigorously stirring the suspension. Note that it is imperative to keep the reaction temperature below 5 °C to avoid the augmented formation of side products. Stirring continued at 0 °C for 3.5 h, followed by another 90 min at room temperature. The reaction was quenched with ice, and the crude product was extracted with diethyl ether (DEE). The combined organic phases were washed with brine until a neutral pH value was obtained and dried using magnesium sulfate ($MgSO_4$). DEE was removed under reduced pressure, and a first distillation at 25 mbar enabled the removal of undesired side products. Fractionated distillation at high vacuum (p= 6·10^{-3} mbar, $T_{b,PreGE}$ = 30 - 33 °C) afforded PreGE as a colorless liquid in yields of 64 %.

Prenyl glycidyl ether

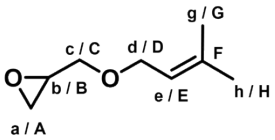

Yield: 64 %

Purification by distillation: p = 6·10^{-3} mbar, $T_{b,PreGE}$ = 30 - 33 °C

^{1}H NMR (400 MHz, chloroform-d_1): δ (ppm) = 5.26 (tdq, J = 7.1, 2.8, 1.4 Hz, 1H, H_e), 4.01 – 3.86 (m, 2H, H_d), 3.59 (dd, J = 11.4, 3.2 Hz, 1H, H_c), 3.29 (dd, J = 11.4, 5.8 Hz, 1H, H_c), 3.05 (ddt, J = 5.9, 4.2, 2.9 Hz, 1H, H_b), 2.69 (dd, J = 5.1, 4.1 Hz, 1H, H_a), 2.51 (dd, J = 5.1, 2.7 Hz, 1H, H_a), 1.66 (s, 3H, H_g), 1.59 (s, 3H, H_h).

^{13}C NMR (100 MHz, chloroform-d_1): δ (ppm) = 137.16 (C_F), 120.72 (C_E), 70.55 (C_C), 67.57 (C_D), 50.71 (C_B), 44.20 (C_A), 25.63 (C_G), 17.86 (C_H).

Isoprenyl glycidyl ether

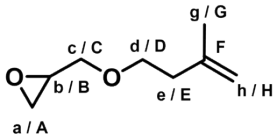

Yield: 59 %

Purification by distillation: $p = 11 \cdot 10^{-3}$ mbar, $T_{b,IsoPreGE} = 32 - 35$ °C

^{1}H NMR (300 MHz, chloroform-d_1): δ (ppm) = 4.81 – 4.67 (d, 2H, H_h), 3.72 (dd, J = 11.6, 3.0 Hz, 1H, H_d), 3.59 (qt, J = 9.4, 6.9 Hz, 2H, H_c), 3.37 (dd, J = 11.6, 5.8 Hz, 1H, H_d), 3.12 (ddt, J = 5.8, 4.1, 2.9 Hz, 1H, H_b), 2.77 (dd, J = 5.1, 4.1 Hz, 1H, H_a), 2.58 (dd, J = 5.0, 2.7 Hz, 1H, H_a), 2.35 – 2.23 (m, 2H, H_e), 1.73 (s, 3H, H_g).

^{13}C NMR (75 MHz, chloroform-d_1): δ (ppm) = 142.72 (C_F), 111.65 (C_H), 71.56 (C_C), 69.98 (C_D), 50.94 (C_B), 44.33 (C_A), 37.82 (C_E), 22.74 (C_G).

Dihydroprenyl glycidyl ether

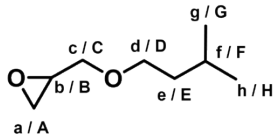

Yield: 51 %

Purification by distillation: $p = 3.5 \cdot 10^{-2}$ mbar, $T_{b,DHPreGE} = 27 – 28$ °C

^{1}H NMR (300 MHz, chloroform-d_1): δ (ppm) = 3.68 (dd, J = 11.5, 3.1 Hz, 1H, H_c), 3.58 – 3.40 (m, 2H, H_d), 3.35 (dd, J = 11.5, 5.8 Hz, 1H, H_c), 3.11 (ddt, J = 5.8, 4.2, 2.9 Hz, 1H, H_b), 2.76 (dd, J = 5.1, 4.1 Hz, 1H, H_a), 2.58 (dd, J = 5.1, 2.7 Hz, 1H, H_a), 1.81 – 1.57 (m, 1H, H_f), 1.46 (q, J = 6.7 Hz, 2H, H_e), 0.88 (d, J = 6.6 Hz, 6H, H_g, H_h).

^{13}C NMR (75 MHz, chloroform-d_1): δ (ppm) = 71.56 (C_C), 70.10 (C_D), 50.98 (C_B), 44.38 (C_A), 38.56 (C_E), 25.10 (C_F), 22.71 (C_G, C_H).

Synthesis of TGEs from mono- and sesquiterpenoids

The procedure refers to the synthesis of geranyl glycidyl ether (GeraGE), neryl glycidyl ether (NerGE), tetrahydrogeranyl glycidyl ether (THGeraGE) and hexahydrofarnesyl glycidyl ether (HHFarGE).[2,3]

A three-necked flask, equipped with a mechanical stirrer and dropping funnel, was charged with an aqueous sodium hydroxide solution (50 % (*w*/*w*) solution, $V_{solution}$ = 96.26 mL; NaOH: 48.13 g, 1.20 mol, 12.7 equiv.), tetrabutylammonium hydrogen sulfate (TBAHS, 1.29 g, 0.004 mol, 0.04 equiv.) and epichlorohydrin (ECH, 39.38 mL, 46.47 g, 0.738 mol, 5.30 equiv.). The reaction mixture was cooled to 0 °C with an ice bath, followed by the dropwise addition of tetrahydrogeraniol (3,7-dimethyloctan-1-ol, 15.0 mL, 17.05 g, 0.095 mol, 1 equiv.) within 30 min under vigorous stirring. Stirring was continued at room temperature until complete consumption of the terpenoid (20 – 24 h). After quenching the reaction with ice, the crude product was extracted with DEE and the combined organic phases were washed with brine until neutrality, then dried over $MgSO_4$. DEE was removed using rotary evaporation and subsequent Kugelrohr distillation served as a first purification step. A high vacuum distillation (p = 5 – 12 $\cdot 10^{-3}$ mbar) enables the removal of potential side products (3-Chloroallyl glycidyl ether (3-Chloro-AGE), diglycidyl ether). Finally, Kugelrohr distillation (p = 12$\cdot 10^{-3}$ mbar, $T_{Kugelrohr,THGeraGE}$ = 130 – 135 °C) isolated purified THGeraGE as a colorless liquid in yields of 81 %.

As previously established for long-chain TGEs, we pretreated the TGEs with methyl iodide (MeI) and sodium hydride (NaH), deactivating any residual protic impurities while extensively drying the monomer.[2] For this purpose, a flame-dried Schlenk flask, charged with NaH (0.22 equiv.), was cooled to 0 °C, followed by the addition of the TGE (1.00 equiv.). MeI (0.10 equiv.) was syringed into the flask after 2 h, and the reaction mixture was allowed to warm up to room temperature. After 22 h, the mixture was diluted with hexane and filtered multiple times to remove accrued sodium iodide. The TGEs were isolated in quantitative yields after Kugelrohr distillation.

Geranyl glycidyl ether

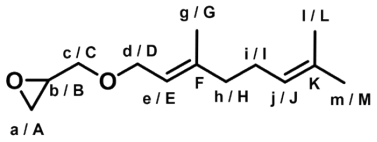

Yield: 83%

Purification by Kugelrohr distillation: p = 7·10^{-3} mbar, $T_{\text{Kugelrohr, GeraGE}}$ = 130 – 135 °C

^{1}H NMR (400 MHz, chloroform-d_1): δ (ppm) = 5.32 (ddq, J = 6.8, 5.4, 1.3 Hz, 1H, H_e), 5.06 (ddp, J = 6.9, 5.7, 1.5 Hz, 1H, H_j), 4.10 – 3.95 (m, 2H, H_d), 3.65 (dd, J = 11.4, 3.2 Hz, 1H, H_c), 3.36 (dd, J = 11.4, 5.8 Hz, 1H, H_c), 3.12 (ddt, J = 5.9, 4.2, 3.0 Hz, 1H, H_b), 2.76 (dd, J = 5.1, 4.1 Hz, 1H, H_a), 2.57 (dd, J = 5.1, 2.7 Hz, 1H, H_a), 2.13 – 1.96 (m, 4H, H_i, H_h), 1.64 (dt, J = 2.3, 1.2 Hz, 6H, H_g, H_l), 1.57 (d, J = 1.4 Hz, 3H, H_m).

^{13}C NMR (100 MHz, chloroform-d_1): δ (ppm) = 140.64 (C_F), 131.66 (C_K), 123.98 (C_J), 120.53 (C_E), 70.63 (C_C), 67.77 (C_D), 50.89 (C_B), 44.45 (C_A), 39.62 (C_H), 26.37 (C_I), 25.71 (C_M), 17.70 (C_L), 16.49 (C_G).

Neryl glycidyl ether

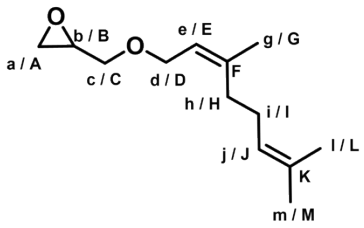

Yield: 81%

Purification by Kugelrohr distillation: p = 7·10^{-3} mbar, $T_{\text{Kugelrohr, NerGE}}$ = 135 – 145 °C

^{1}H NMR (400 MHz, chloroform-d_1): δ (ppm) = 5.35 (tq, J = 6.9, 1.5 Hz, 1H, H_e), 5.08 (ttd, J = 5.9, 3.0, 1.5 Hz, 1H, H_j), 4.09 – 3.94 (m, 2H, H_d), 3.66 (dd, J = 11.3, 3.3 Hz, 1H, H_c), 3.38 (dd, J = 11.3, 5.8 Hz, 1H, H_c), 3.14 (ddt, J = 5.9, 4.1, 3.0 Hz, 1H, H_b), 2.78 (dd, J = 5.0, 4.1 Hz, 1H, H_a), 2.59 (dd, J = 5.0, 2.7 Hz, 1H, H_a),

2.12 – 1.99 (m, 4H, H_h, H_i), 1.74 (s, 3H, H_g), 1.68 (s, 3H, H_m), 1.59 (s, 3H, H_l).

^{13}C NMR (100 MHz, chloroform-d_1): δ (ppm) = 140.97 (C_F), 132.08 (C_K), 123.90 (C_J), 121.59 (C_E), 70.79 (C_C), 67.60 (C_D), 50.97 (C_B), 44.56 (C_A), 32.35 (C_H), 26.79 (C_I), 25.80 (C_M), 23.59 (C_G), 17.74 (C_L).

Tetrahydrogeranyl glycidyl ether

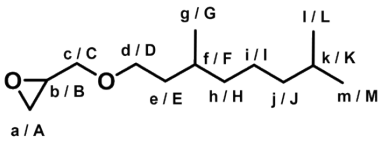

Yield: 81 %

Purification by Kugelrohr distillation: p = 12·10^{-3} mbar, $T_{Kugelrohr,THGeraGE}$ = 130 – 135 °C

^{1}H NMR (300 MHz, chloroform-d_1): δ (ppm) = 3.71 (dt, J = 11.5, 2.9 Hz, 1H, H_c), 3.63 – 3.42 (m, 2H, H_d), 3.38 (ddd, J = 11.5, 5.8, 3.0 Hz, 1H, H_c), 3.15 (ddt, J = 5.8, 4.1, 2.9 Hz, 1H, H_b), 2.80 (dd, J = 5.1, 4.1 Hz, 1H, H_a), 2.61 (dd, J = 5.1, 2.7 Hz, 1H, H_a), 1.73 – 1.01 (m, 8H, H_e, H_f, H_h, H_i, H_j, H_k), 0.88 (dd, J = 6.6, 5.2 Hz, 9H, H_g, H_l, H_m).

^{13}C NMR (75 MHz, chloroform-d_1): δ (ppm) = 71.59 (C_C), 70.07 (C_D), 51.00 (C_B), 44.41 (C_A), 39.36 (C_J), 37.46 (C_H), 36.79 (C_E), 29.91 (C_F), 28.06 (C_K), 24.76 (C_I), 22.80 (C_M, C_L), 19.76 (C_G).

Hexahydrofarnesyl glycidyl ether

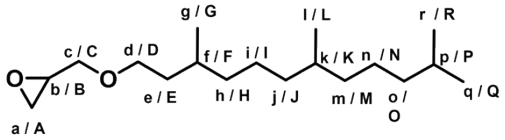

Yield: 78 %

Purification by Kugelrohr distillation: p = 5·10^{-3} mbar, $T_{Kugelrohr,HHFarGE}$ = 160 °C

^{1}H NMR (400 MHz, chloroform-d_1): δ (ppm) = 3.70 (dt, J = 11.5, 3.4 Hz, 1H, H_c), 3.60 – 3.43 (m, 2H, H_d), 3.38 (ddd, J = 11.5, 5.8, 4.2 Hz, 1H, H_c), 3.14 (ddt, J = 5.8, 4.1, 2.9 Hz, 1H, H_b), 2.79 (dd, J = 5.1, 4.1 Hz, 1H, H_a), 2.60 (ddd, J = 5.1, 2.8, 0.9 Hz, 1H, H_a), 1.70 – 0.96 (m, H_e, H_f, H_h, H_i, H_j, H_k, H_m, H_n, H_o), 0.96 – 0.78 (m, H_g, H_l H_r, H_q).

^{13}C NMR (100 MHz, chloroform-d_1): δ (ppm) = 71.63 (C_C), 70.17, 70.14 (C_D), 51.05 (C_B), 44.50, 44.49 (C_A), 39.50 (C_O), 37.63, 37.59 (C_M), 37.51 (C_H), 37.47, 37.40 (C_J), 36.88, 36.80, (C_E), 32.91 (C_K), 30.00, 29.99, 29.97 (C_F), 28.12 (C_P), 24.96, 24.93 (C_N), 24.49 (C_I), 22.86, 22.77 (C_Q, C_R), 19.88, 19.84, 19.81, 19.78 (C_G, C_L).

3. Polymerization Procedures

Synthesis procedure for statistical copolymerization of TGEs with EO

The statistical copolymerization of TGEs and EO was conducted in an equal manner for all epoxide monomers applied. In the following, the general polymerization procedure is exemplified for P(EG_{120}-*co*-$GeraGE_{12}$) (Table 1, entry 12). In a flame-dried anionic polymerization flask, cesium hydroxide monohydrate (95.4 mg, 0.57 mmol, 0.9 equiv.) and 2-(benzyloxy)ethanol (91.0 mg, 0.59 mmol, 1.0 equiv., BzEtOH), were suspended in benzene (10 mL) under an argon atmosphere. After stirring the mixture for 1 h at 60 °C, the removal of benzene under reduced pressure afforded the partially deprotonated initiator salt. Subsequently, the dried initiator was dissolved in anhydrous DMSO (0.80 mL) and tetrahydrofuran (THF, 4.2 mL) (V_{DMSO}/V_{THF}=1:5) and stirred for 20 min at room temperature. THF was added via cryo-transfer to remove protic stabilizers from THF. The reaction mixture was cooled to -82 °C using an ethanol/liquid nitrogen bath, and previously dried GeraGE (1.63 mL, 1.43 g, 6.82 mmol, 11.4 equiv.) was syringed into the flask. Quantification of EO (2.82 mL, 2.70 g, 61.3 mmol, 102.6 equiv.) was realized via distillation into a graduated ampule under vacuum, followed by a cryo-transfer into the cooled polymerization flask. The polymerization was carried out at 40 °C for 24 h and terminated with an excess of methanol (MeOH). All solvents were evaporated under reduced pressure and dialysis (MWCO = 1000 g·mol^{-1}) against a Milli-Q® water/MeOH mixture (V_{MeOH}/V_{water}=5/1) removed salt impurities and DMSO traces. Lyophilization afforded a brown viscous copolymer in yields of 77 %. Table 1 summarizes the copolymer characterization data.

In situ ^{1}H NMR kinetic study of a statistical copolymerization of TGEs with EO

In situ ^{1}H NMR kinetic investigations for the copolymerization of a variety of TGEs with EO were performed in a sealable Norell S-500-VT-7 NMR tube, relying on a procedure by Herzberger et al.[4] In general, the polymerization set up in an NMR tube is restricted by its volume. To reproduce the optimized polymerization conditions (40 °C, THF-d_8/DMSO-d_6 = 5/1 (V_{THF}/V_{DMSO})) for the TGE copolymerizations, batch calculations and theoretical comonomer ratios vary with each monomer in dependence of its chain length. This is a consequence of the varying molecular weights and densities of the applied TGEs. Note that EO is a highly toxic, flammable gas, which requires careful handling. As small amounts of EO are required for the *in situ* kinetic measurements, comonomer ratios are further impacted by small variations of the measured EO volumes.

The pre-dried initiator salt, cesium 2-(benzyloxy)ethanolate (degree of deprotonation: 95 %), was prepared in a 10-fold excess and dissolved in anhydrous DMSO-d_6 under stirring for 30 min (initiator stock solution). Its preparation was carried out in accordance with the statistical copolymerization protocol described in the previous section. After evacuating the oven-dried NMR tube, using a Teflon stopcock using Schlenk-line vacuum, EO was cryo-transferred into the NMR tube under static vacuum at -45 °C with an acetone/nitrogen bath. Subsequently, an aliquot of the initiator stock solution and THF-d_8 were syringed into the tube under argon atmosphere while cooling was maintained. After a final evacuation cycle, the reaction mixture was allowed to warm to room temperature and shaken vigorously to homogenize the solution. Then, the NMR tube was placed in the preheated NMR spectrometer (40 °C) and a control spectrum was recorded once a stable temperature in the probe head was reached (~10 min, ΔT = 0.1 K). The sample rotation was turned off and ^{1}H NMR spectra with 1 scan per spectrum were recorded in 2 min intervals. After the kinetic study, the copolymer was characterized via SEC analysis.

Monitoring the integrals of the epoxide functionality of EO and the respective TGE enables the calculation of the monomer consumption with preceding copolymerization. To this end, the normalized monomer consumption was analyzed using the NIREVAL software from Johann *et al*.[5] For the evaluation of the reactivity ratios of the comonomer pair the Jaacks method was applied for a 90 % TGE conversion to ensure a significant signal-to-noise ratio.[6]

4. Procedures for Post-polymerization Functionalizations

Thiol-Ene Click

The following procedure was applied to all double bond-containing monomers. As an example, the modification of P(EG_{120}-*co*-$GeraGE_{12}$) is described. The polymer (50 mg, 6.76 µmol) and 2,2-dimethoxy-2-phenylacetophenone (DMPA, 83.1 mg, 0.324 mmol, 48 eq., 0.01 eq. to the thiol) were added to a Schlenk flask, equipped with a magnetic stirrer and rubber septum. 8 ml of DCM was added, followed by 2-mercaptoethanol (2.53 g, 32.4 mmol, 4800 eq., 200 eq. per double bond). After mixing, three freeze-pump-thaw cycles were applied. Subsequently, an argon-filled balloon was attached to the Schlenk flask through the septum. The stirred mixture was irradiated overnight using a UV lamp (254 nm) at 5 cm. After the reaction the mixture was extracted against water (20 ml) thrice. Additionally, the polymer was purified by dialysis against MeOH (*Orange Scientific*, Molecular weight cut-off 1000 g/mol, 1 L, solvent changed three times). The solvents were evaporated to obtain the modified polymer in typical yields of 80 %.

Since every copolymer required slightly different ratios of DMPA and 2-mercaptoethanol, the set-ups are displayed in the following table. The authors would like to emphasize that the quantities mentioned are not necessarily the lowest possible. The experimental procedure was optimized for P(EG_{120}-*co*-$GeraGE_{12}$) first. The amounts were adjusted to the polymers. DMPA was modified and/or 2-mercaptoethanol was increased to suppress crosslinking.

Table S 1: Precursor polymers and the respective equivalents of Thiol and DMPA in the thiol-ene click postpolymerization modification.

Entry	Polymer	Thiol/Double bond	DMPA eq./Thiol
1	P(EG_{102}-*co*-$PreGE_{10}$)	600	0.010
2	P(EG_{126}-*co*-$IsoPreGE_{12}$)	200	0.010
3	P(EG_{120}-*co*-$GeraGE_{12}$)	200	0.010
4	P(EG_{123}-*co*-$NerGE_{13}$)	600	0.015

Recovery of unreacted 2-mercaptoethanol

After the reaction, the volatile compounds, mainly DCM and 2-mercaptoethanol, were cryo-transferred into a Schlenk flask equipped with a magnetic stirrer. The volatile compounds were fractionally distilled, 2-mercaptoethanol was received in a yield of 80 %.

Synthesis of potassium azodicarboxylate (PADA)

PADA was synthesized according to Groves and Ma.[7] 30 mL of a 40 *w*.-% aqueous potassium hydroxide solution was added to a 50 mL round-bottom flask equipped with a magnetic stirrer. The flask was immersed into a water bath at 6 °C. Azodicarboxylate (4.84 g, 41.7 mmol) was added portion wise over 2 h. The precipitate was filtered off using a glass frit and washed 20 times with ice cold methanol. The product was dried in a desiccator over 1.5 d employing vacuum, giving an intense yellow powder. The yield was 7.18 g, 37.0 mmol, 89 %.

Hydrogenation

Hydrogenation of polymers with potassium azodicarboxylate (PADA) is rarely employed.[8] The described procedure was developed during the optimization experiments and represents the best result. We oriented on the procedures described from Groves and Ma[7] as well as Snyder and Hamersma.[9]

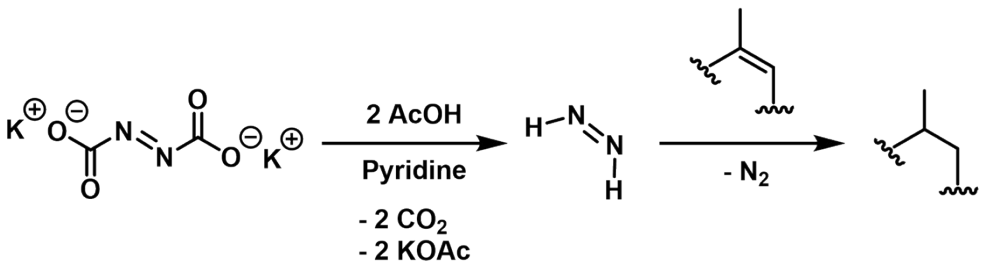

Scheme S1: Acidic decomposition of potassium azodicarboxylate (PADA) to generate diimide and subsequent polymer hydrogenation. Gaseous carbon dioxide and nitrogen as well as readily water-soluble potassium acetate are produced as coupling products.

The hydrogenation was applied to P(EG_{120}-*co*-GeraGE_{12}). 50 mg (6.76 µmol) were transferred in a flame dried Schlenk flask equipped with a rubber septum and a magnetic stirrer using toluene. The solvent was removed *in vacuo* yielding the dried polymer due to azeotropic distillation. PADA (423 mg, 360 eq., 15 eq. per double bond) and 3 ml of dry pyridine (stored over mole sieve, *Fisher Scientific*) were added. To the stirred slurry glacial acetic acid (distilled from P_4O_{10} and stored over Argon, 0.28 ml, 720 eq., 2 eq. per PADA) was slowly added dropwise with a syringe. After the complete addition of the glacial acetic acid the mixture was allowed to react overnight. The now colorless suspension was suspended in $CHCl_3$, solids were filtered off, and the organic phase was washed with water twice (20 ml). The solvents were evaporated, yielding the polymer in a yield of 85 %.

Table S 2: Reaction conditions of the hydrogenation of P(EG_{120}-*co*-$GeraGE_{12}$) employing potassium azodicarboxylate (PADA).

				Remaining signal of the DB		
Entry	**T / °C**	**Eq. PADA/DB**	**V(Py) / mL**	**5.30 ppm**	**5.08 ppm**	**avg. efficiency**
1	0	2.5	0.4	58 %	64 %	39 %
2	25	2.5	0.4	92 %	89 %	10 %
3	0	15	0.4	44 %	49 %	53 %
4	25	15	0.4	73 %	78 %	25 %
5	0	2.5	3	71 %	74 %	28 %
6	25	2.5	3	74 %	80 %	23 %
7	0	15	3	48 %	55 %	48 %
8	25	15	3	43 %	49 %	53 %

5. NMR Spectra of TGEs

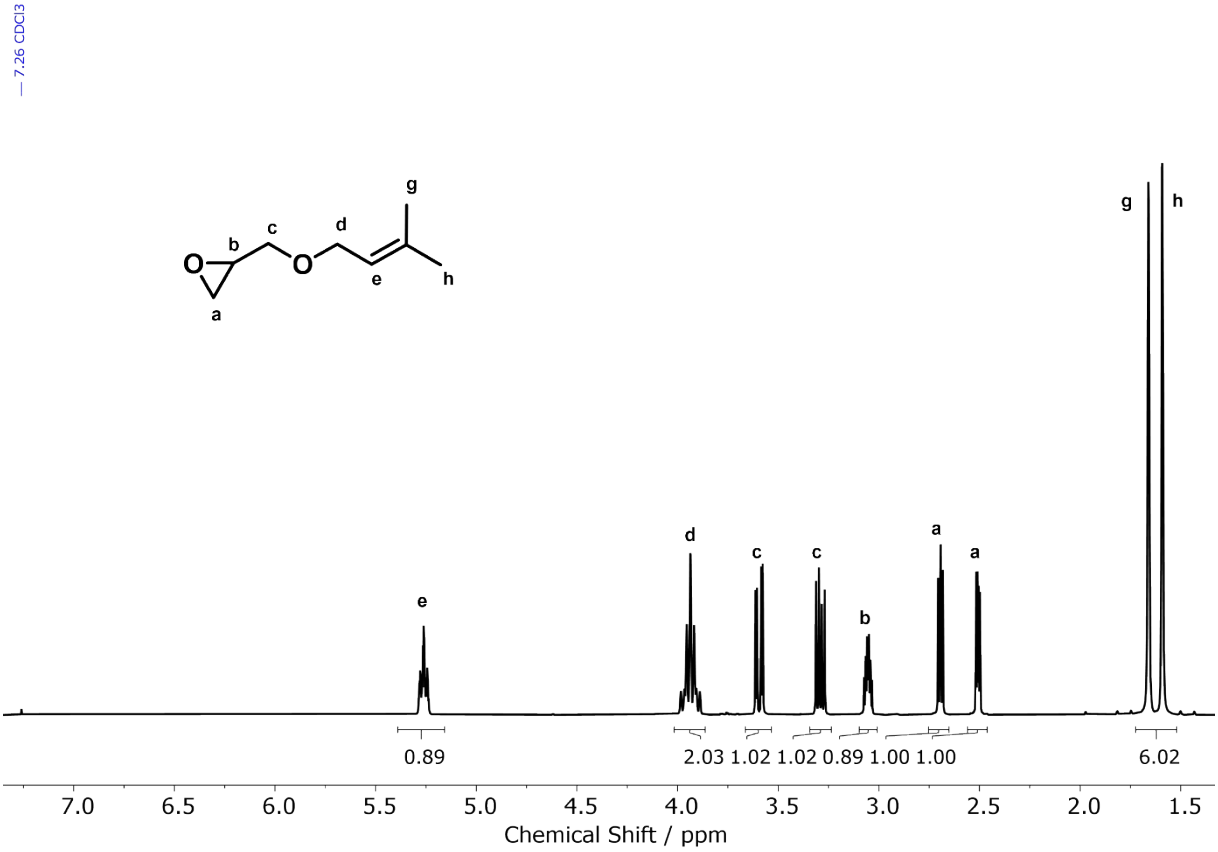

Figure S1: ^{1}H NMR spectrum (300 MHz, $CDCl_3$) of PreGE.

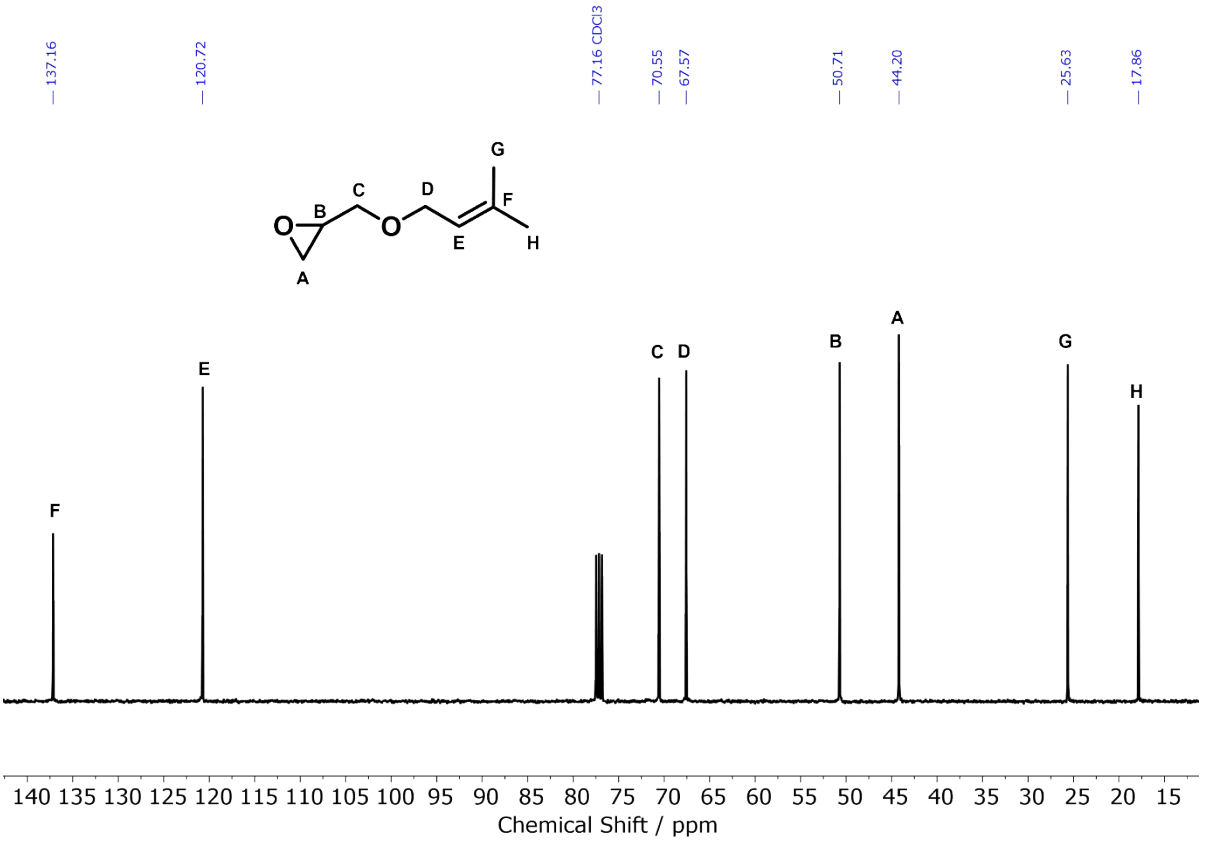

Figure S2: ^{13}C NMR spectrum (75 MHz, $CDCl_3$) of PreGE.

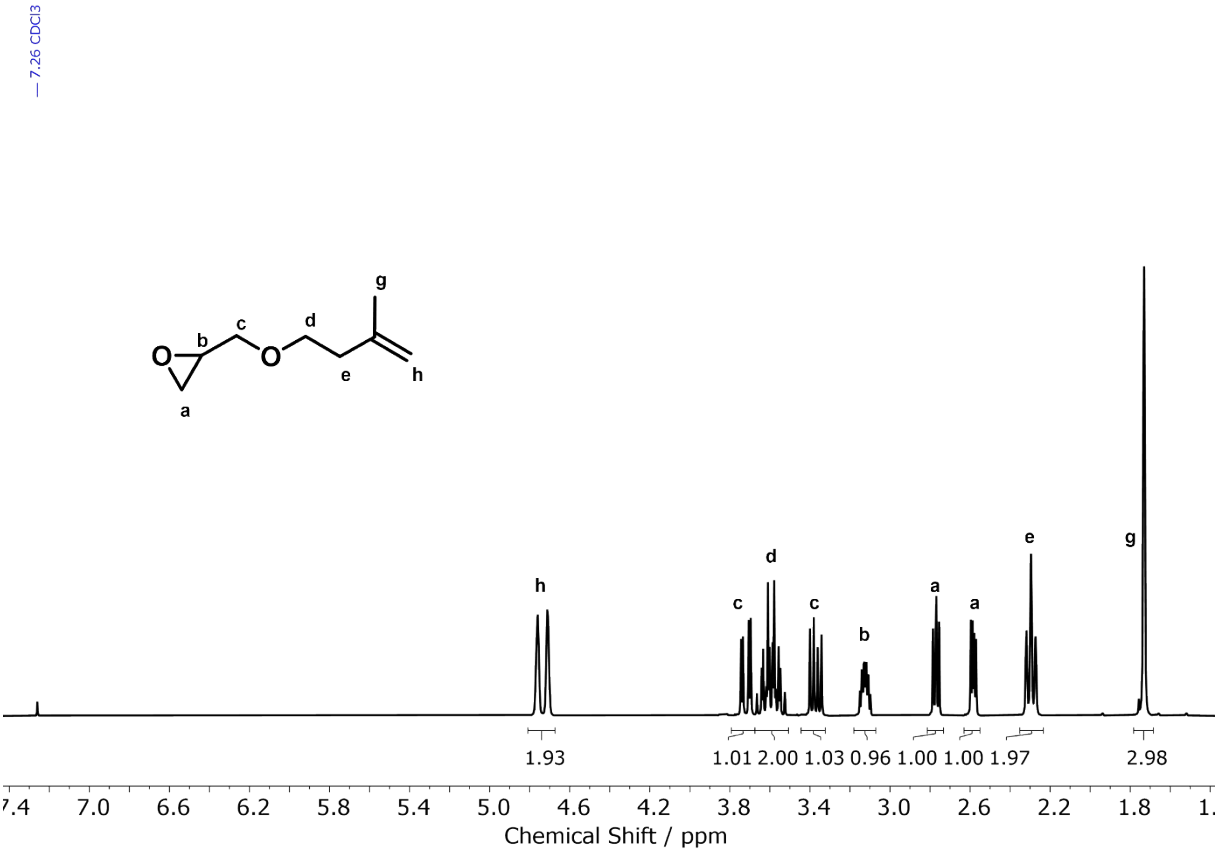

Figure S3: ^{1}H NMR spectrum (300 MHz, $CDCl_3$) of IsoPreGE.

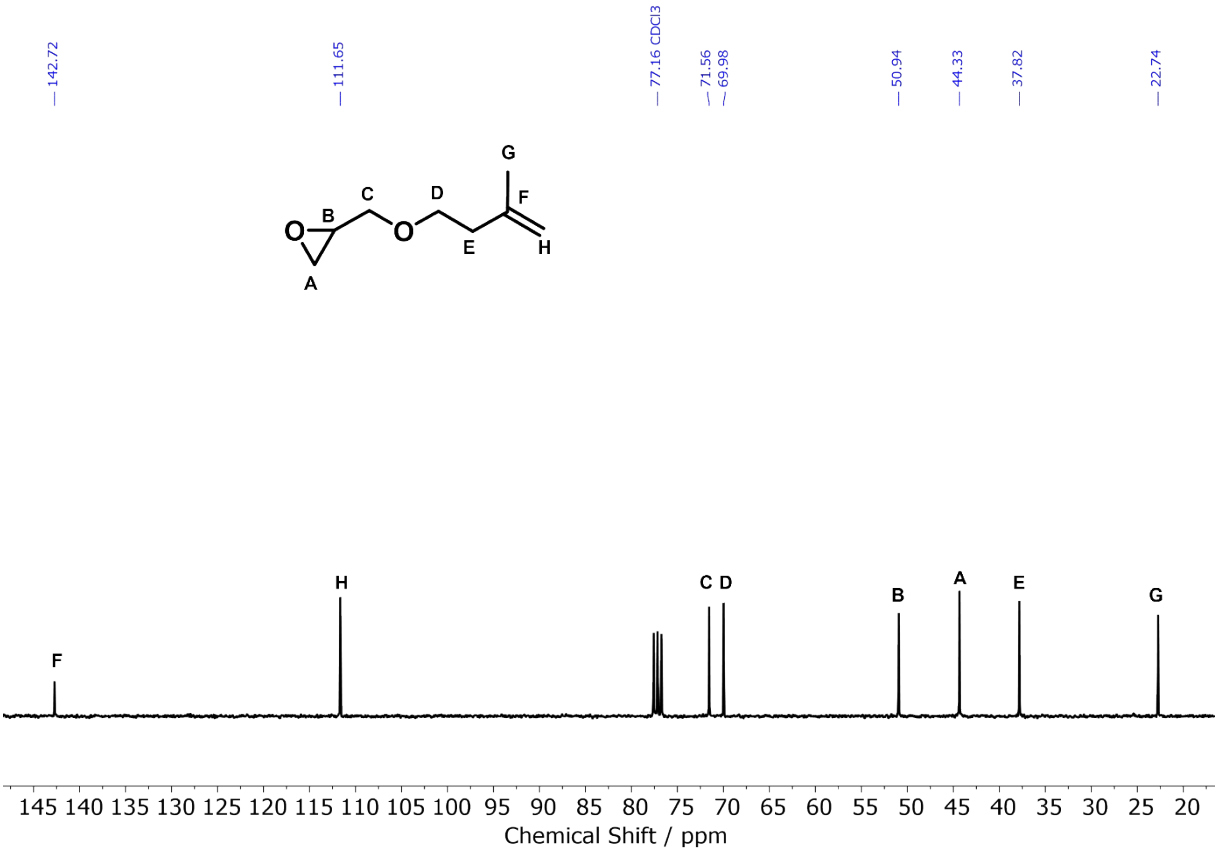

Figure S4: ^{13}C NMR spectrum (75 MHz, $CDCl_3$) of IsoPreGE.

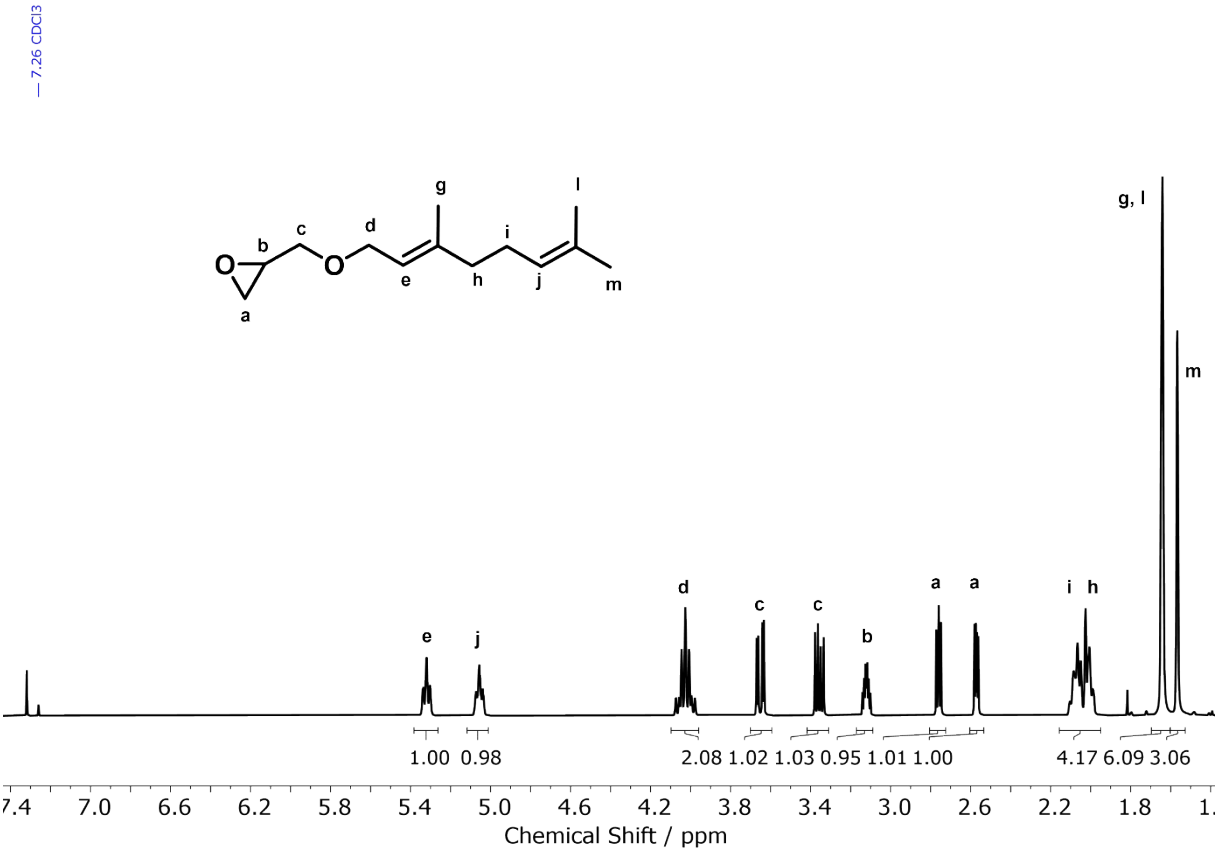

Figure S5: ^{1}H NMR spectrum (400 MHz, $CDCl_3$) of GeraGE.

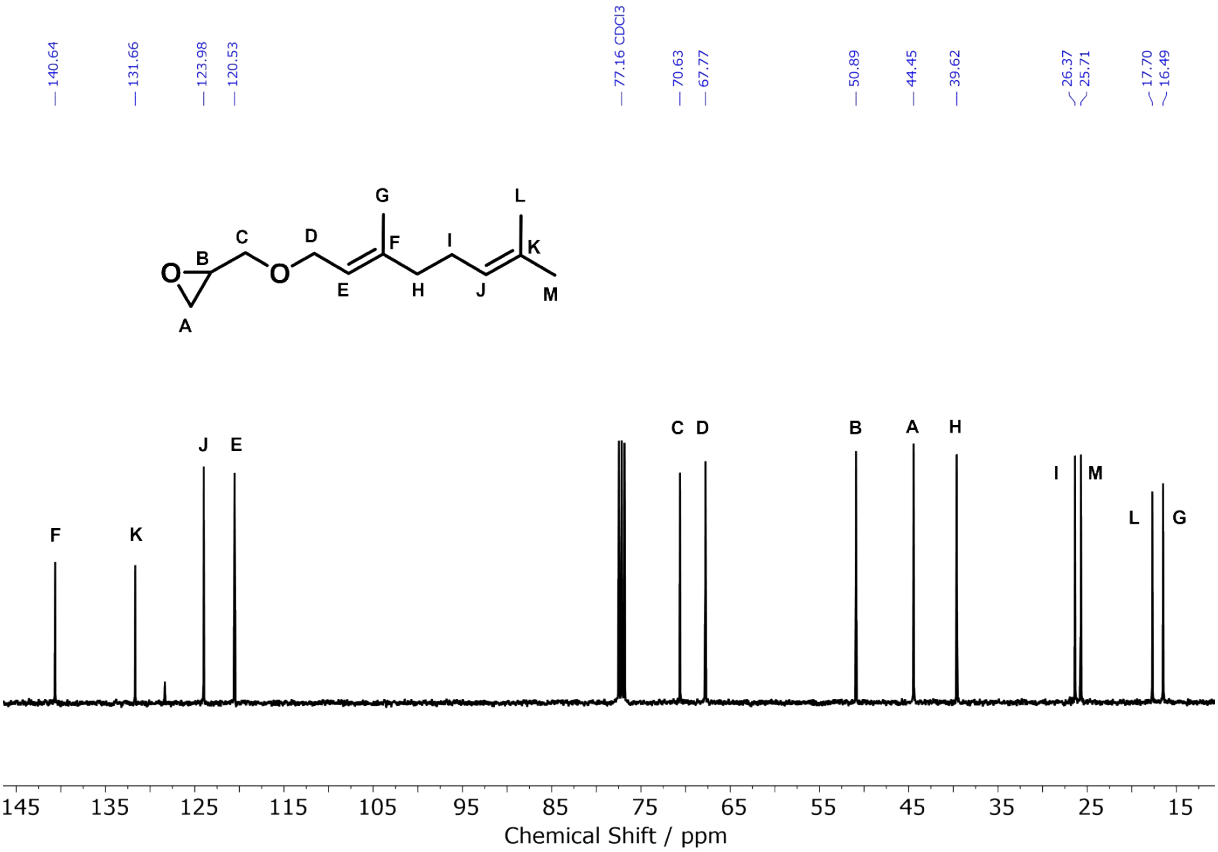

Figure S6: ^{13}C NMR spectrum (100 MHz, $CDCl_3$) of GeraGE.

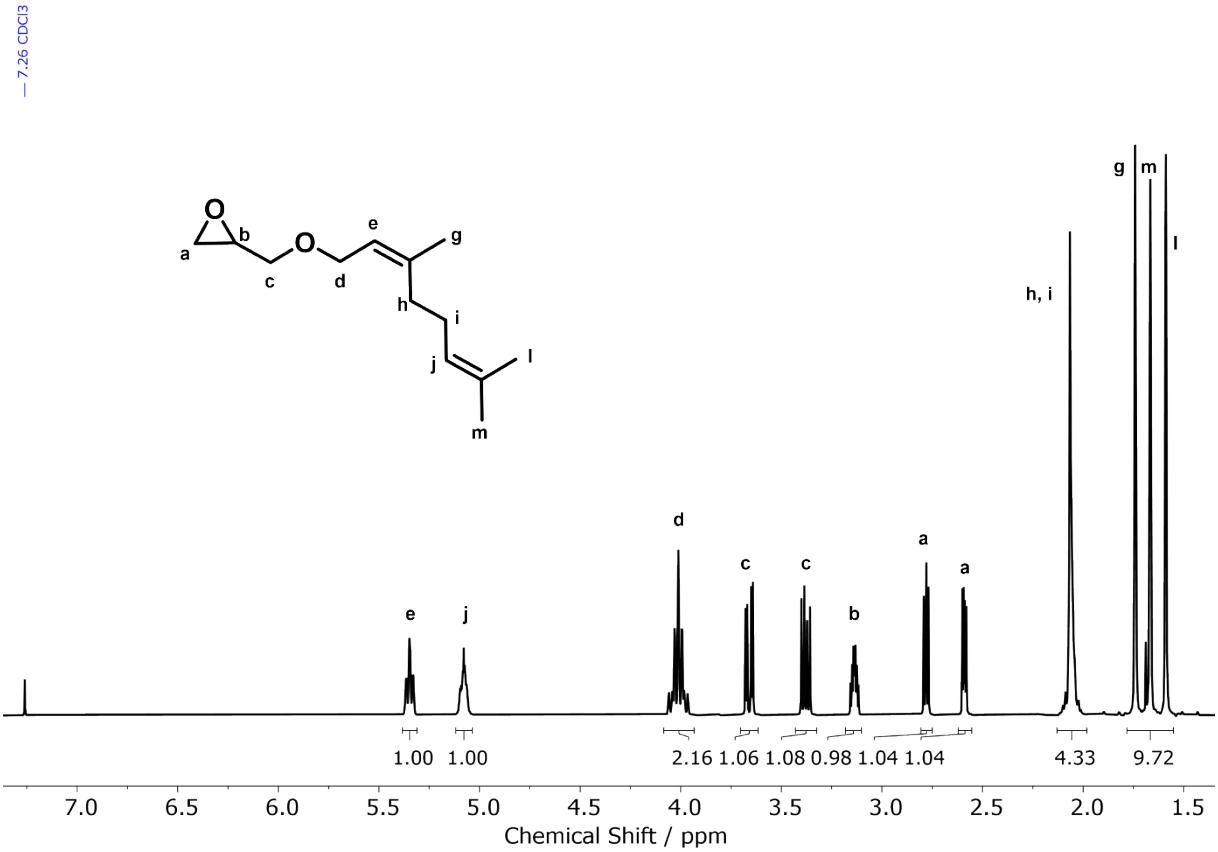

Figure S7: ^{1}H NMR spectrum (400 MHz, $CDCl_3$) of NerGE.

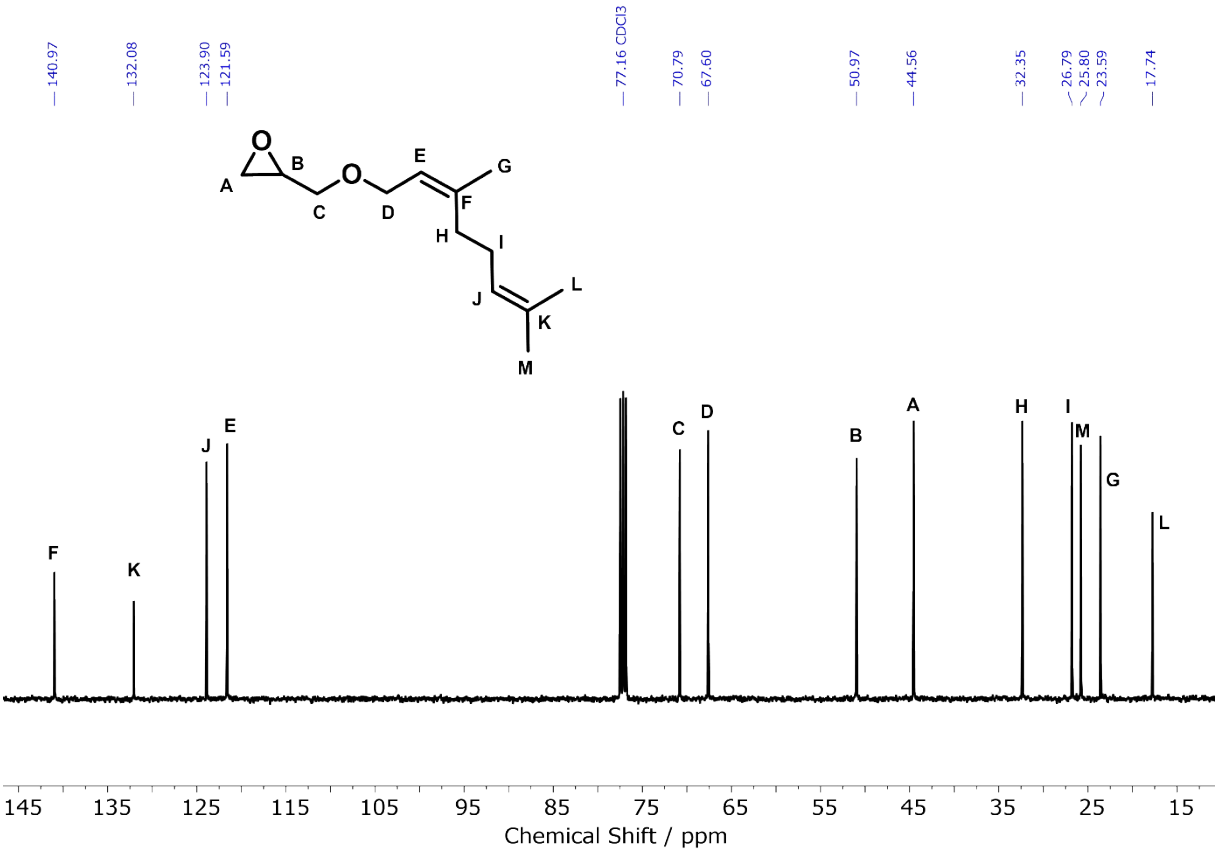

Figure S8: ^{13}C NMR spectrum (100 MHz, $CDCl_3$) of NerGE.

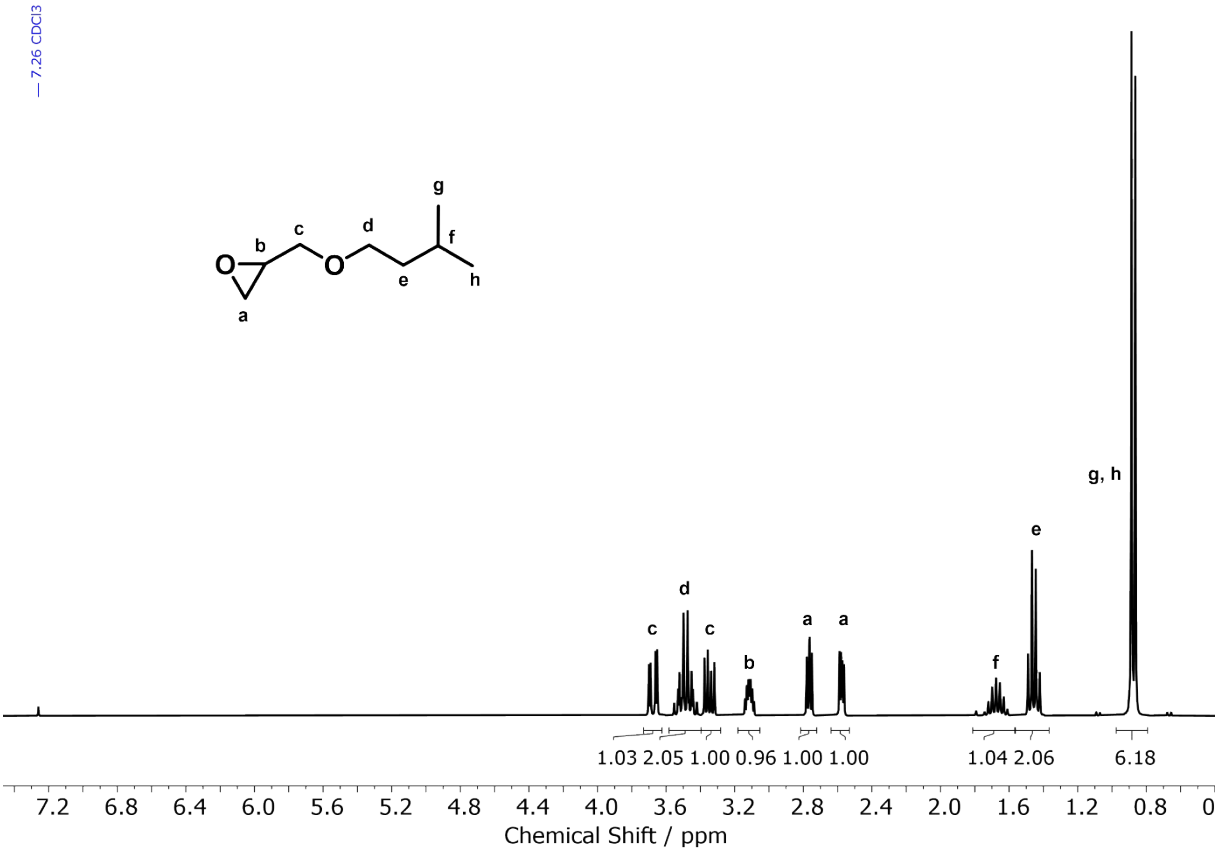

Figure S9: ^{1}H NMR spectrum (300 MHz, $CDCl_3$) of DHPreGE.

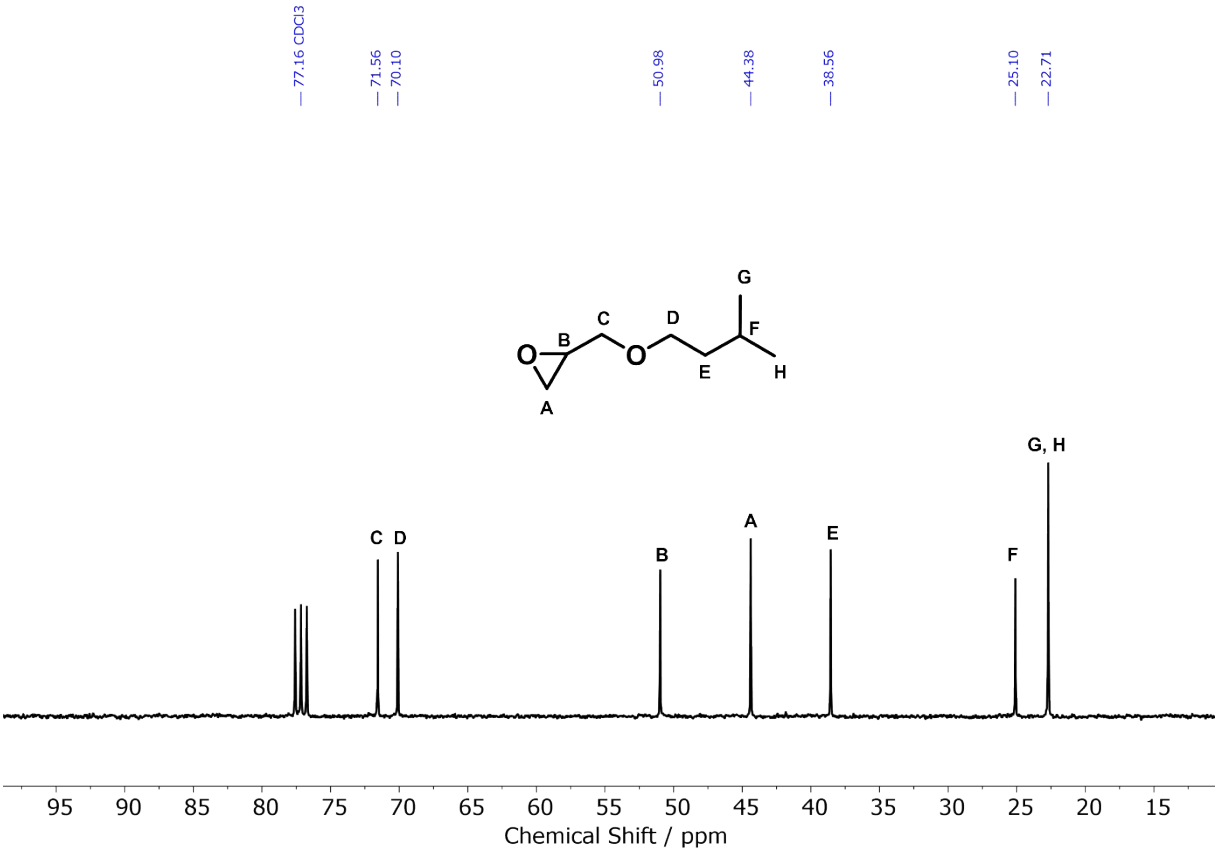

Figure S10: ^{13}C NMR spectrum (75 MHz, $CDCl_3$) of DHPreGE.

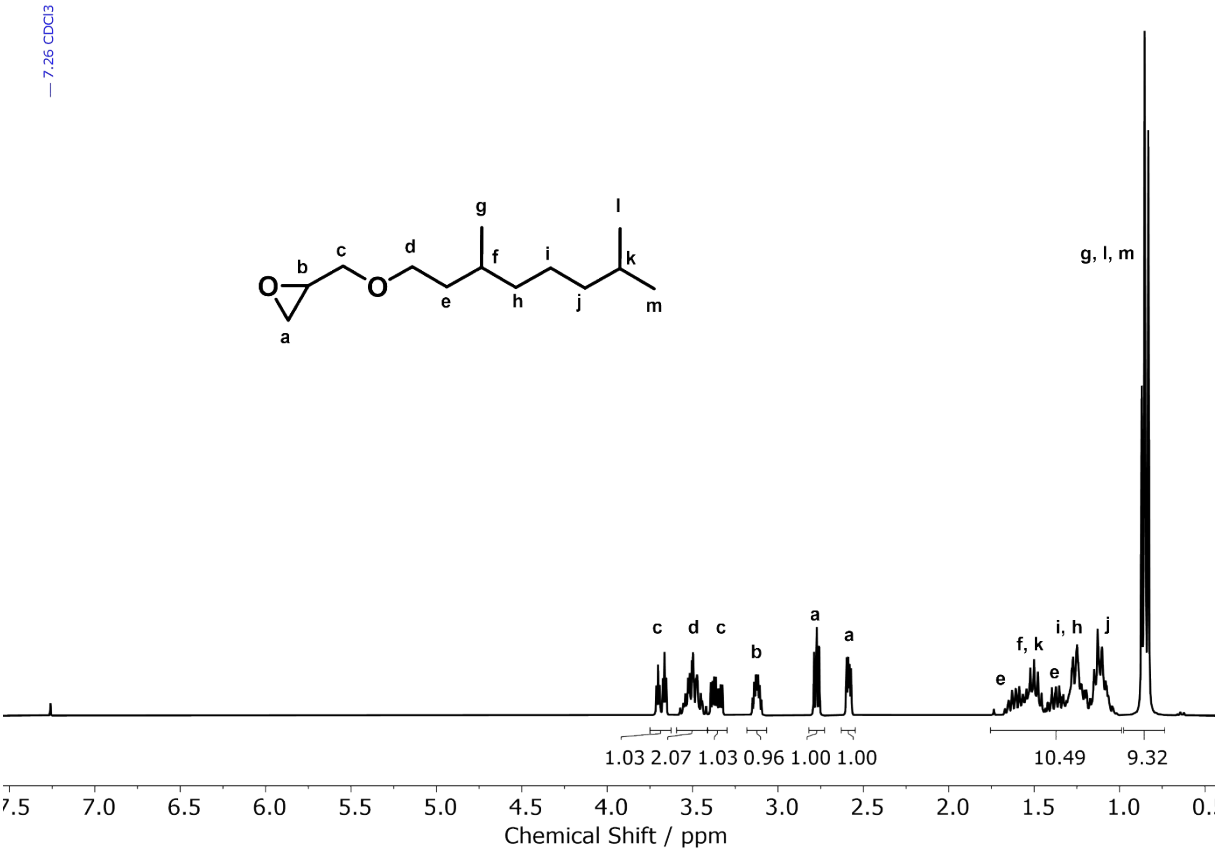

Figure S11: ^{1}H NMR spectrum (300 MHz, $CDCl_3$) of THGeraGE.

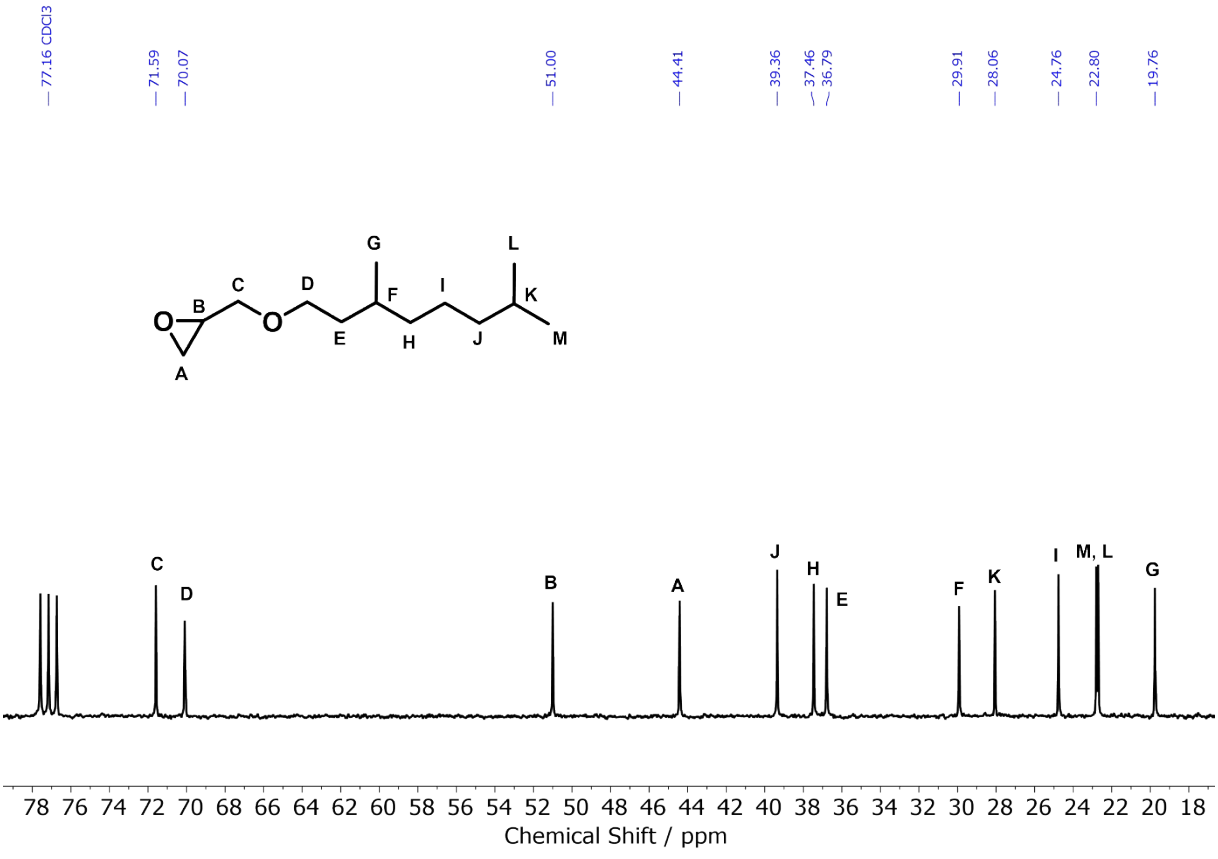

Figure S12: ^{13}C NMR spectrum (75 MHz, $CDCl_3$) of THGeraGE.

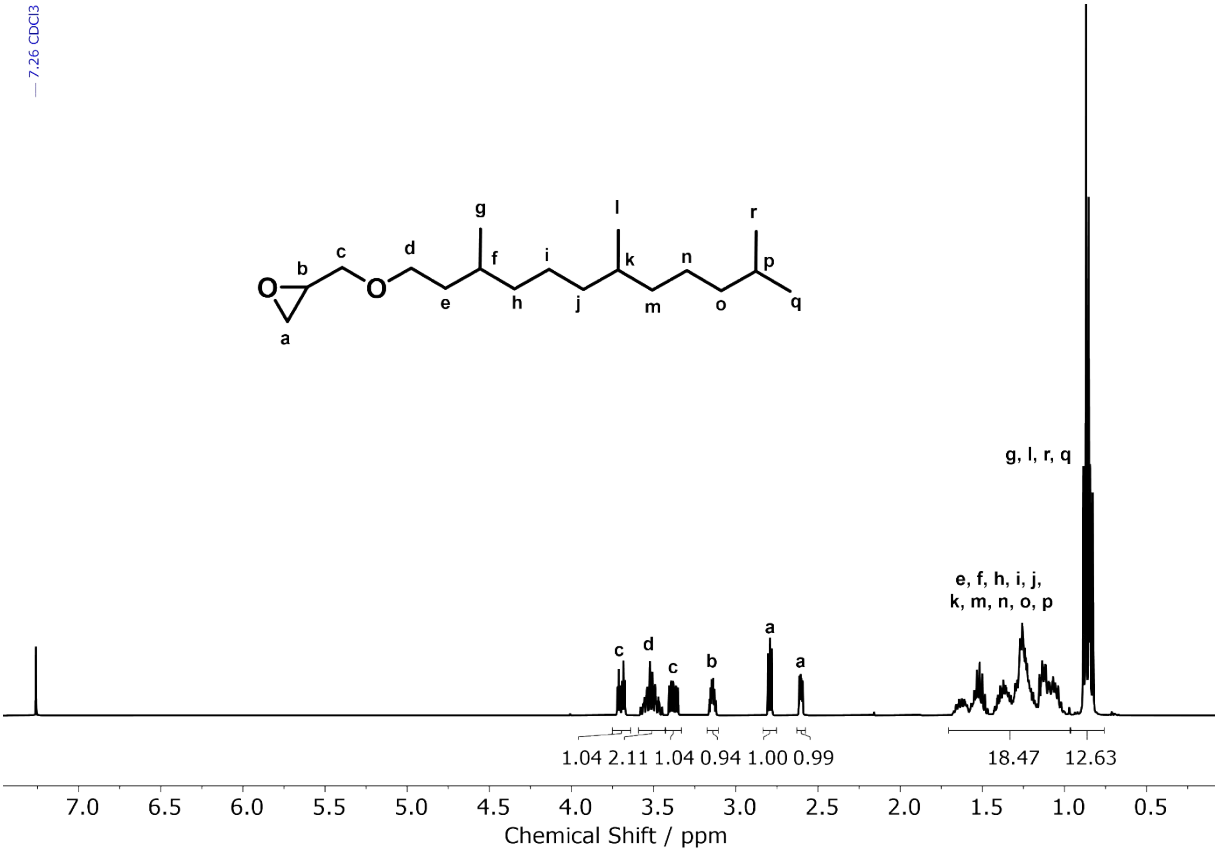

Figure S13: ^{1}H NMR spectrum (400 MHz, $CDCl_3$) of HHFarGE.

Figure S14: ^{13}C NMR spectrum (100 MHz, $CDCl_3$) of HHFarGE.

6. Characterization of Statistical Copolymers of TGEs and EO

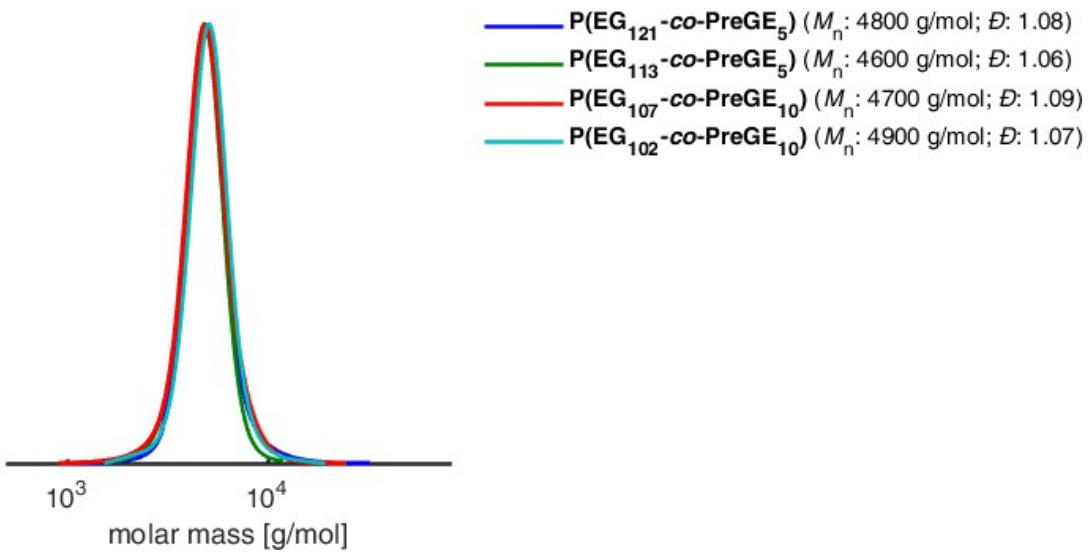

Figure S15: SEC traces of P(EG_n-*co*-$PreGE_m$) (RI detector, eluent: DMF, PEG calibration).

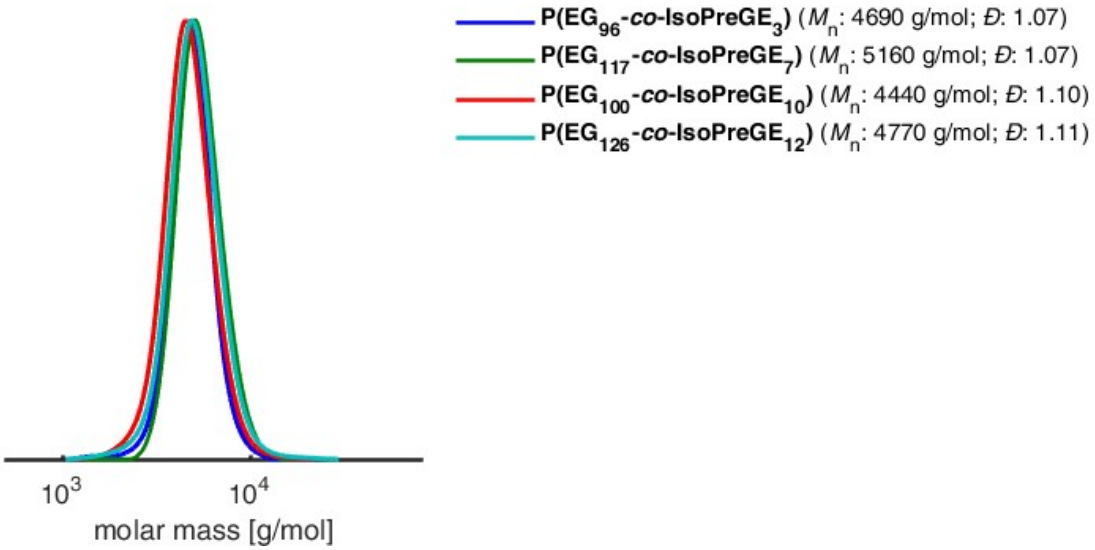

Figure S16: SEC traces of P(EG_n-*co*-$IsoPreGE_m$) (RI detector, eluent: DMF, PEG calibration).

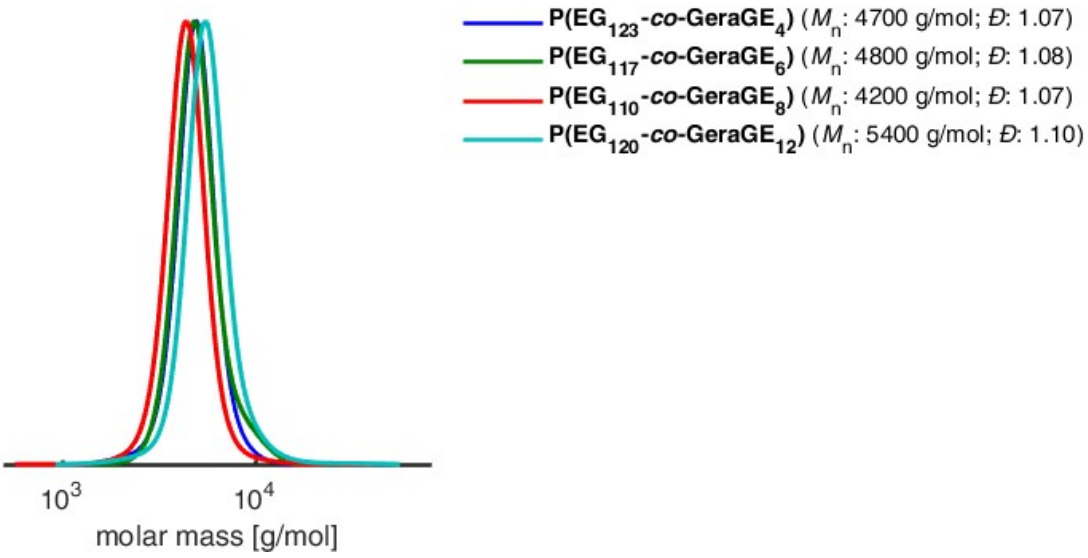

Figure S17: SEC traces of P(EG_n-*co*-$GeraGE_m$) (RI detector, eluent: DMF, PEG calibration).

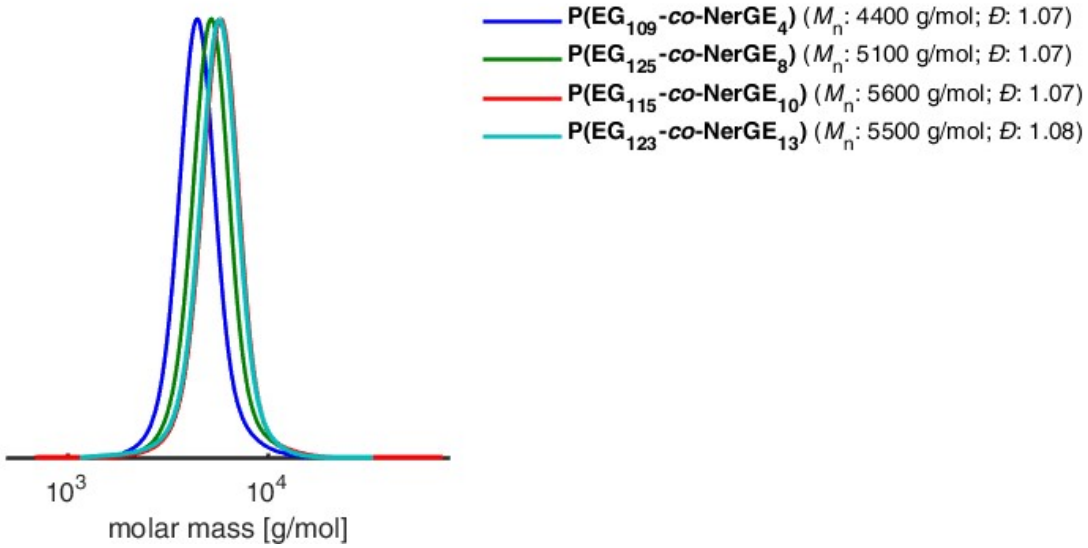

Figure S18: SEC traces of P(EG_n-*co*-$NerGE_m$) (RI detector, eluent: DMF, PEG calibration).

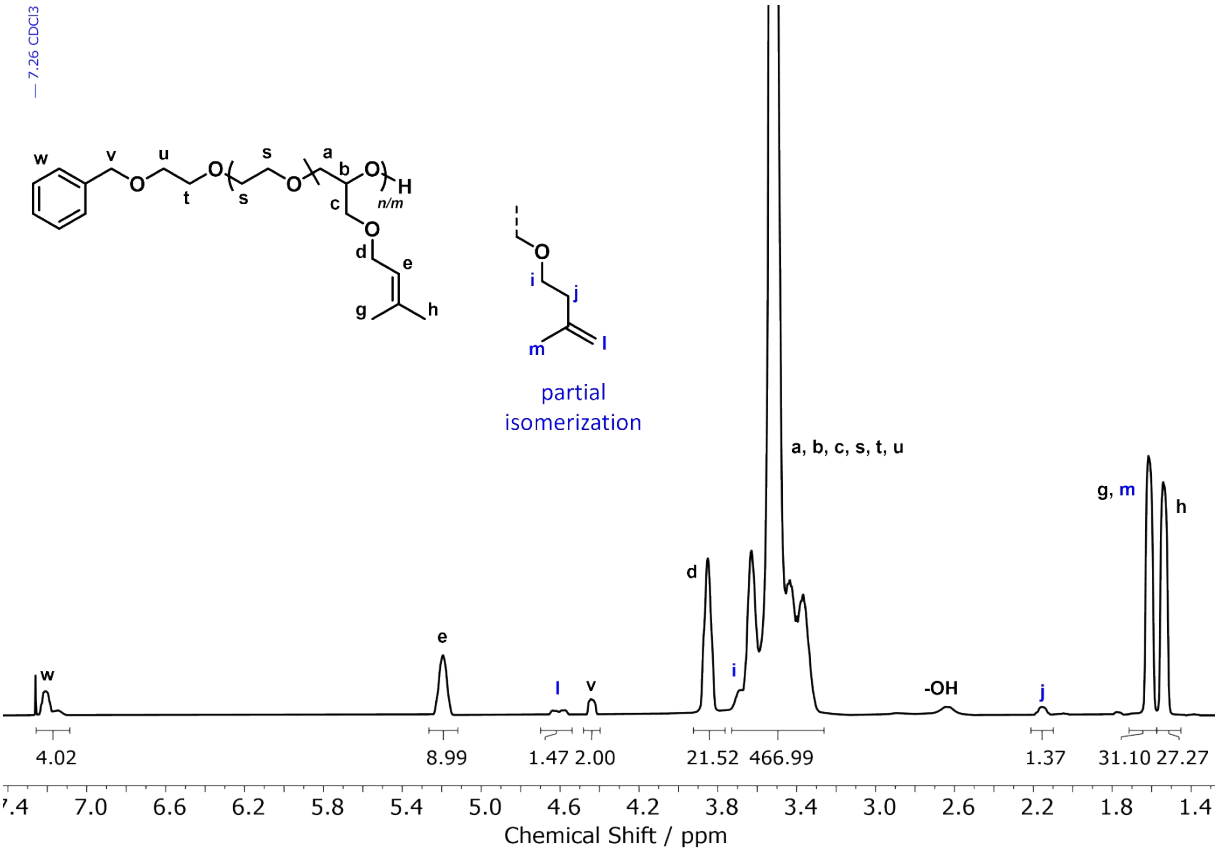

Figure S19: ^{1}H NMR spectrum (400 MHz, $CDCl_3$) of P(EG_{102}-*co*-PreGE_{10}).

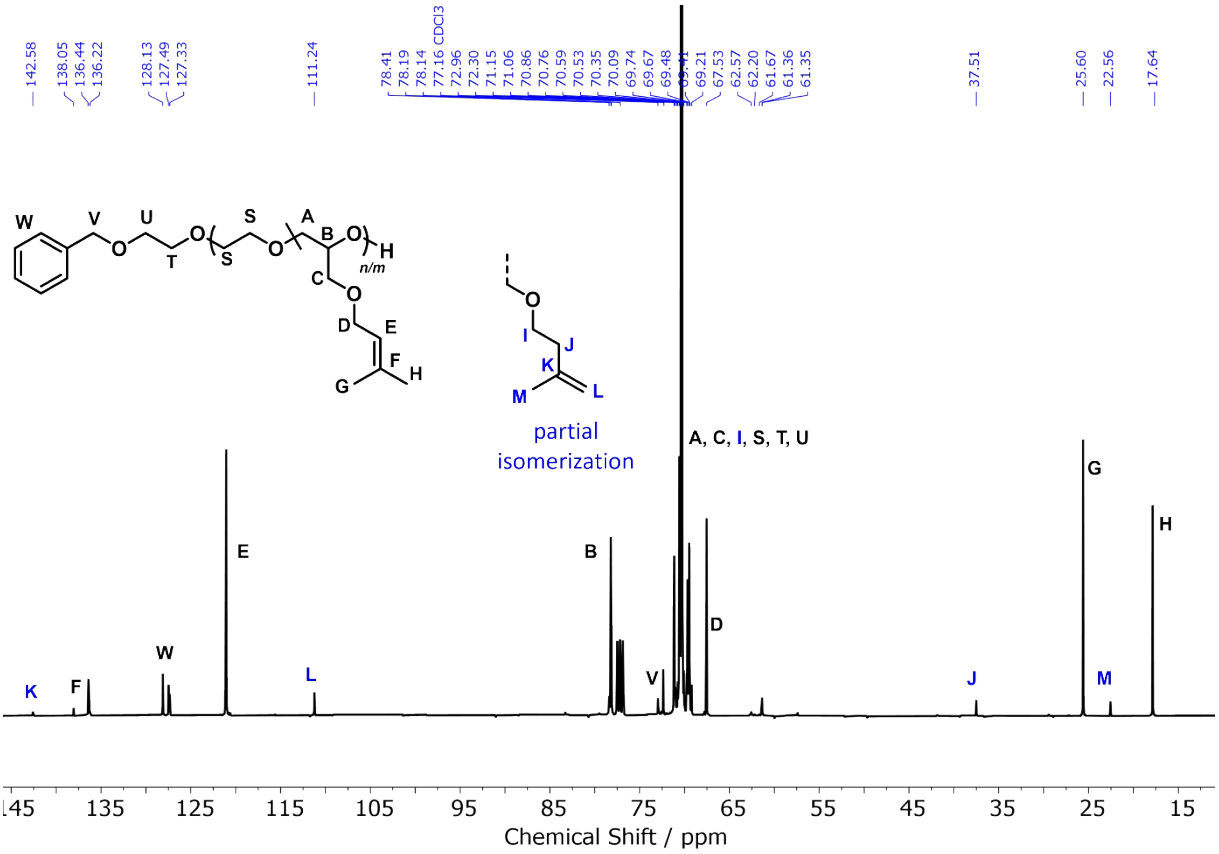

Figure S20: ^{13}C NMR spectrum (100 MHz, $CDCl_3$) of P(EG_{102}-*co*-PreGE_{10}).

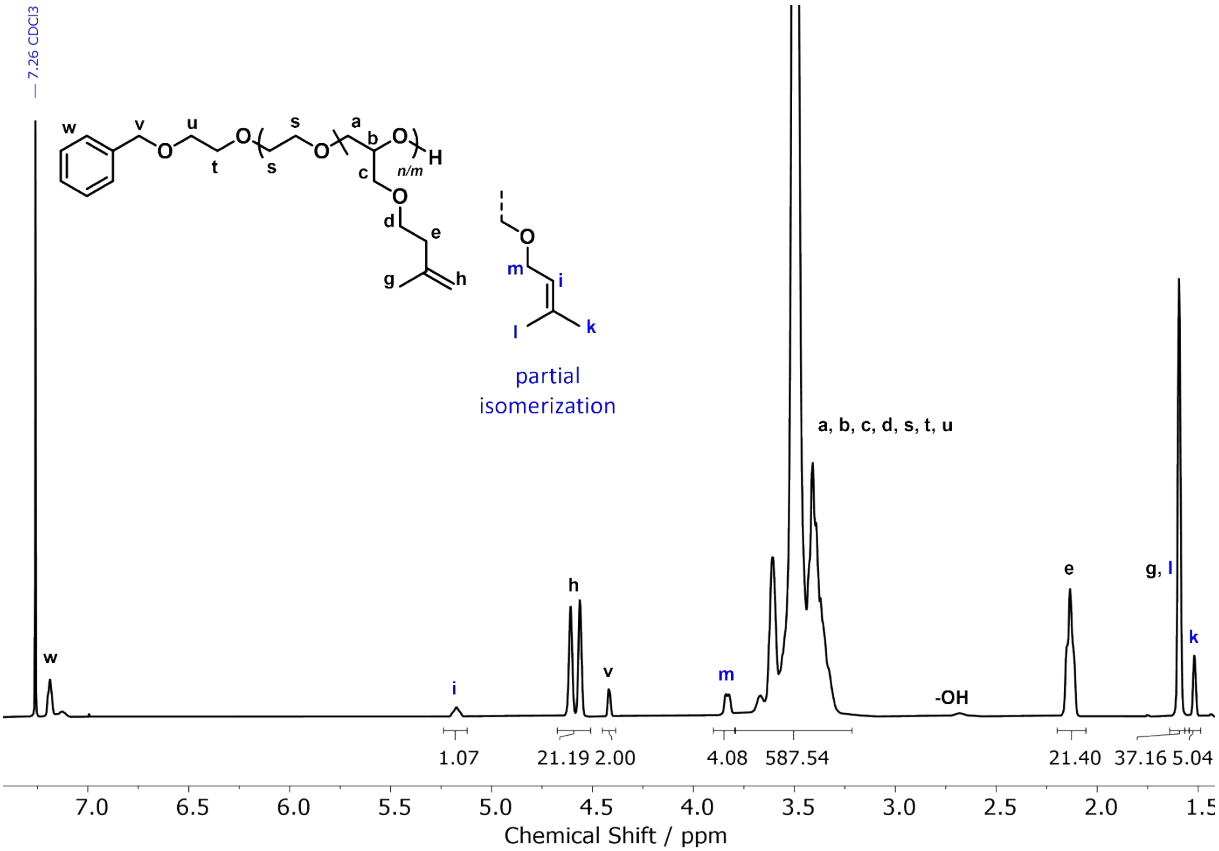

Figure S21: ^{1}H NMR spectrum (400 MHz, $CDCl_3$) of P(EG_{126}-*co*-IsoPreGE_{12}).

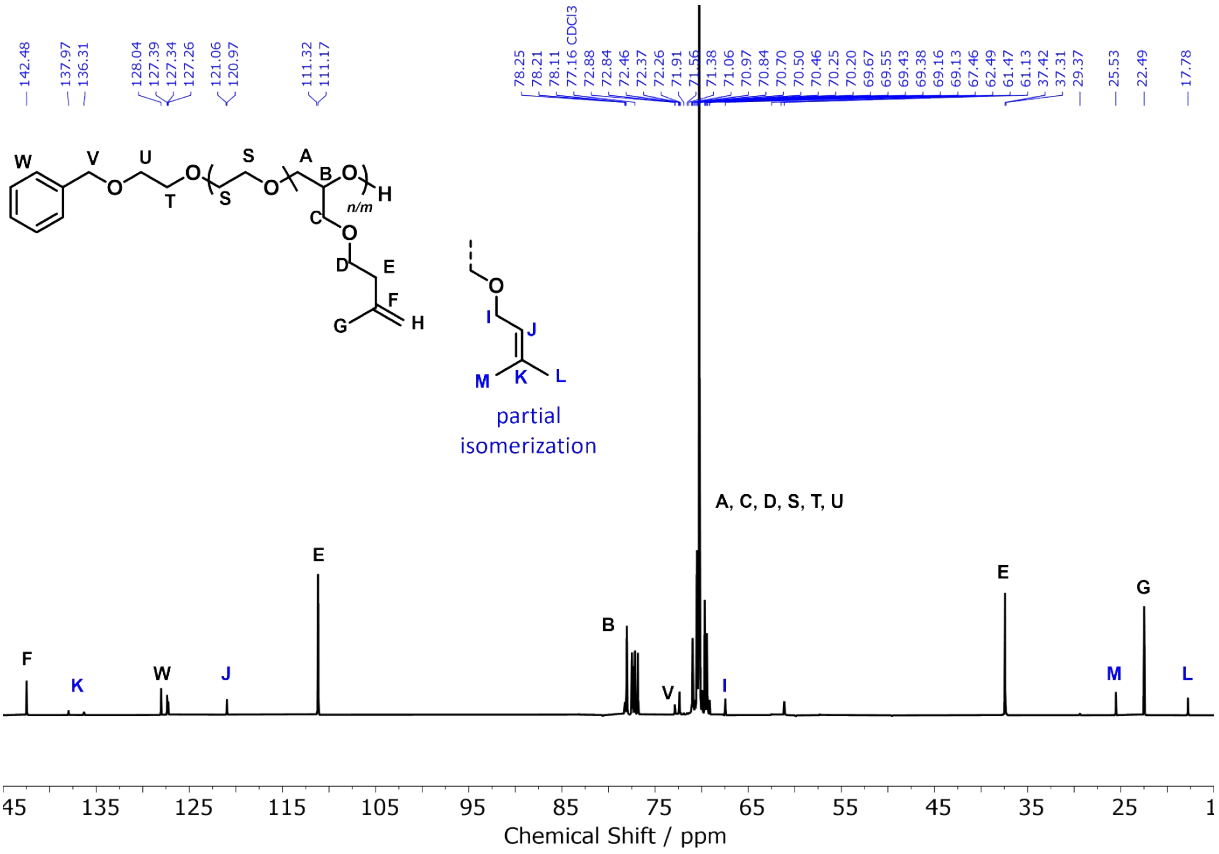

Figure S22: ^{13}C NMR spectrum (100 MHz, $CDCl_3$) of P(EG_{126}-*co*-IsoPreGE_{12}).

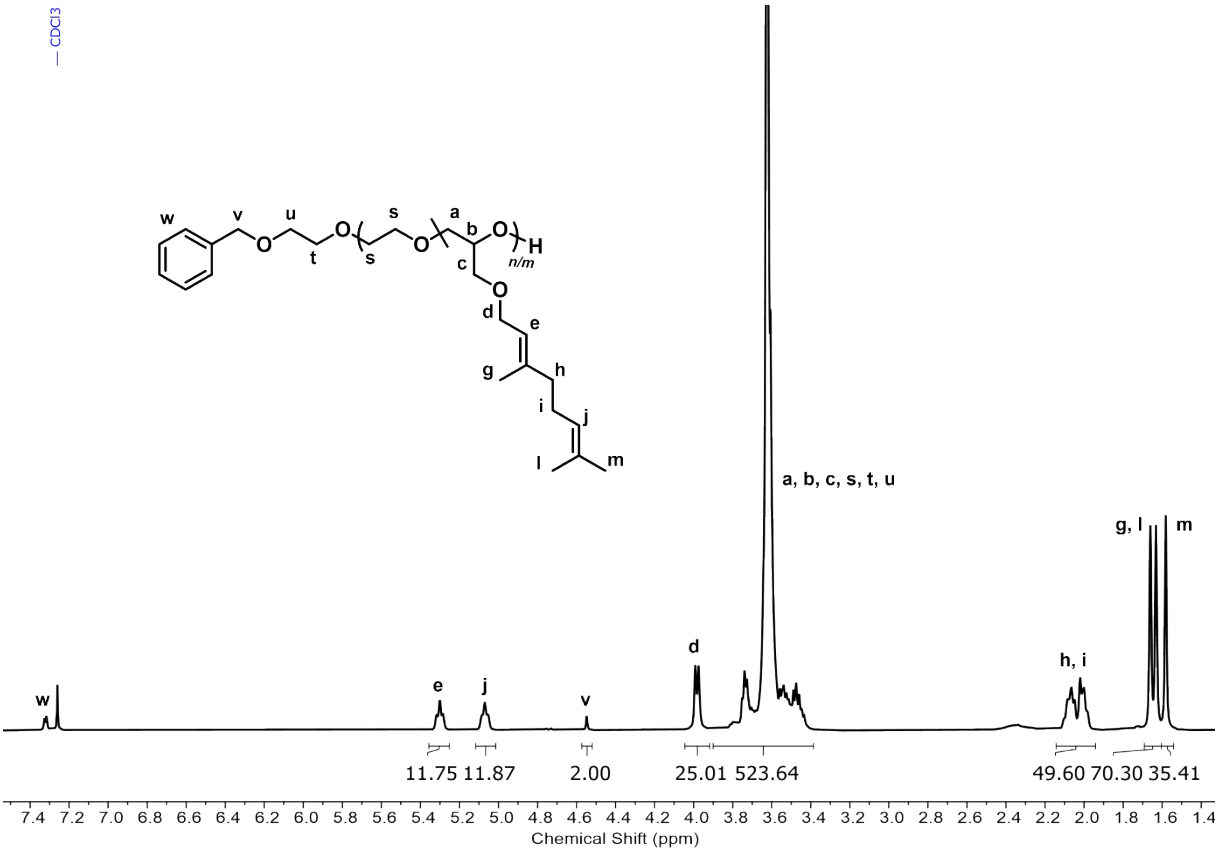

Figure S23: ^{1}H NMR spectrum (400 MHz, $CDCl_3$) of P(EG_{120}-*co*-GeraGE_{12}).

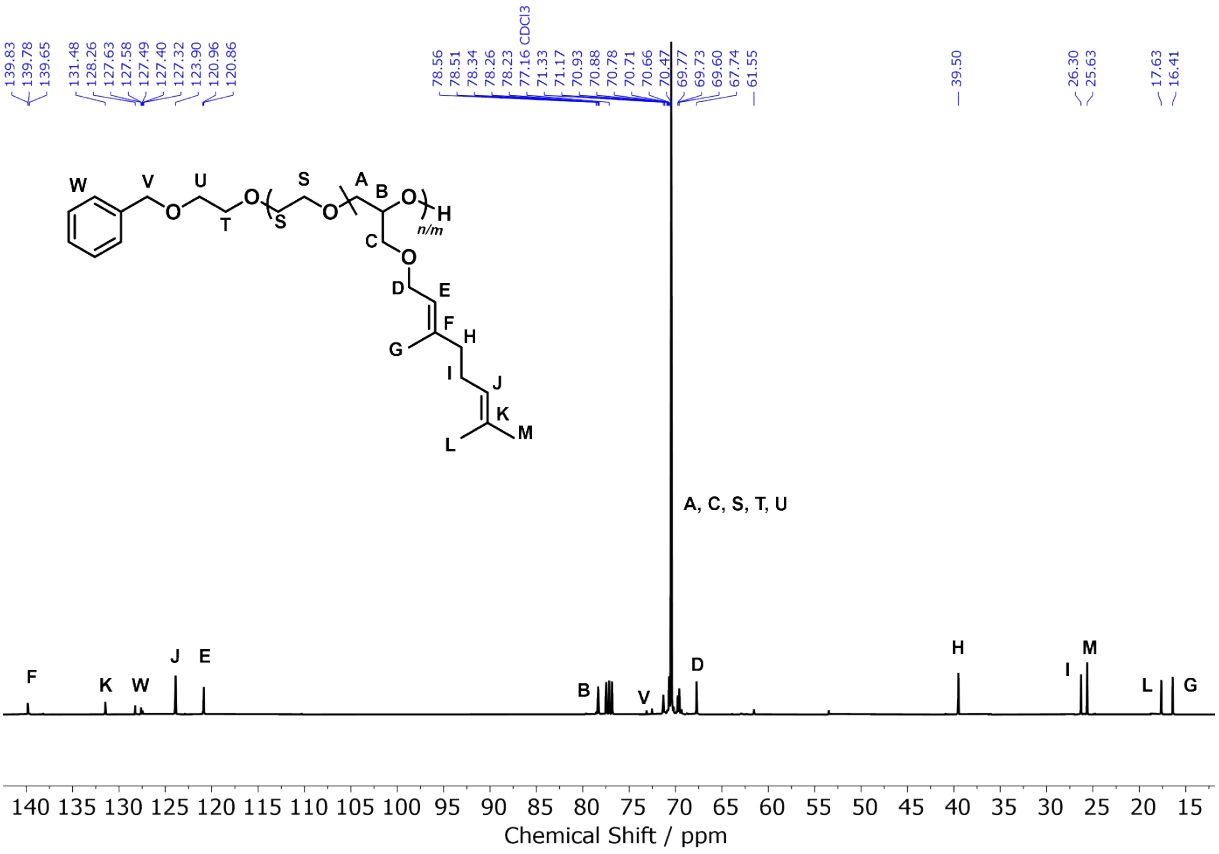

Figure S24: ^{13}C NMR spectrum (100 MHz, $CDCl_3$) of P(EG_{120}-*co*-GeraGE_{12}).

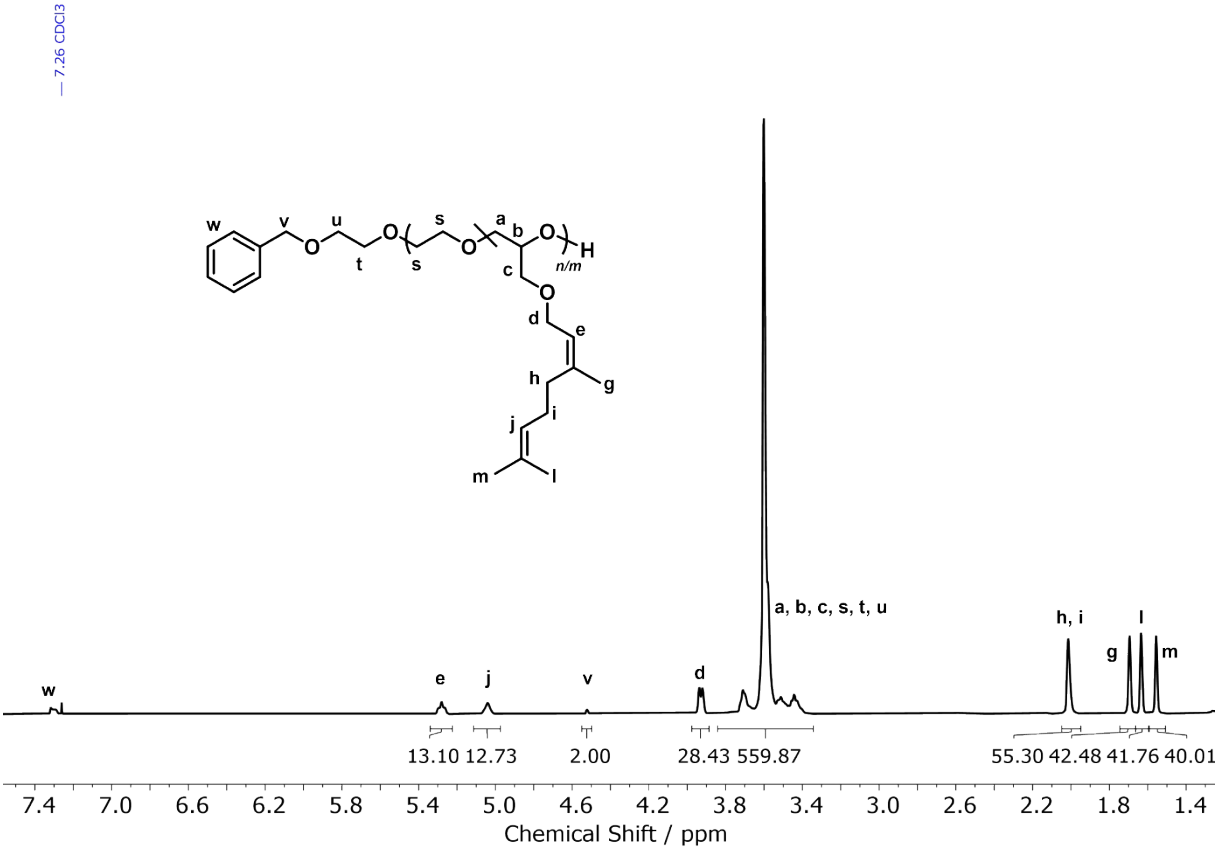

Figure S25: ^{1}H NMR spectrum (400 MHz, $CDCl_3$) of P(EG_{123}-*co*-$NerGE_{13}$).

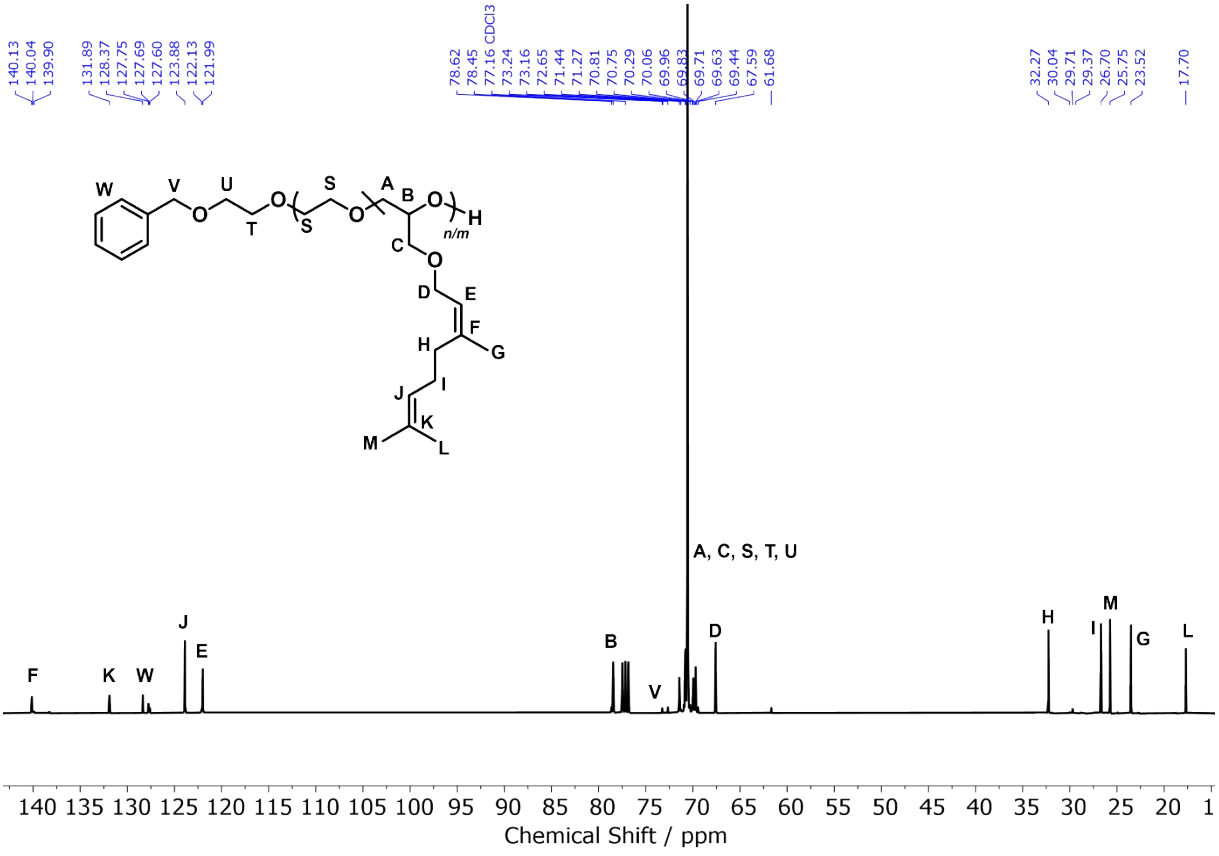

Figure S26: ^{13}C NMR spectrum (100 MHz, $CDCl_3$) of P(EG_{123}-*co*-$NerGE_{13}$).

7. *In situ* ^{1}H NMR Copolymerization Kinetics of TGEs with EO

Non-terminal, ideal copolymerization model and Jaacks fit.

The evaluation of the reactivity ratios is based on the non-terminal, ideal copolymerization model, which was introduced by Wall in 1941.[10] Assuming first order polymerizations, the following polymerization rates apply for a binary copolymerization system:

$$\frac{d[M_1]}{dt} = -k_1[M_1][P] \quad (1)$$

$$\frac{d[M_2]}{dt} = -k_2[M_2][P] \quad (2)$$

[P] refers to the active chain end. Eliminating *t* from the equations by dividing rate (1) by rate (2), followed by rearrangement, the time-independent differential equation (4) is obtained:

$$\frac{d[M_1]}{d[M_2]} = \frac{k_1[M_1]}{k_2[M_2]} \quad (3)$$

$$\frac{d[M_1]}{[M_1]} = r_1\frac{d[M_2]}{[M_2]} \quad \text{with} \quad r_1 = \frac{k_1}{k_2} \quad (4)$$

Wall was the first to use relative rates to describe copolymerizations and the resulting reactivity ratios r_1 and r_2 represent the compositional drift due to different comonomer reactivities.[11] The model assumes a copolymerization behavior that is not dependent on the identity of the growing chain end, but solely on the comonomer reactivities.

The integration of the rearranged Wall's equation (4) leads to the Jaacks equation (5)[6]:

$$log\frac{[M_{1,\ t=x}]}{[M_{1,t=0}]} = r_1 log\frac{[M_{2,\ t=x}]}{[M_{2,t=0}]} \quad (5)$$

The Jaacks equation allows for the determination of the reactivity ratios at any comonomer ratio when ideal copolymerization conditions are applicable *($r_1 \cdot r_2$* = 1).[6]

In line with the Ockhams razor, the non-terminal model represents the most basic model for the determination of the reactivity ratios and poses the model of choice to avoid overfitting.[12,13] Experimental data suggest its suitability for the copolymerization of EO and monosubstituted epoxides, which tend to obey ideal copolymerization behavior.[11]

Jaacks fit for the copolymerization of TGEs with EO

The signal scattering noticeably increases at high copolymerization conversions while the signal-to-noise ratio decreases. Hence, all reactivity ratios were calculated for a TGE monomer conversion of approximately 90 %. The results are summarized in Table 2.

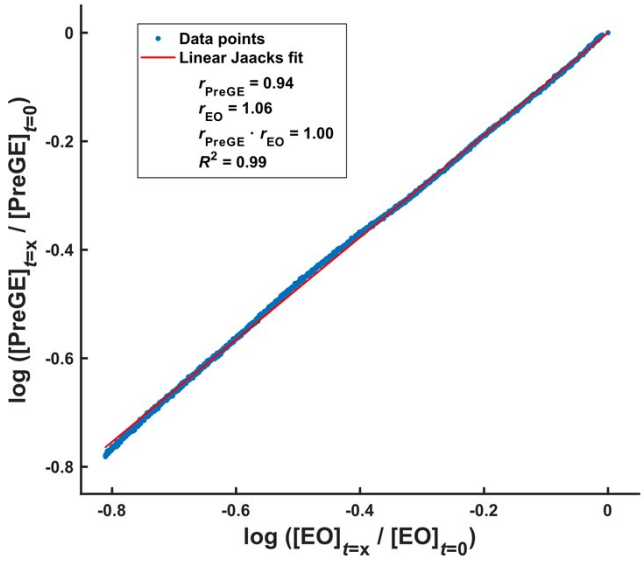

Figure S27: Jaacks fit of the *in situ* ^{1}H NMR copolymerization kinetics of PreGE with EO in a mixture of THF-d_8 and DMSO--d_6 (5:1) at 40 °C.

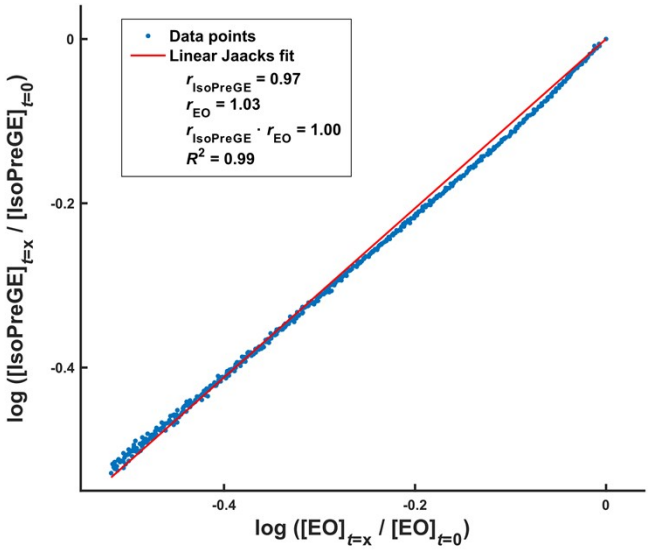

Figure S28: Jaacks fit of the *in situ* ^{1}H NMR copolymerization kinetics of IsoPreGE with EO in a mixture of THF-d_8 and DMSO--d_6 (5:1) at 40 °C.

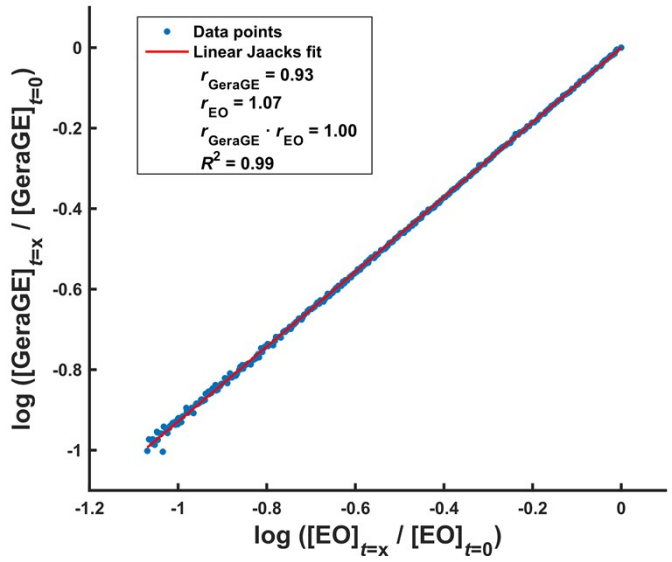

Figure S29: Jaacks fit of the *in situ* ^{1}H NMR copolymerization kinetics of GeraGE with EO in a mixture of THF-d_8 and DMSO--d_6 (5:1) at 40 °C.

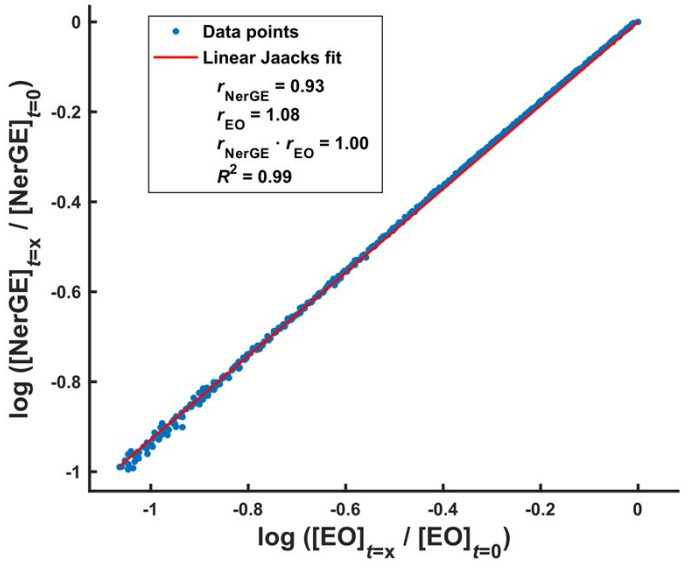

Figure S30: Jaacks fit of the *in situ* ^{1}H NMR copolymerization kinetics of NerGE with EO in a mixture of THF-d_8 and DMSO--d_6 (5:1) at 40 °C.

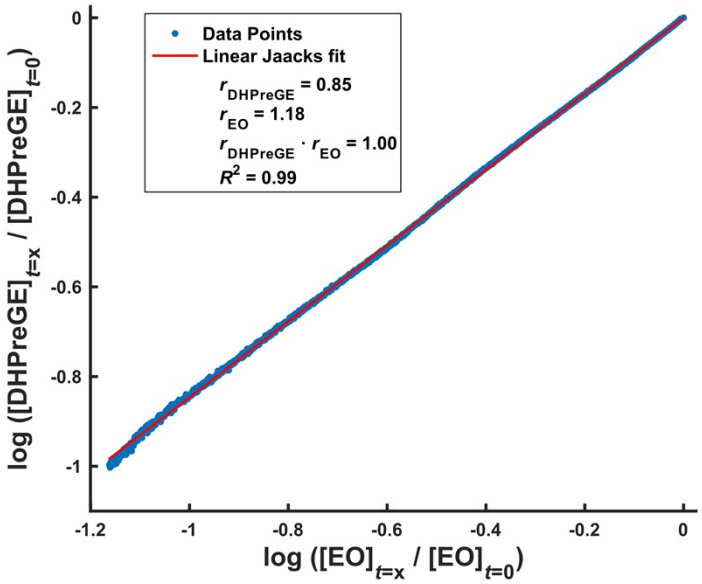

Figure S31: Jaacks fit of the *in situ* ^{1}H NMR copolymerization kinetics of DHPreGE with EO in a mixture of THF-d_8 and DMSO--d_6 (5:1) at 40 °C.

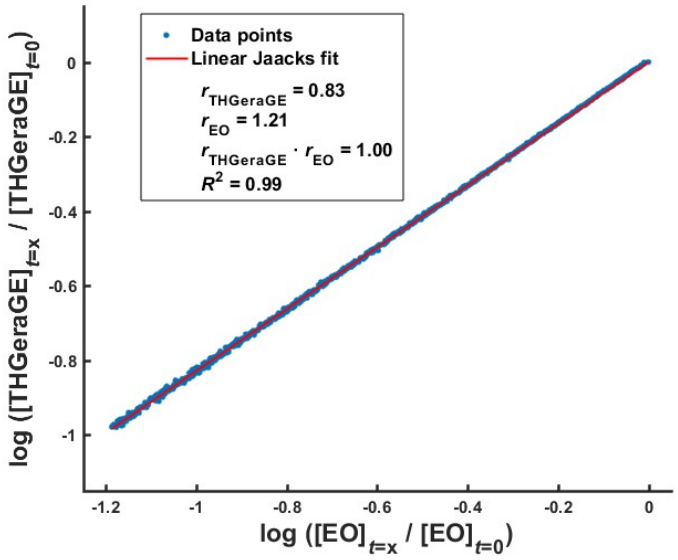

Figure S32: Jaacks fit of the *in situ* ^{1}H NMR copolymerization kinetics of THGeraGE with EO in a mixture of THF-d_8 and DMSO-d_6 (5:1) at 40 °C.

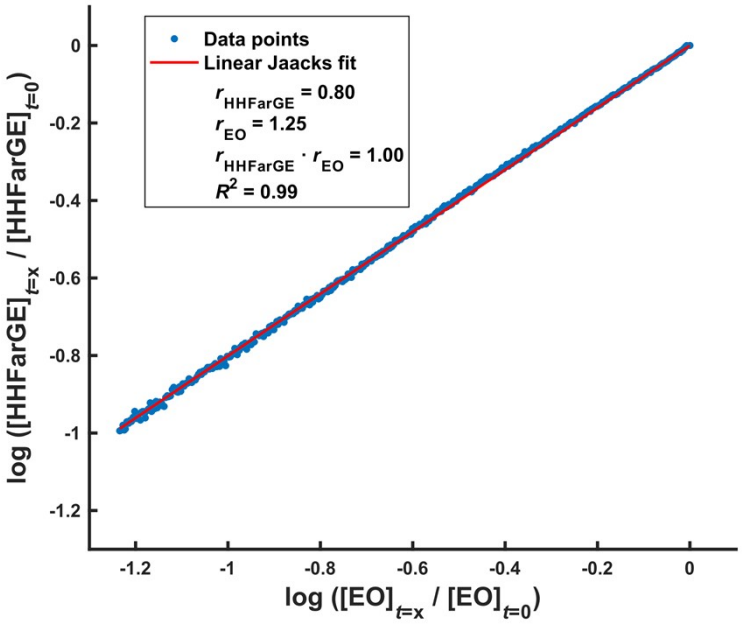

Figure S33: Jaacks fit of the *in situ* ^{1}H NMR copolymerization kinetics of HHFarGE with EO in a mixture of THF-d_8 and DMSO--d_6 (5:1) at 40 °C.

Investigation of side reaction during *in situ* copolymerization kinetics of PreGE with EO

Note that we unexpectedly observed the appearance of new signals between 4.9 – 6.6 ppm during the *in situ* copolymerization kinetics (Figure 3 + Figure S34). Chain transfer to the monomer due to proton abstraction of the α-methylene proton is a literature-known side reaction of the AROP, prevailing proton signals in a similar down-field region.[14] To reliably determine the reactivity ratios, we sought to further investigate this phenomenon as proton abstraction would falsely simulate an increased PreGE consumption. On account of previous reports applying the prenyl functionality as an OH protective group, we hypothesized that a base-catalyzed elimination by the alkoxide chain end leads to the formation of isoprene.[15,16] Scheme S2 suggests a six-membered transition state prior to elimination, which tentatively explains the elimination predominantly occuring for the short TGEs.

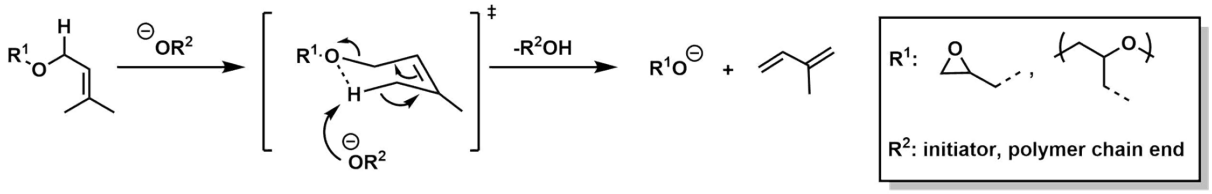

Scheme S2: Proposed base-catalyzed elimination of isoprene during the copolymerization of PreGE with EO.

In a second *in situ* kinetic experiment, all volatile components were cryo-transferred (THF-d_8, DMSO-d_6, isoprene) into a Young NMR tube. Subsequent NMR and GC analyses corroborate the hypothesis of isoprene forming during the copolymerization (Figure S35 – Figure S37). In summary, monomer consumption is solely caused by monomer incorporation into the polymer chain, legitimizing the determined reactivity ratios and the related copolymer microstructure. Figure S38 additionally reveals the partial base-catalyzed prenyl-to-isoprenyl isomerization of the side chain under basic conditions (and vice versa for IsoPreGE).[17,18]

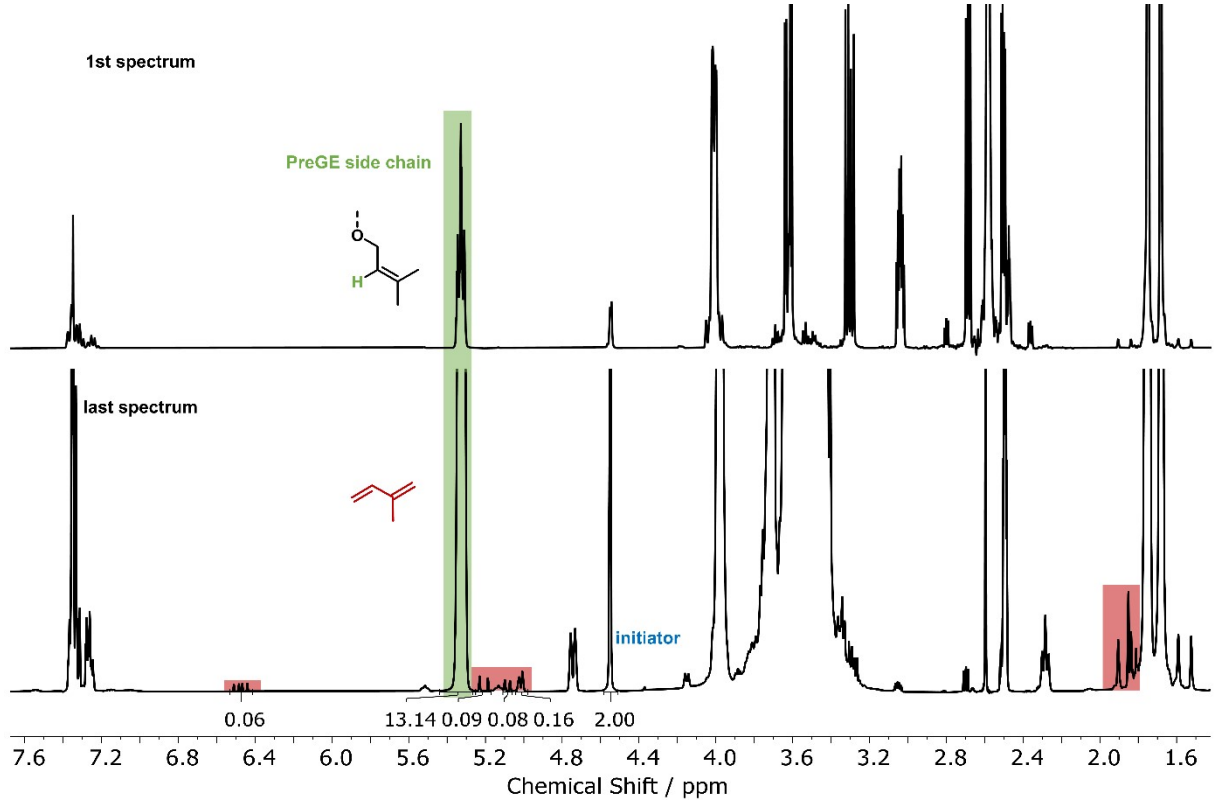

Figure S34: Overlay of the first and last ^{1}H NMR spectrum (400 MHz, THF-d_8) of the *in situ* kinetics, proving the elimination of isoprene in small quantities during copolymerization. The monomer amount undergoing elimination is below 0.5%.

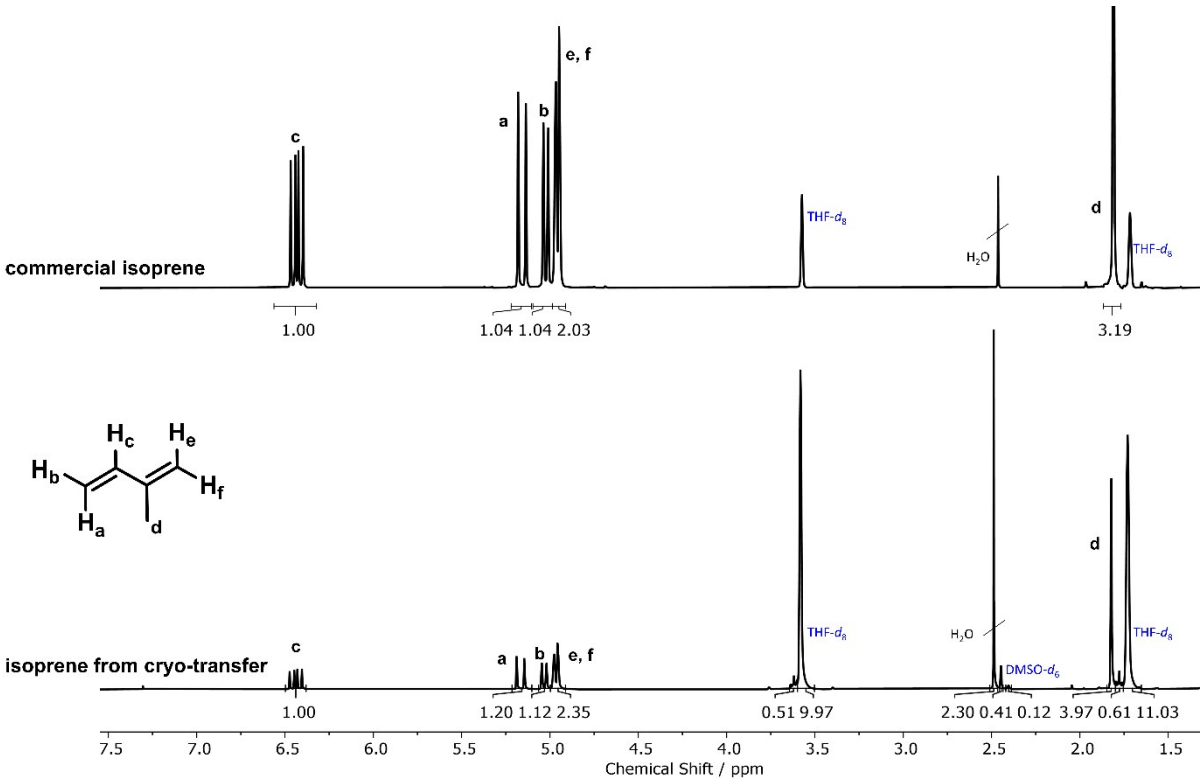

Figure S35: Overlay of ^{1}H NMR spectra (400 MHz, THF-d_8) of the commercial isoprene and cryo-transferred isoprene.

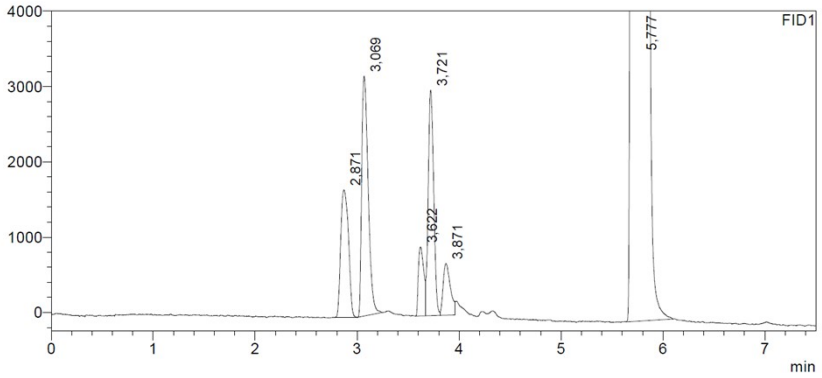

Figure S36: GC analysis of isoprene eliminated during the copolymerization with a $t_{retention,\ isorprene}$ = 3.721 (area 98.8 %). Isoprene and THF-d_8 were isolated via cryo-transfer from the NMR tube and the major peak can be ascribed to THF-d_8 with a $t_{retention,\ THF}$ = 5.777. All other signals are impurities in DMSO, which was used to prepare the GC sample.

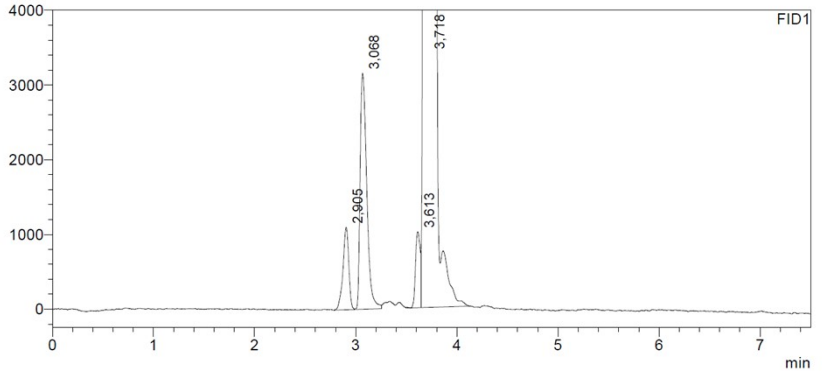

Figure S37: GC analysis of commercial isoprene with a $t_{retention,\ isorprene}$ = 3.718 (area 98.8 %). All other signals are impurities in DMSO, which was used to prepare the GC sample.

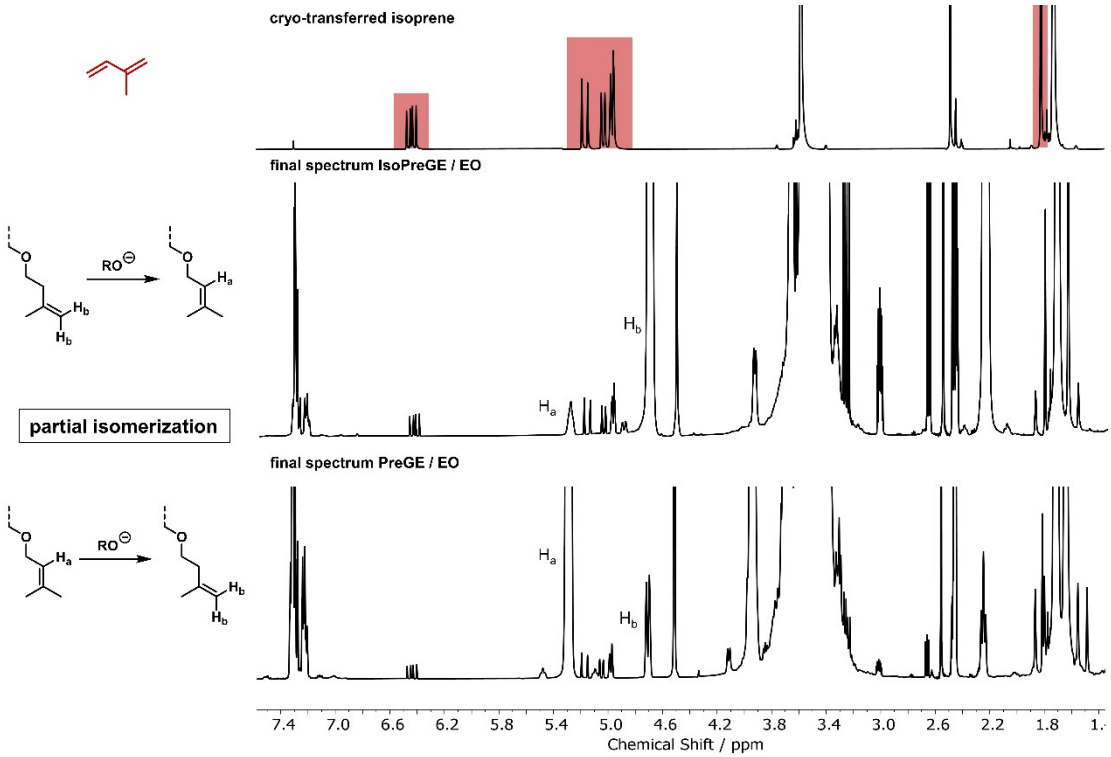

Figure S38: Overlay of ^{1}H NMR spectra (400 MHz, $CDCl_3$) of the spectrum of the cryo-transferred isoprene (top) and the final spectra of the in situ kinetic measurements of IsoPreGE (middle) with EO and PreGE with EO (bottom). *In situ* NMR

kinetics mirror the formation of isoprene in trace amounts. The overlay also demonstrates a slight isomerization of the prenyl and isoprenly side chain to the respective isomer (H_a and H_b).

Kinetic data of the copolymerization of PreGE with EO.

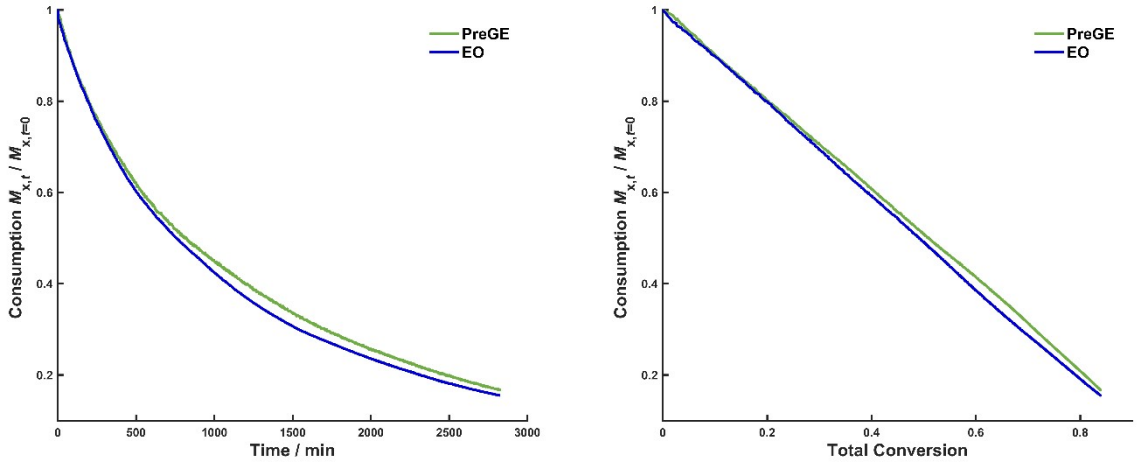

Figure S39: Time-conversion plot of the anionic copolymerization of IsoPreGE and with EO, determined via *in situ* ^{1}H NMR kinetics (left). Individual monomer conversion versus total monomer conversion (right).

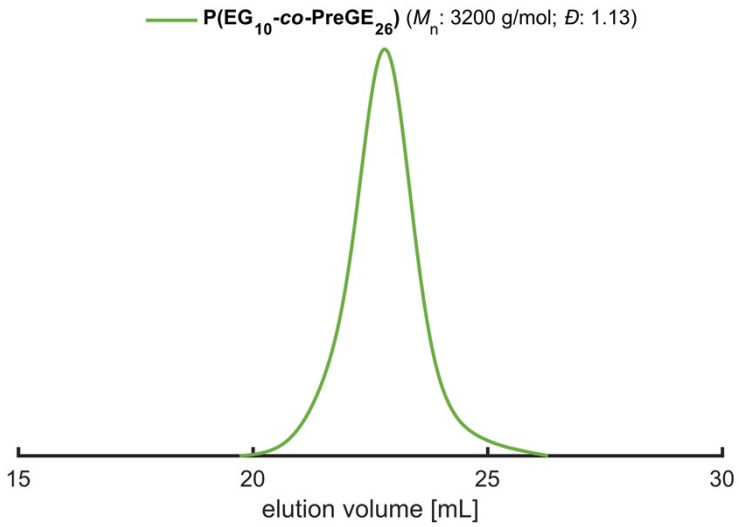

Figure S40: SEC elugram (RI detector, eluent: DMF, PEG calibration) of the P(EG_{10}-*co*-$PreGE_{26}$) copolymer synthesized from the *in situ* ^{1}H NMR copolymerization kinetics. SEC analysis: M_n = 3200 g·mol^{-1}, $Đ$ = 1.13.

Kinetic data of the copolymerization of IsoPreGE with EO.

Note that the isoprene formation has additionally been observed during the copolymerization of IsoPreGE and EO. We conclude an elimination of isoprene (Scheme S2) from the glycidyl side chain occurring, which is confirmed in analogy to the PreGE/EO comonomer pair in the previous section (Figure S38).

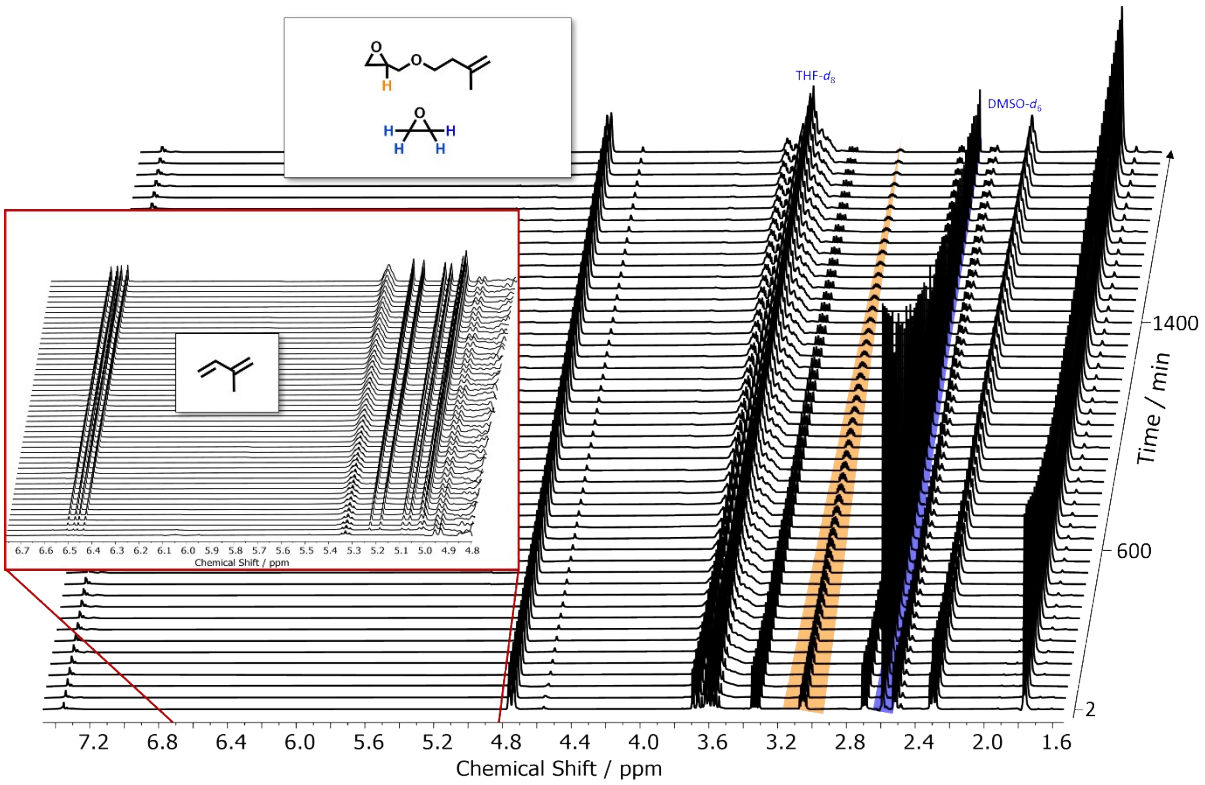

Figure S41: Selection of ^{1}H NMR spectra (400 MHz, THF-d_8 : DMSO-d_6= 5:1) for the *in situ* NMR kinetics of the statistical copolymerization of IsoPreGE with EO at 40 °C. Relevant epoxide signals for evaluation are highlighted in green at 3.05 ppm (IsoPreGE) and blue at 2.59 ppm (EO). Since spectra were recorded at 2 min intervals over a period of 32.9 h, only every 20th spectrum is displayed. The zoom-in section displays the appearance of new signals, which is ascribed to isoprene formation during the copolymerization.

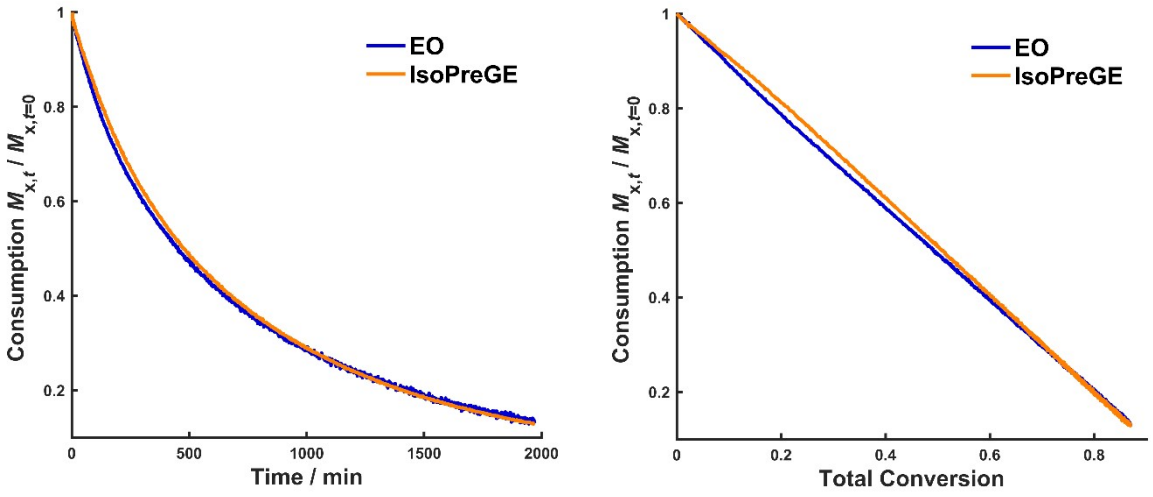

Figure S42: Time-conversion plot of the anionic copolymerization of IsoPreGE and with EO, determined via *in situ* ^{1}H NMR kinetics (left). Individual monomer conversion versus total monomer conversion (right).

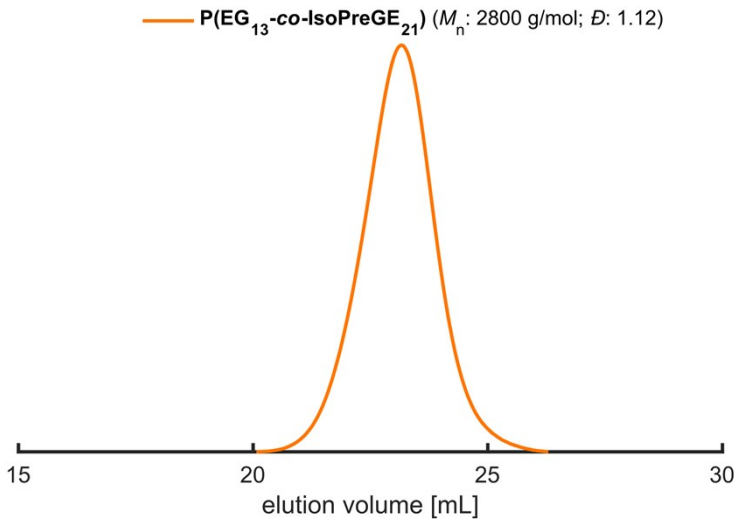

Figure S43: SEC elugram (RI detector, eluent: DMF, PEG calibration) of the P(EG$_{13}$-*co*-IsoPreGE$_{21}$) copolymer synthesized from the *in situ* ^{1}H NMR copolymerization kinetics. SEC analysis: M_n = 2800 g·mol^{-1}, $Đ$ = 1.12.

Kinetic data of the copolymerization of GeraGE with EO.

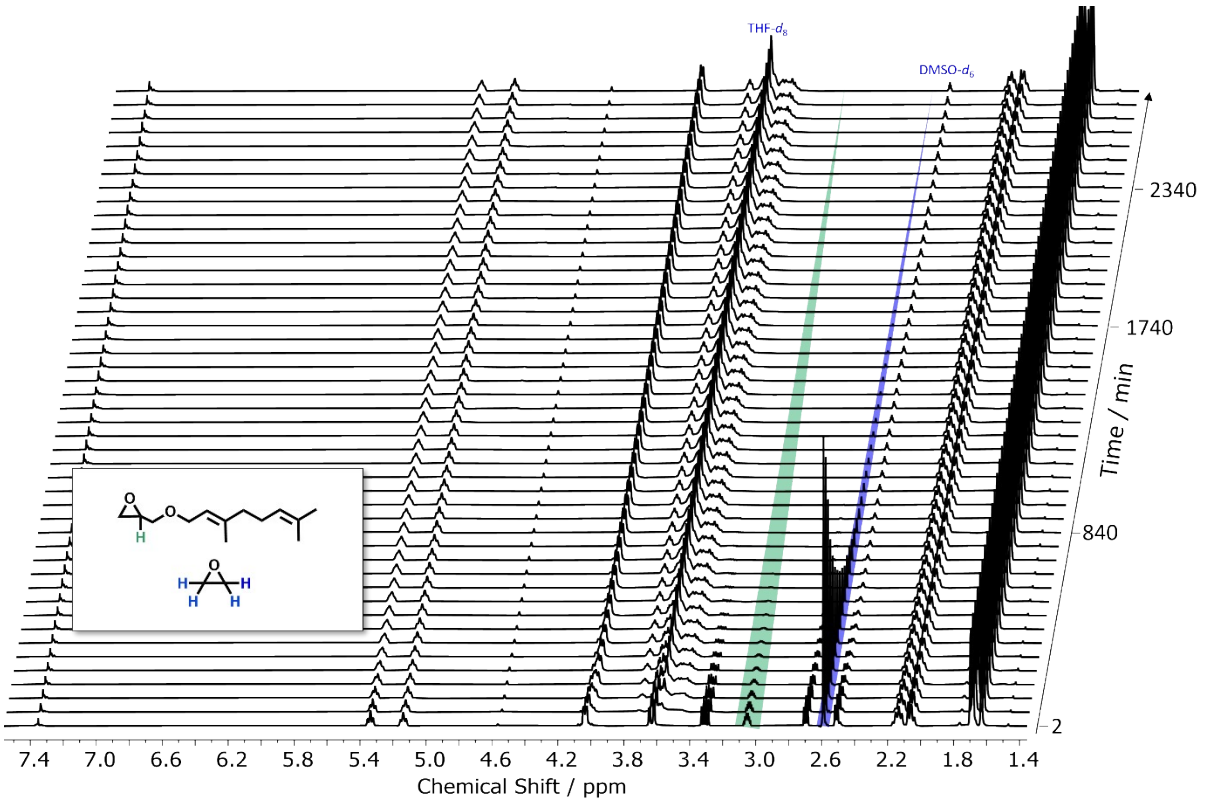

Figure S44: Selection of ^{1}H NMR spectra (400 MHz, THF-d_8 : DMSO-d_6= 5:1) for the *in situ* NMR kinetics of the statistical copolymerization of GeraGE with EO at 40 °C (top). Relevant epoxide signals for evaluation are highlighted in green at 3.05 ppm (GeraGE) and blue at 2.59 ppm (EO). Since spectra were recorded at 2 min intervals over a period of 46.0 h, only every 30th spectrum is displayed.

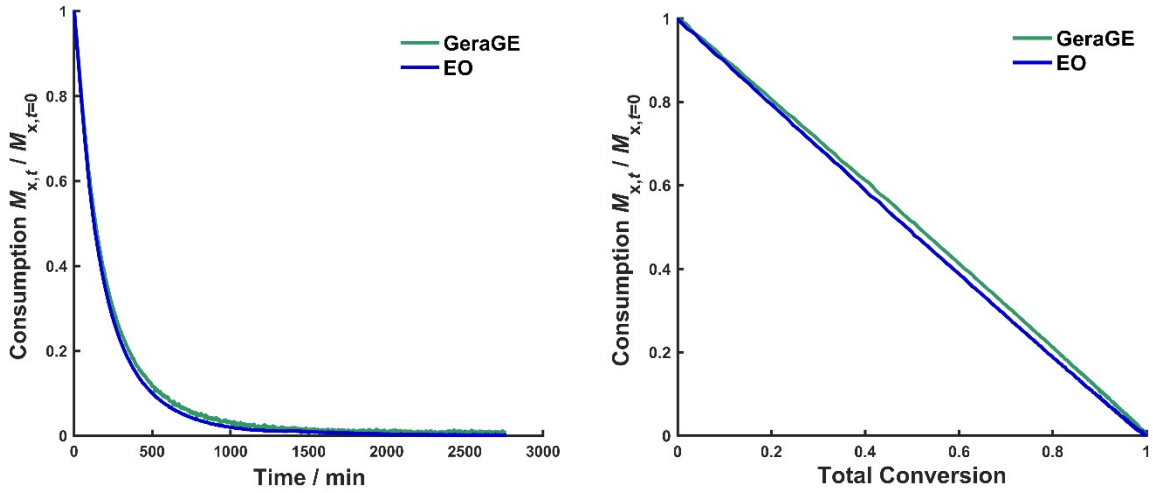

Figure S45: Time-conversion plot of the anionic copolymerization of GeraGE and with EO, determined via *in situ* ^{1}H NMR kinetics (left). Individual monomer conversion versus total monomer conversion (right).

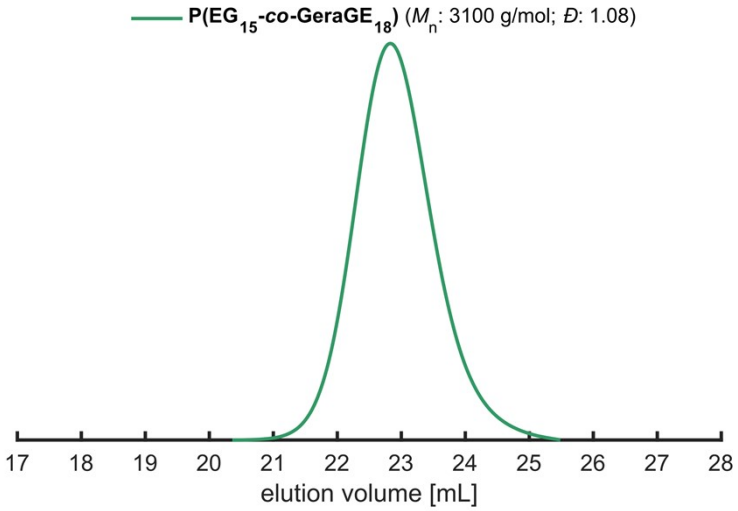

Figure S46: SEC elugram (RI detector, eluent: DMF, PEG calibration) of the P(EG_{15}-*co*-$GeraGE_{18}$) copolymer synthesized from the *in situ* ^{1}H NMR copolymerization kinetics. SEC analysis: M_n = 3100 g·mol^{-1}, $Đ$ = 1.08.

Kinetic data of the copolymerization of NerGE with EO.

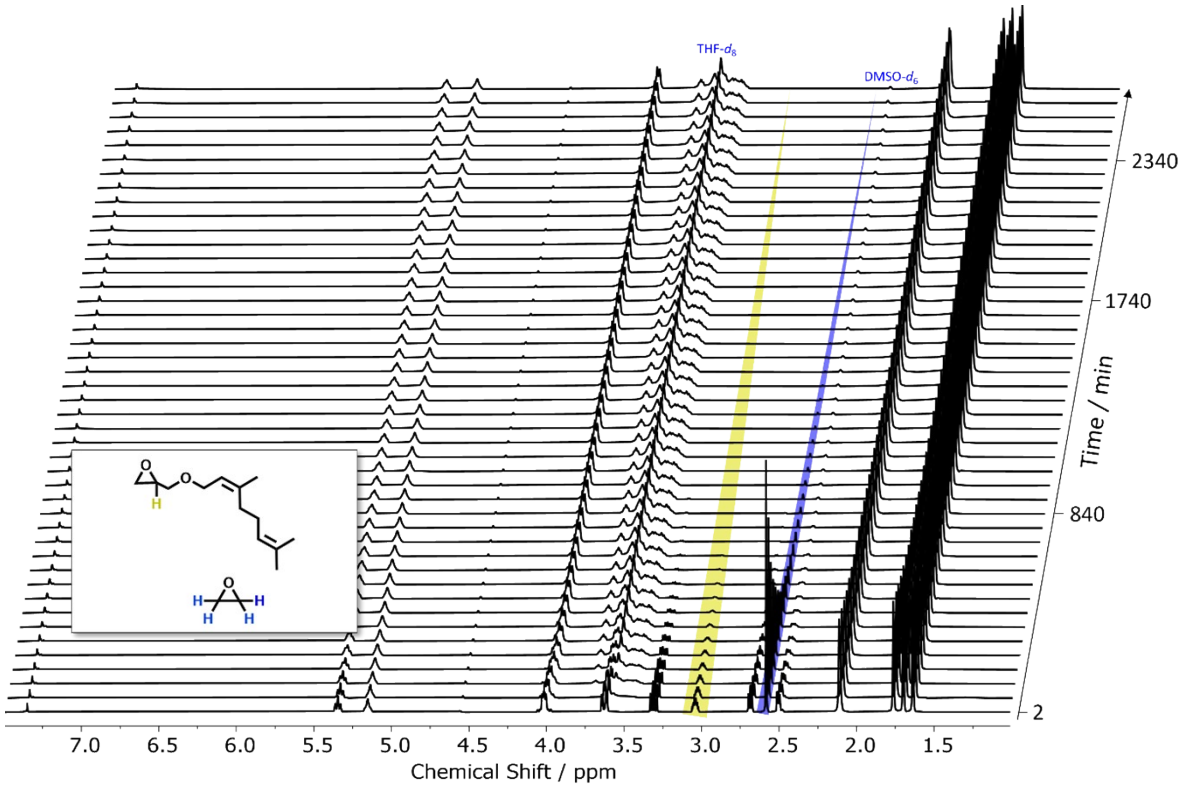

Figure S47: Selection of ^{1}H NMR spectra (400 MHz, THF-d_8 : DMSO-d_6= 5:1) for the *in situ* NMR kinetics of the statistical copolymerization of NerGE with EO at 40 °C. Relevant epoxide signals for evaluation are highlighted in yellow at 3.04 ppm (NerGE) and blue at 2.59 ppm (EO). Since spectra were recorded at 2 min intervals over a period of 44.6 h, only every 30th spectrum is displayed.

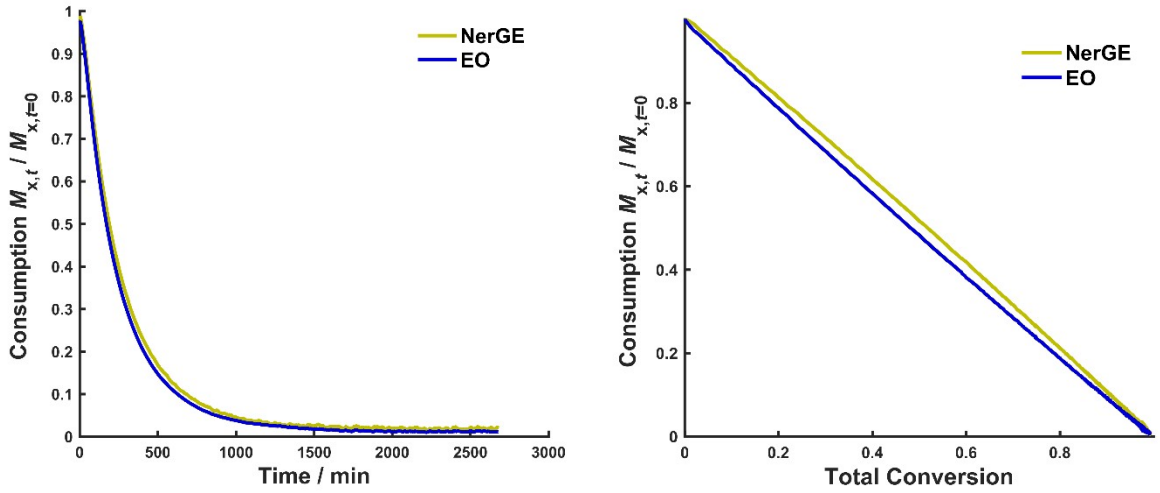

Figure S48: Time-conversion plot of the anionic copolymerization of NerGE and with EO, determined via *in situ* ^{1}H NMR kinetics (left). Individual monomer conversion versus total monomer conversion (right).

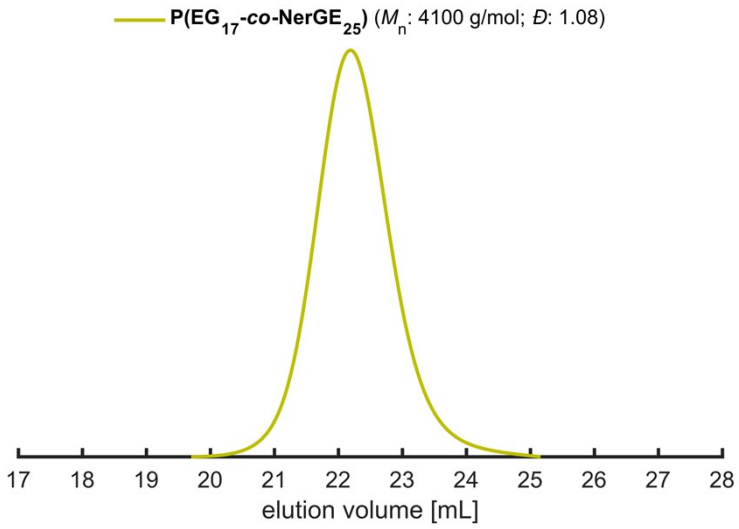

Figure S49: SEC elugram (RI detector, eluent: DMF, PEG calibration) of the P(EG_{17}-*co*-$NerGE_{25}$) copolymer synthesized from the *in situ* ^{1}H NMR copolymerization kinetics. SEC analysis: M_n = 4100 g·mol^{-1}, $Đ$ = 1.08.

Kinetic data of the copolymerization of DHPreGE with EO.

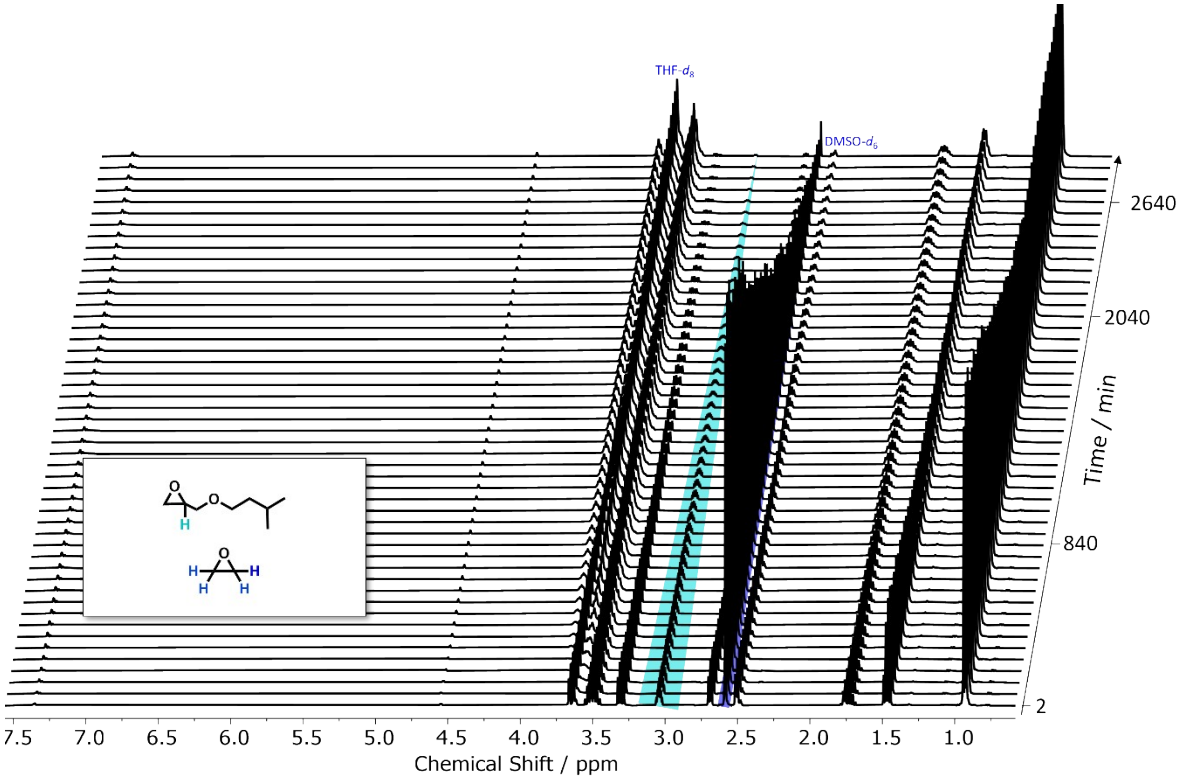

Figure S50: Selection of ^{1}H NMR spectra (400 MHz, THF-d_8 : DMSO-d_6= 5:1) for the *in situ* NMR kinetics of the statistical copolymerization of DHPreGE with EO at 40 °C. Relevant epoxide signals for evaluation are highlighted in cyan at 3.04 ppm (DHPreGE) and blue at 2.59 ppm (EO). Since spectra were recorded at 2 min intervals over a period of 48.4 h, only every 30th spectrum is displayed.

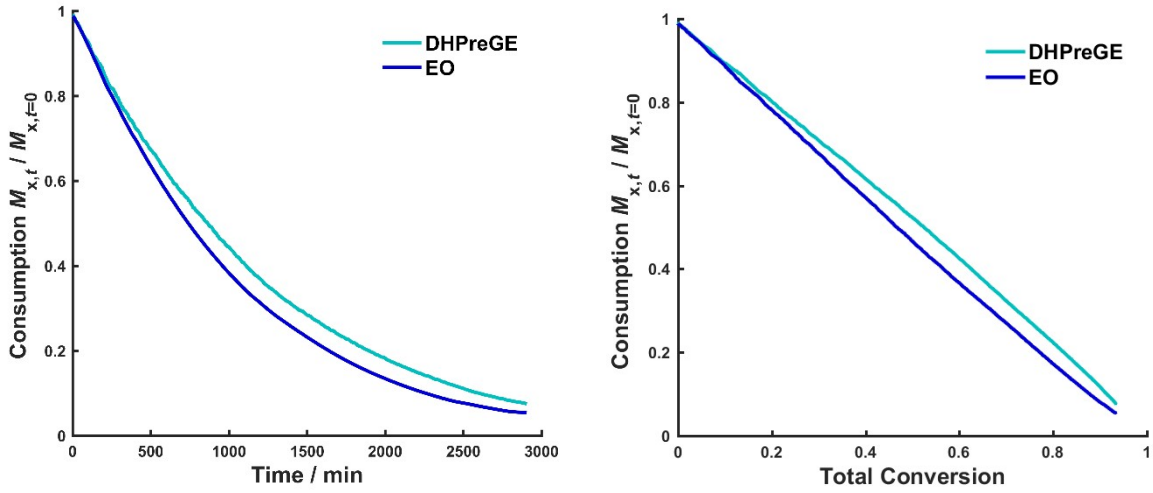

Figure S51: Time-conversion plot of the anionic copolymerization of DHPreGE and with EO, determined via *in situ* ^{1}H NMR kinetics (left). Individual monomer conversion versus total monomer (right).

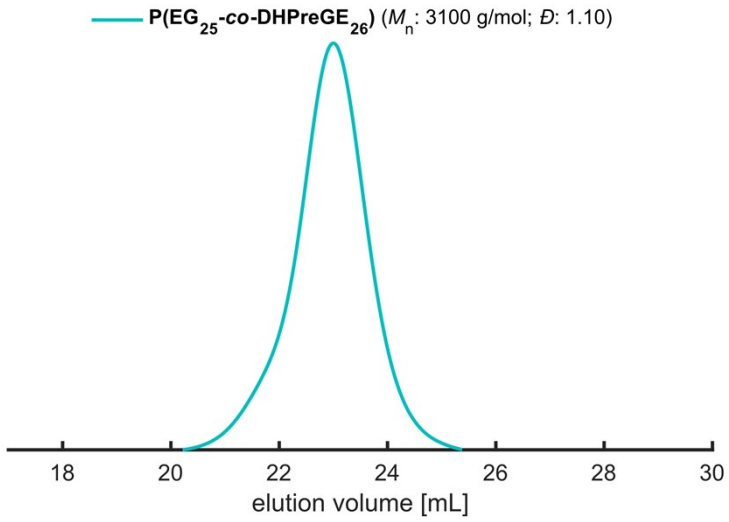

Figure S52: SEC elugram (RI detector, eluent: DMF, PEG calibration) of the P(EG_{25}-*co*-$DHPreGE_{26}$) copolymer synthesized from the *in situ* ^{1}H NMR copolymerization kinetics. SEC analysis: M_n = 3100 g·mol^{-1}, $Đ$ = 1.10.

Kinetic data of the copolymerization of THGeraGE with EO.

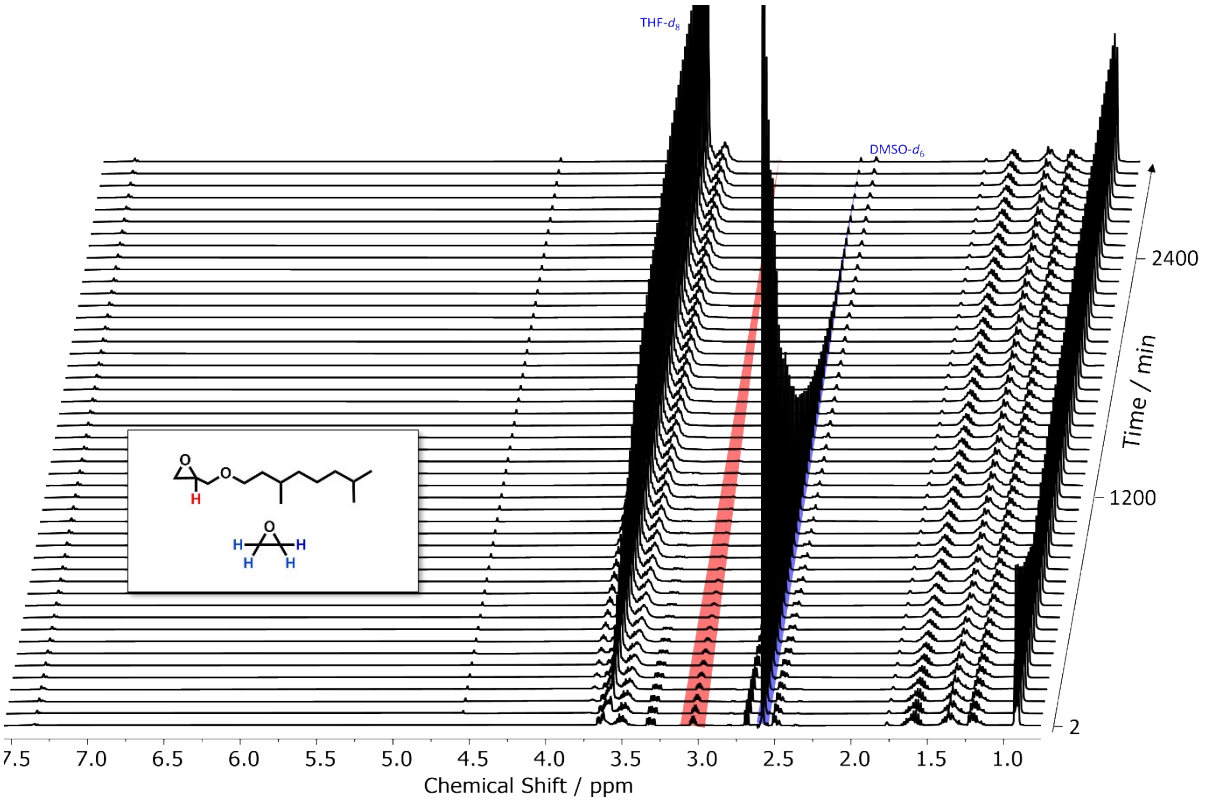

Figure S53: Selection of ^{1}H NMR spectra (400 MHz, THF-d_8 : DMSO-d_6= 5:1) for the *in situ* NMR kinetics of the statistical copolymerization of THGeraGE with EO at 40 °C. Relevant epoxide signals for evaluation are highlighted in red at 3.03 ppm (THGeraGE) and blue at 2.59 ppm (EO). Since spectra were recorded at 2 min intervals over a period of 48 h, only every 30th spectrum is displayed.

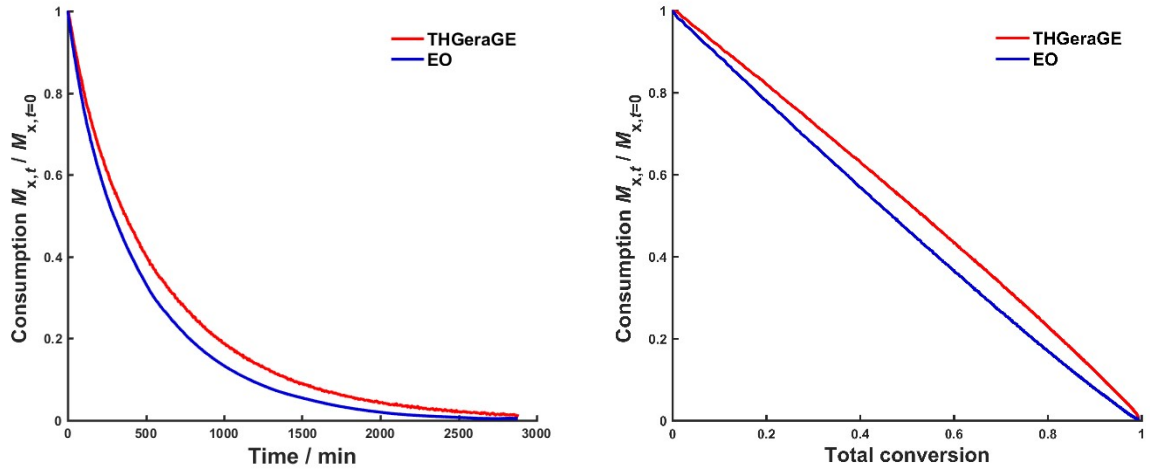

Figure S54: Time-conversion plot of the anionic copolymerization of THGeraGE and with EO, determined via *in situ* ^{1}H NMR kinetics (left). Individual monomer conversion versus total monomer conversion (right).

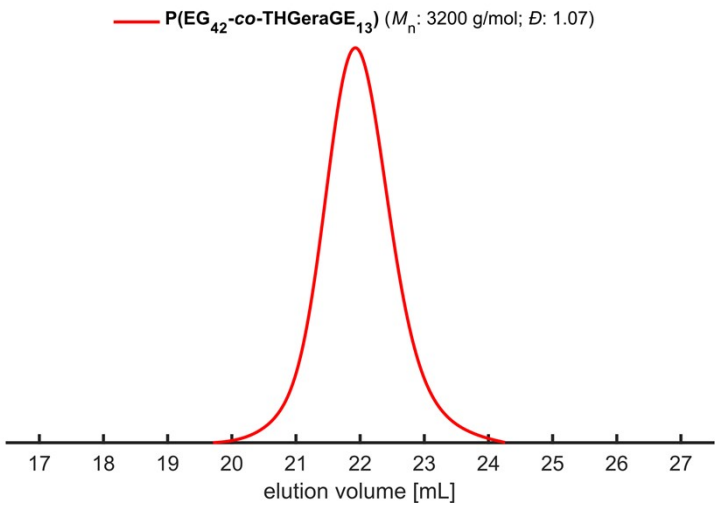

Figure S55: SEC elugram (RI detector, eluent: DMF, PEG calibration) of the P(EG_{42}-*co*-$THGeraGE_{13}$) copolymer synthesized from the *in situ* ^{1}H NMR copolymerization kinetics. SEC analysis: M_n = 3200 g·mol^{-1}, $Đ$ = 1.07.

Kinetic data of the copolymerization of HHFarGE with EO.

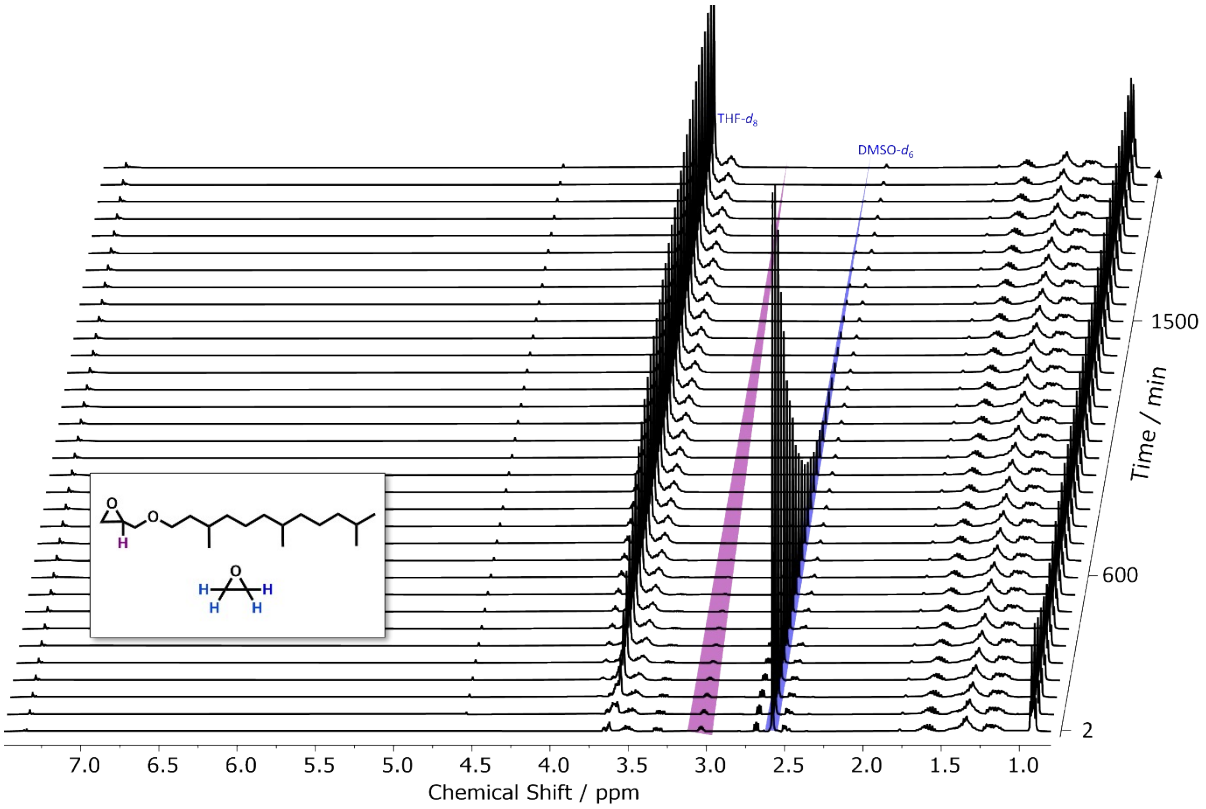

Figure S56: Selection of ^{1}H NMR spectra (400 MHz, THF-d_8 : DMSO-d_6= 5:1) for the *in situ* kinetics of the statistical copolymerization of HHFarGE with EO at 40 °C. Relevant epoxide signals for evaluation are highlighted in purple (HHFarGE) at 3.05 ppm and blue (EO) at 2.59 ppm. Since spectra were recorded every 2 min over a period of 34.0 h, only every 30th spectrum is displayed.

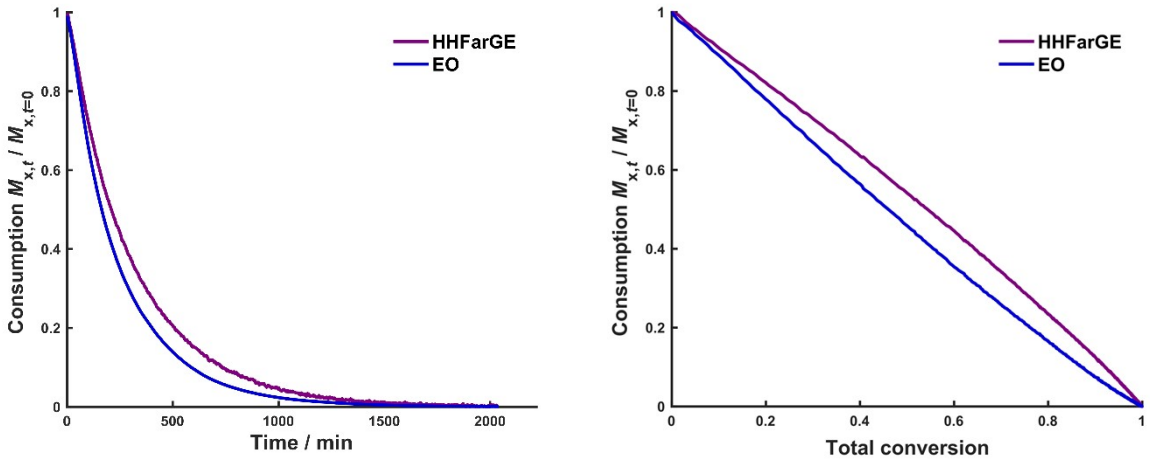

Figure S57: Time-conversion plot of the anionic copolymerization of HHFarGE and with EO, determined via *in situ* ^{1}H NMR kinetics (left). Individual monomer conversion versus total monomer conversion (right).

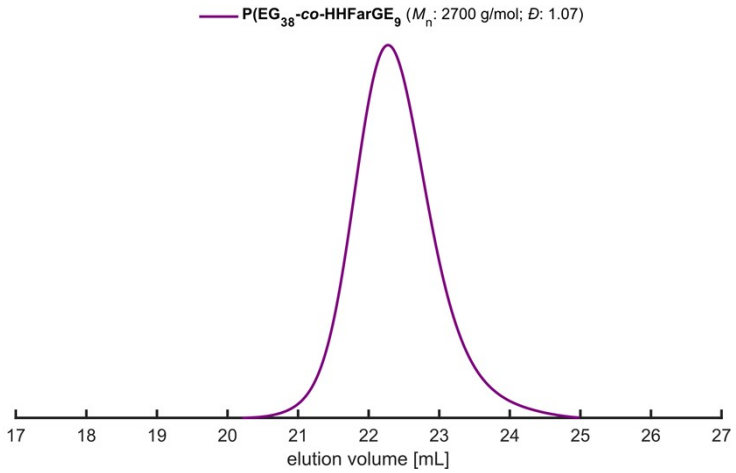

Figure S58: SEC elugram (RI detector, eluent: DMF, PEG calibration) of the P(EG_{38}-*co*-$HHFarGE_9$) copolymer synthesized from the *in situ* ^{1}H NMR copolymerization kinetics. SEC analysis: M_n = 2700 g·mol^{-1}, $Đ$ = 1.07.

7. Postpolymerization Functionalizations

7.1. Thiol-Ene Click

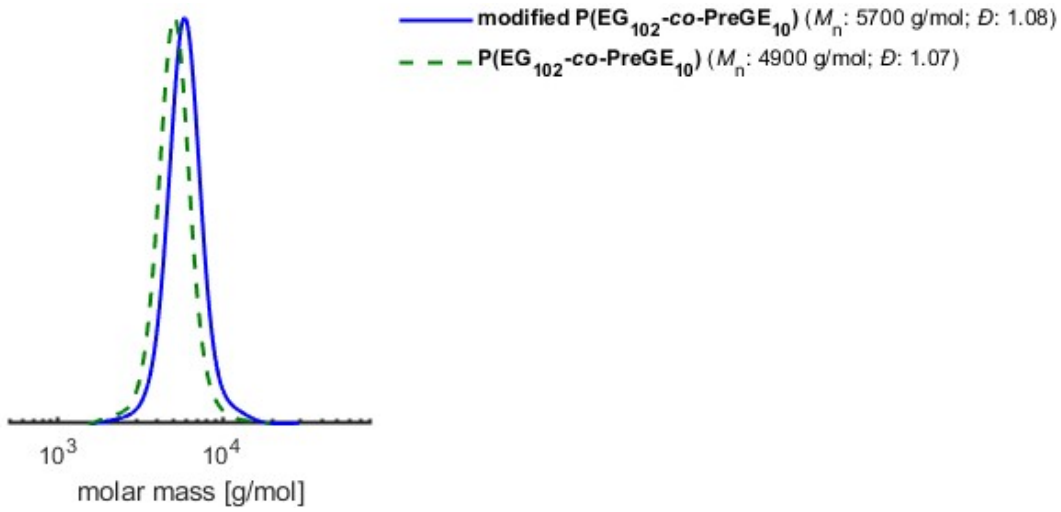

Figure S59: SEC traces of modified P(EG_{102}-*co*-$PreGE_{10}$) (blue) and its respective precursor polymer (green, dotted line). (Eluent: DMF, RI-Detector, PEG calibration).

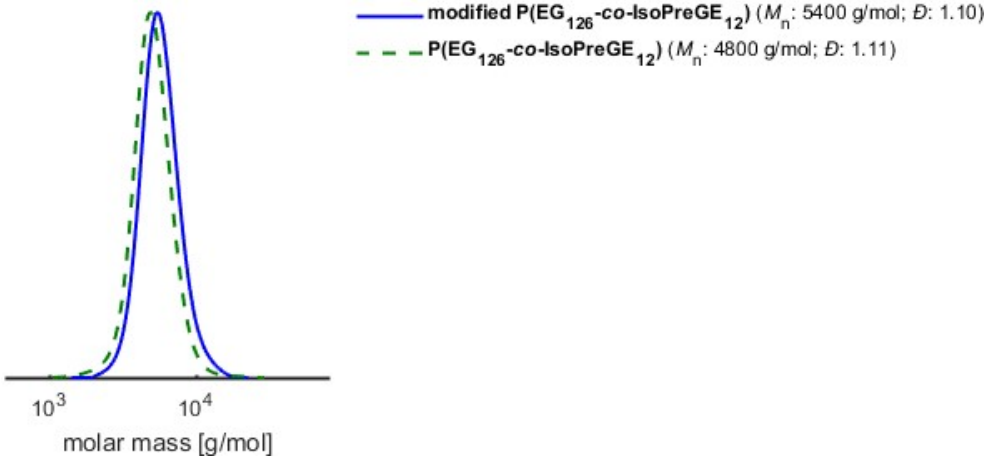

Figure S60: SEC traces of modified P(EG_{126}-*co*-$IsoPreGE_{12}$) (blue) and its respective precursor polymer (green, dotted line). (Eluent: DMF, RI-Detector, PEG calibration).

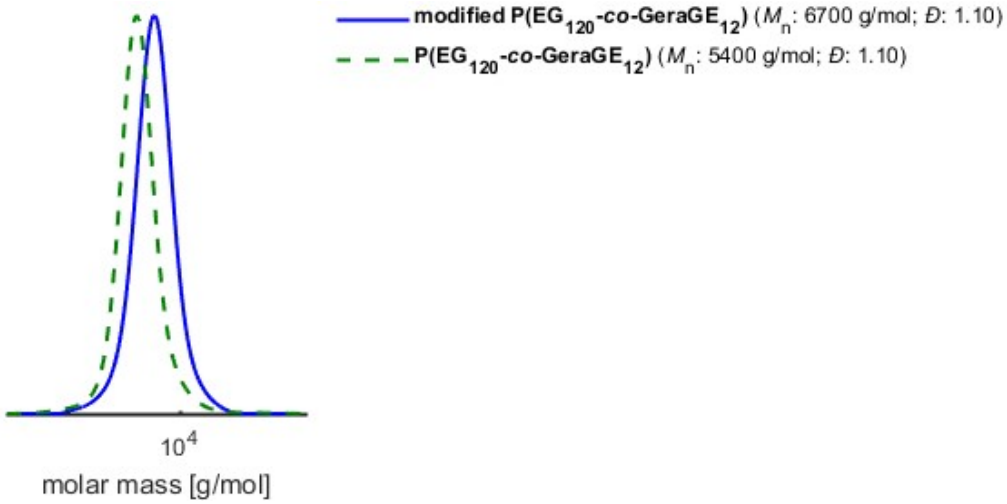

Figure S61: SEC traces of modified P(EG_{120}-*co*-$GeraGE_{12}$) (blue) and its respective precursor polymer (green, dotted line). (Eluent: DMF, RI-Detector, PEG calibration).

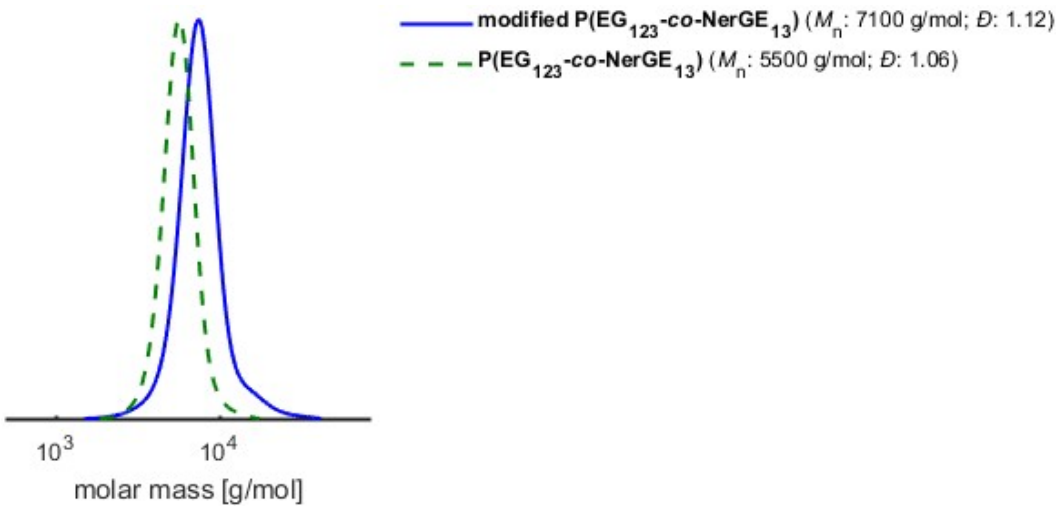

Figure S62: SEC traces of modified P(EG_{123}-*co*-$NerGE_{13}$) (blue) and its respective precursor polymer (green, dotted line) (Eluent: DMF, RI-Detector, PEG calibration).

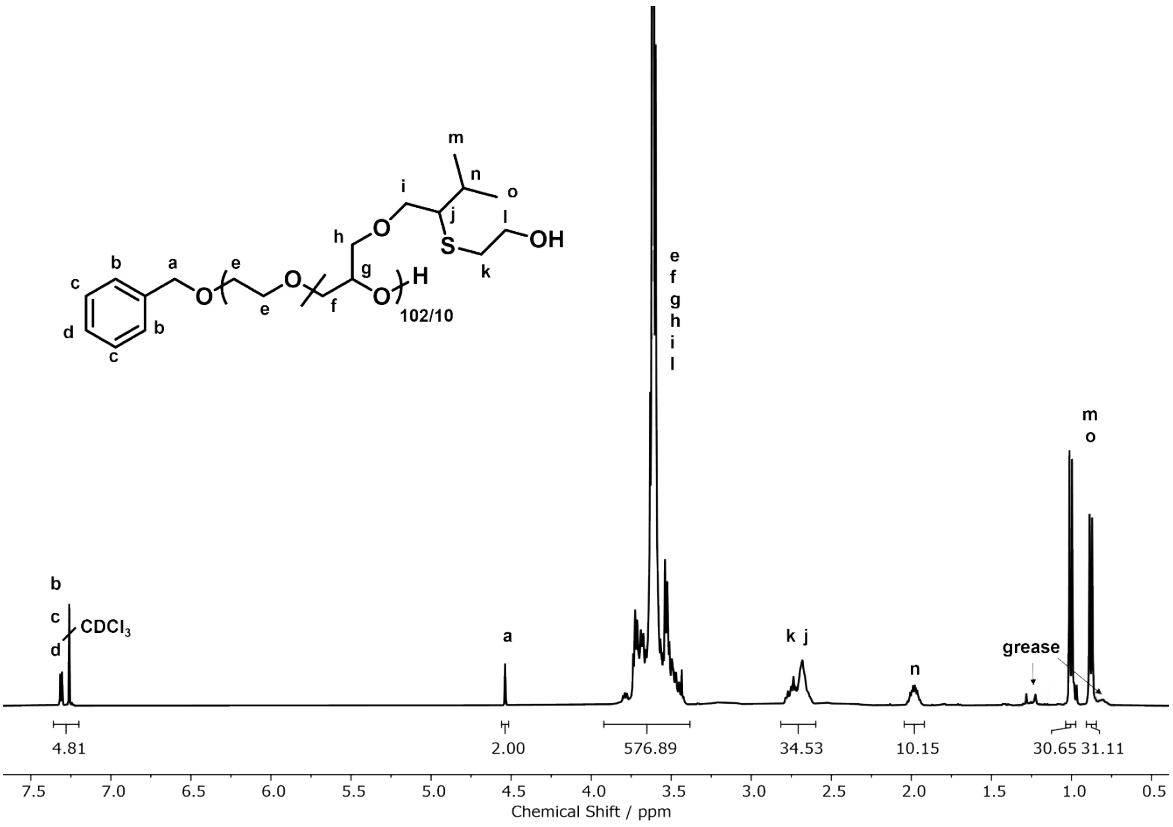

Figure S63: ^{1}H NMR spectrum of P(EG_{102}-*co*-$PreGE_{10}$) functionalized with 2-mercaptoethanol via Thiol-ene click reaction (400 MHz, $CDCl_3$).

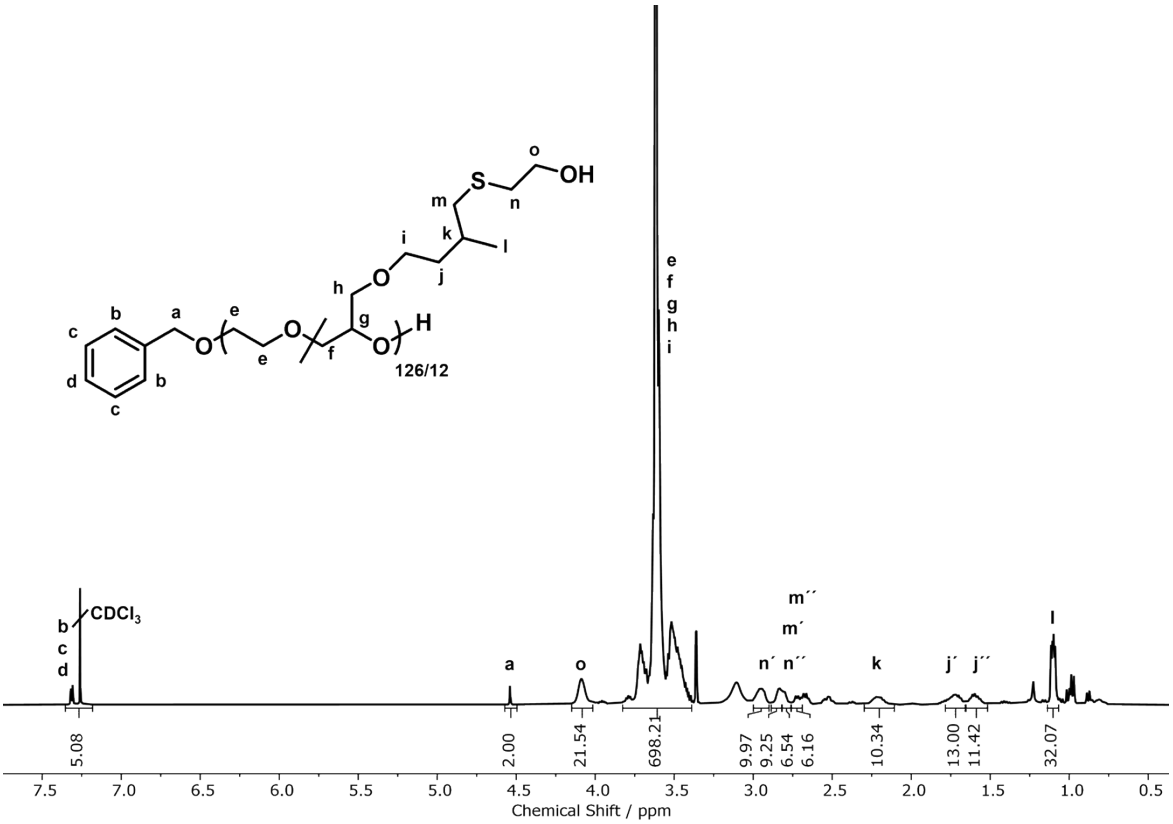

Figure S64: ^{1}H NMR spectrum of P(EG_{126}-*co*-IsoPreGE$_{12}$) functionalized with 2-mercaptoethanol via Thiol-ene click reaction (400 MHz, $CDCl_3$). Isoprenyl glycidyl ether partially isomerized to prenyl glycidyl ether during polymerization and was also functionalized. Signals are omitted for clarity.

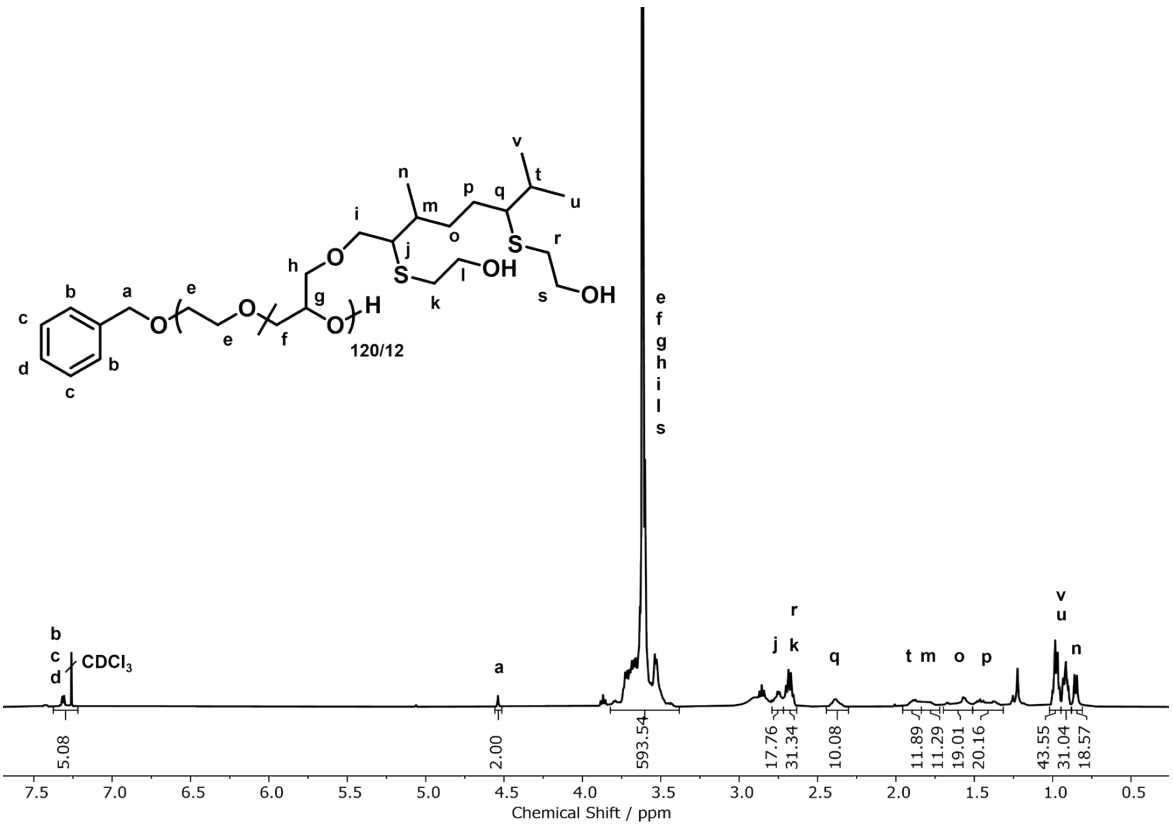

Figure S65: ^{1}H NMR spectrum of P(EG_{120}-*co*-$GeraGE_{12}$) functionalized with 2-mercaptoethanol via thiol-ene click reaction (400 MHz, $CDCl_3$).

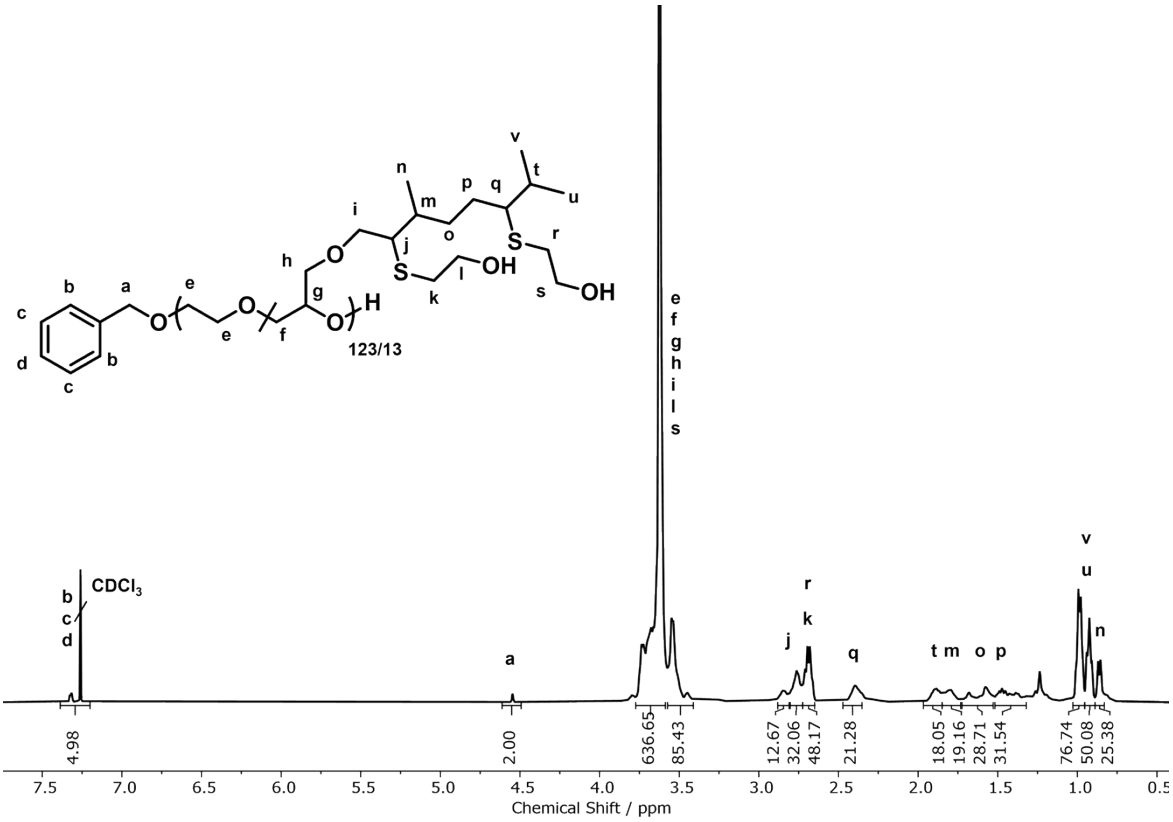

Figure S66: ^{1}H NMR spectrum of P(EG_{123}-*co*-$NerGE_{13}$) functionalized with 2-mercaptoethanol via thiol-ene click reaction (400 MHz, $CDCl_3$).

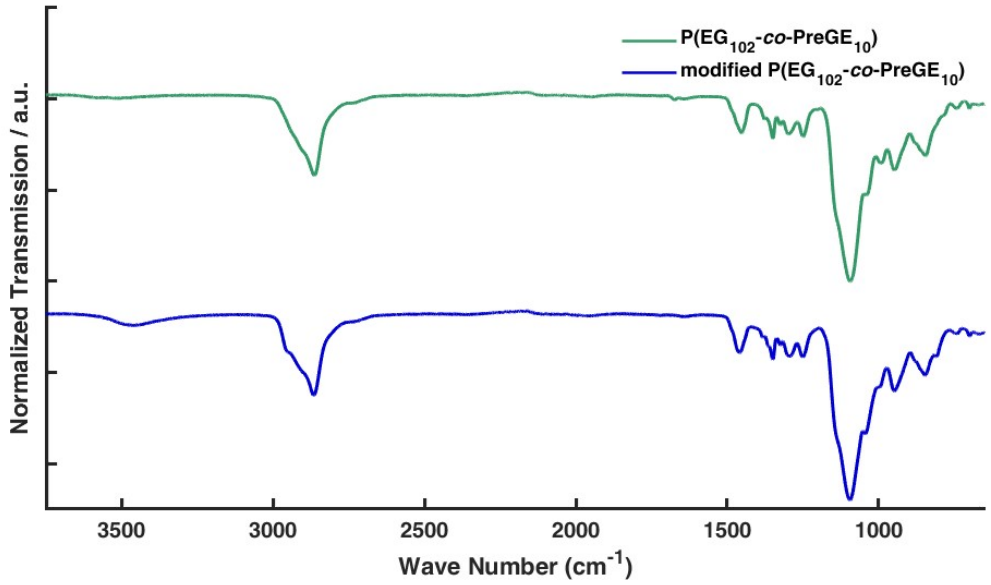

Figure S67: IR spectrum of P(EG_{102}-*co*-$PreGE_{10}$) functionalized with 2-mercaptoethanol via thiol-ene click reaction.

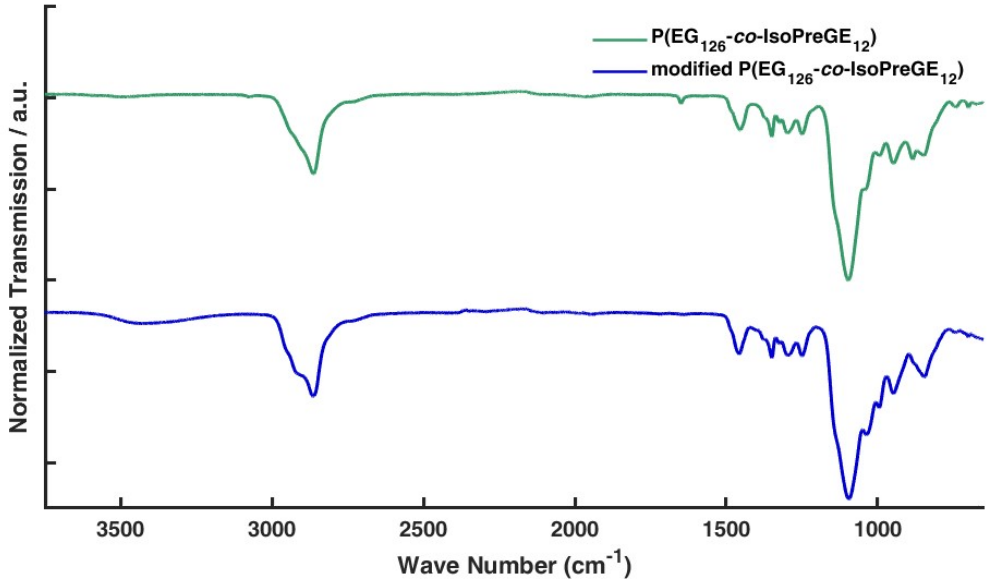

Figure S68: IR spectrum of P(EG_{126}-co-$IsoPreGE_{12}$) functionalized with 2-mercaptoethanol via thiol-ene click reaction.

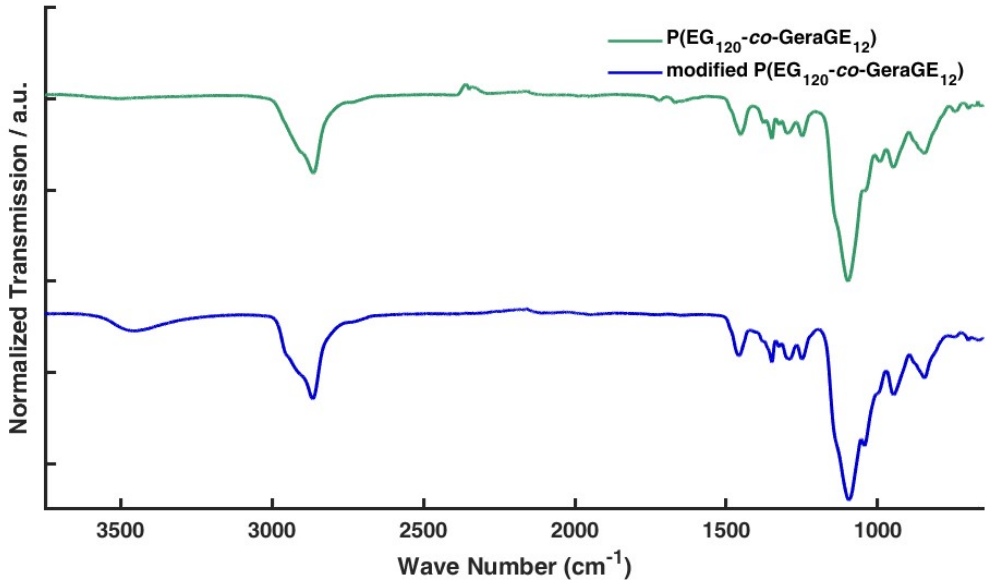

Figure S69: IR spectrum of P(EG_{120}-*co*-$GeraGE_{12}$) functionalized with 2-mercaptoethanol via thiol-ene click reaction.

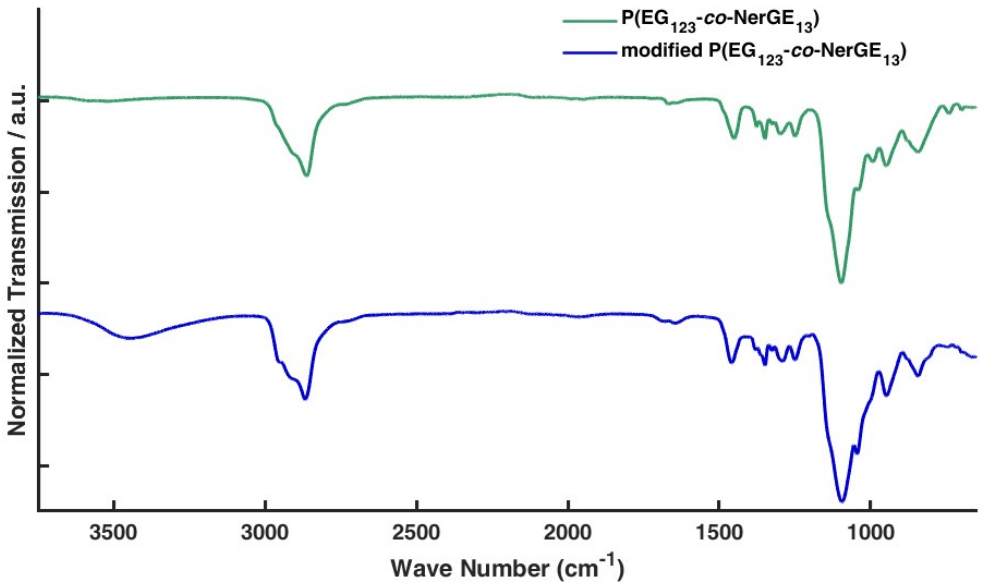

Figure S70: IR spectrum of P(EG_{123}-*co*-$NerGE_{13}$) functionalized with 2-mercaptoethanol via Thiol-ene click reaction.

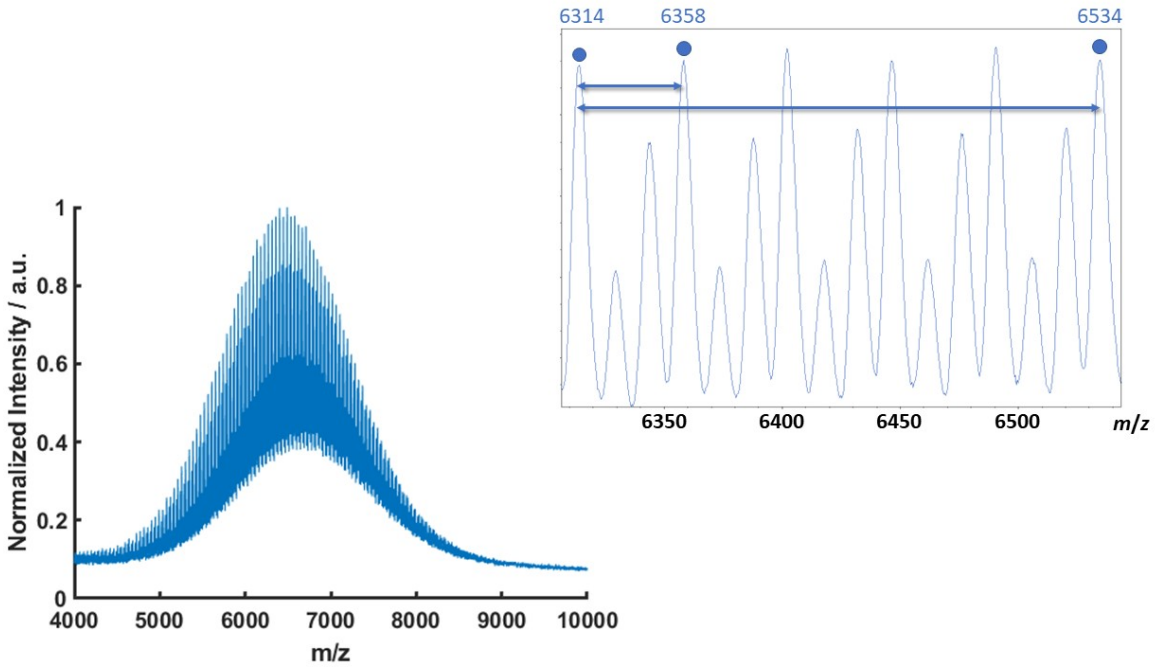

Figure S71: MALDI-ToF of P(EG_{102}-*co*-$PreGE_{10}$) functionalized with 2-mercaptoethanol via Thiol-ene click reaction. Small arrow denotes the mass difference of one EO unit with 44 g/mol. Large arrow denotes the mass difference of the functionalized PreGE unit with a mass difference of 220 g/mol. To be exact, 220 g/mol could also be a multiple of 44 g/mol.

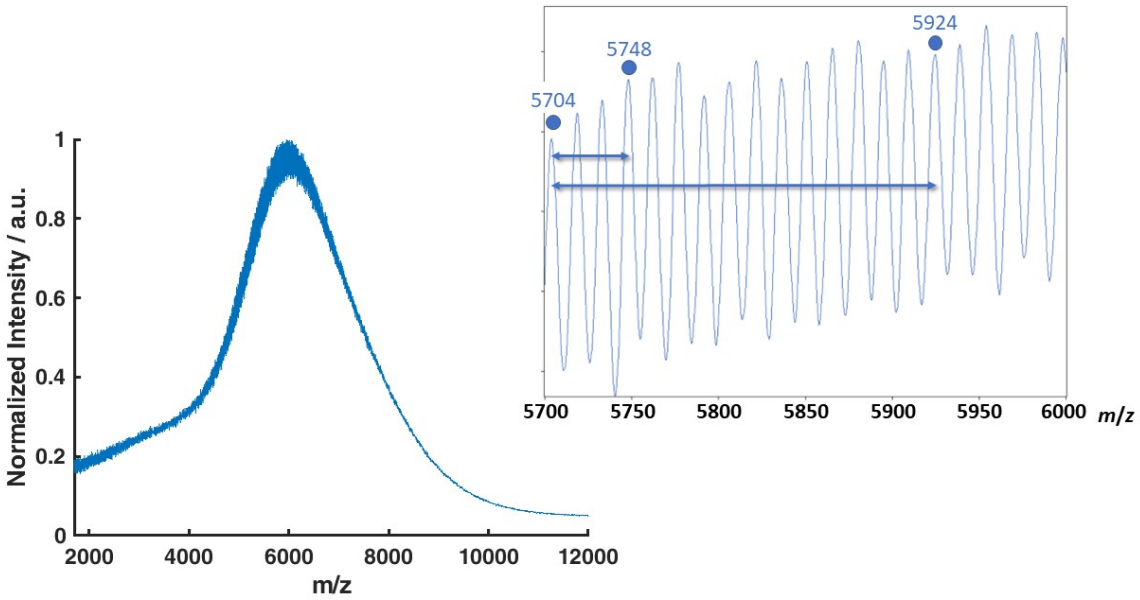

Figure S72: MALDI-ToF of P(EG_{126}-*co*-IsoPreGE$_{12}$) functionalized with 2-mercaptoethanol via Thiol-ene click reaction. Small arrow denotes the mass difference of one EO unit with 44 g/mol. Large arrow denotes the mass difference of the functionalized IsoPreGE unit with a mass difference of 220 g/mol. To be exact, 220 g/mol could also be a multiple of 44 g/mol.

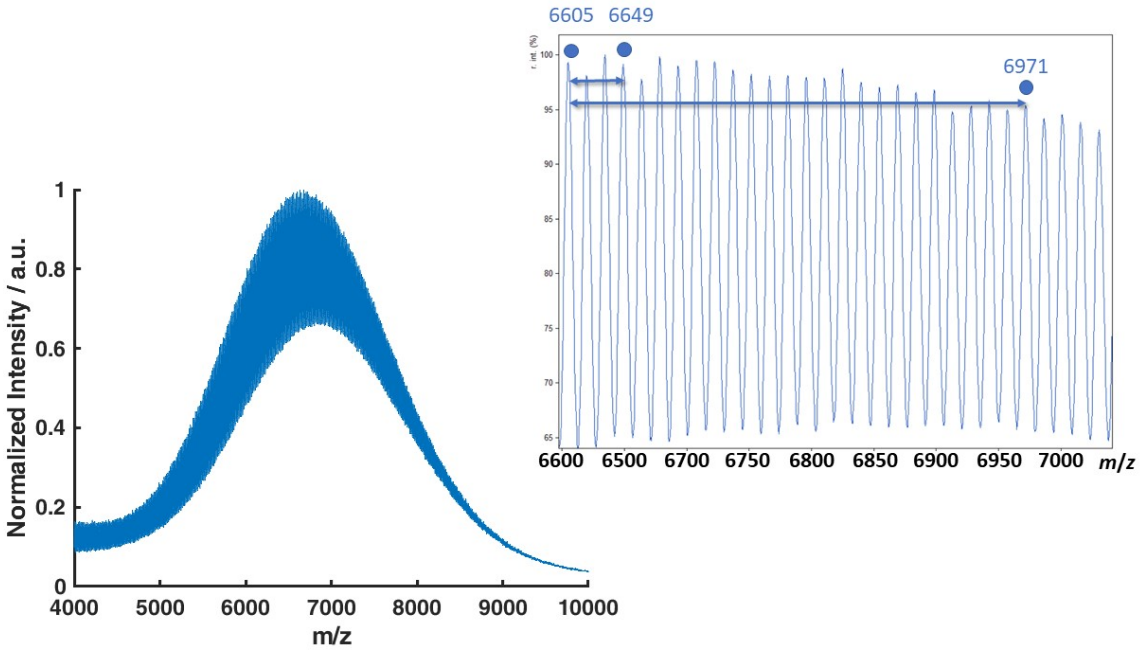

Figure S73: MALDI-ToF of P(EG_{120}-*co*-GeraGE$_{12}$) functionalized with 2-mercaptoethanol via Thiol-ene click reaction. Small arrow denotes the mass difference of one EO unit with 44 g/mol. Large arrow denotes the mass difference of the double functionalized GeraGE unit with a mass difference of 366 g/mol.

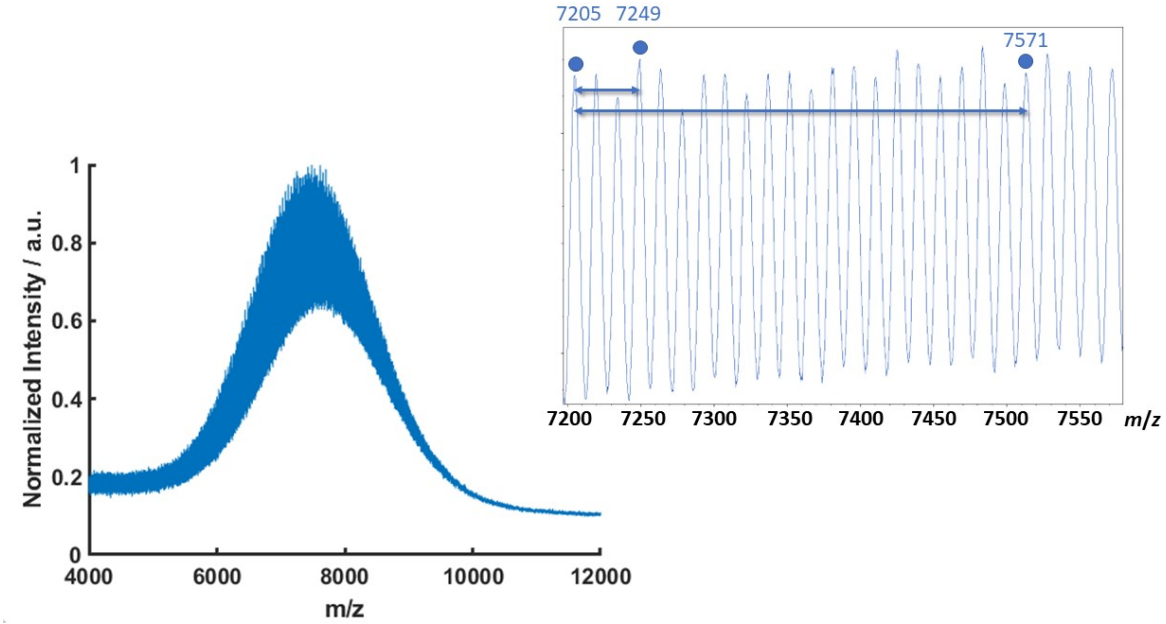

Figure S74: MALDI-ToF of P(EG_{123}-*co*-$NerGE_{13}$) functionalized with 2-mercaptoethanol via Thiol-ene click reaction. Small arrow denotes the mass difference of one EO unit with 44 g/mol. Large arrow denotes the mass difference of the double functionalized NerGE unit with a mass difference of 366 g/mol.

7.2. Hydrogenation

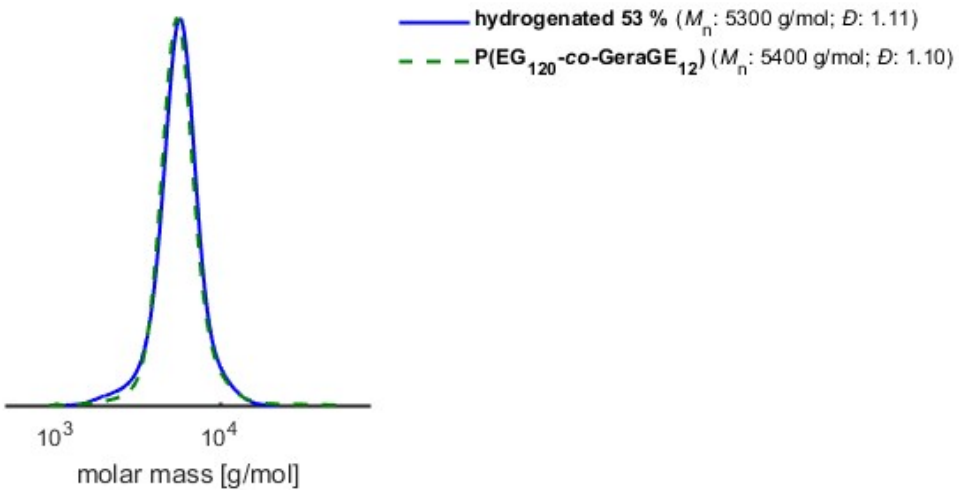

Figure S75: SEC traces of P(EG_{120}-*co*-$GeraGE_{12}$) with a degree of hydrogenation of 53 %. (Eluent: DMF, RI-Detector, PEG calibration).

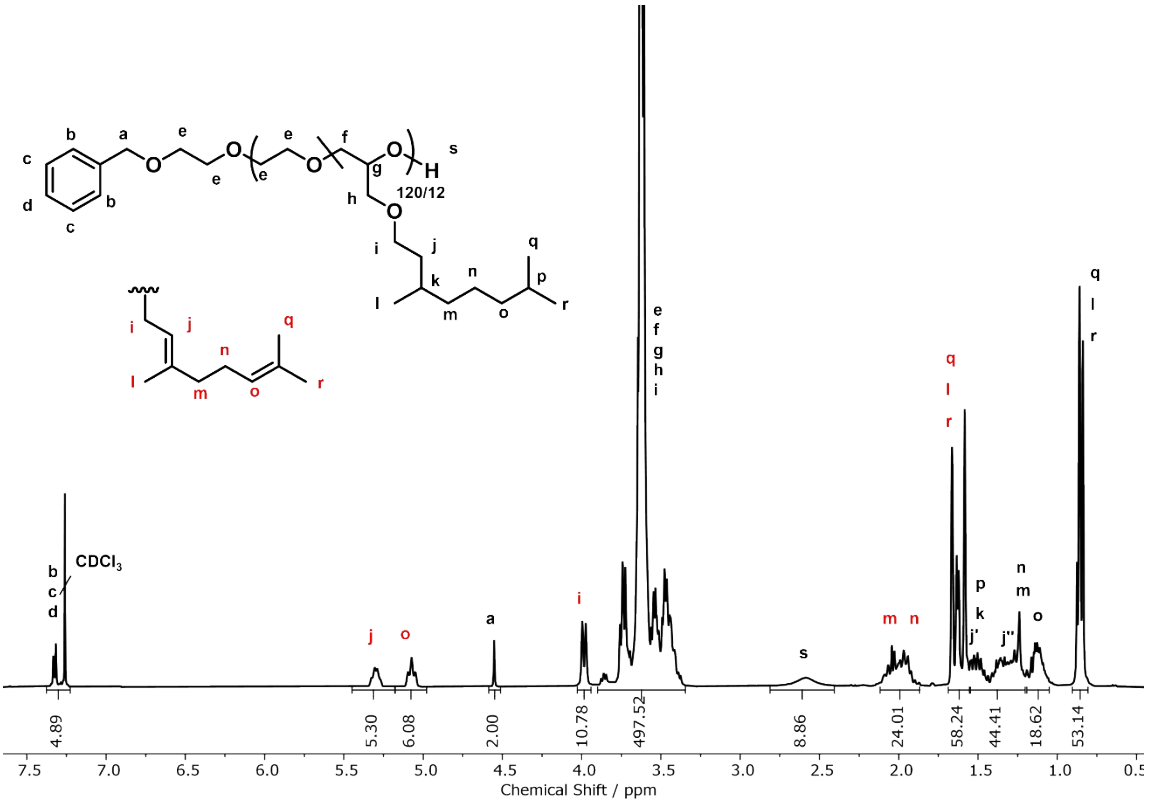

Figure S76: ^{1}H NMR spectrum of P(EG$_{120}$-*co*-GeraGE$_{12}$) hydrogenated with PADA (300 MHz, $CDCl_3$). The degree of hydrogenation is 53 %. Note that the electron-poor double bond is hydrogenated preferentially. Red letters denote atoms of residual not hydrogenated precursor polymer.

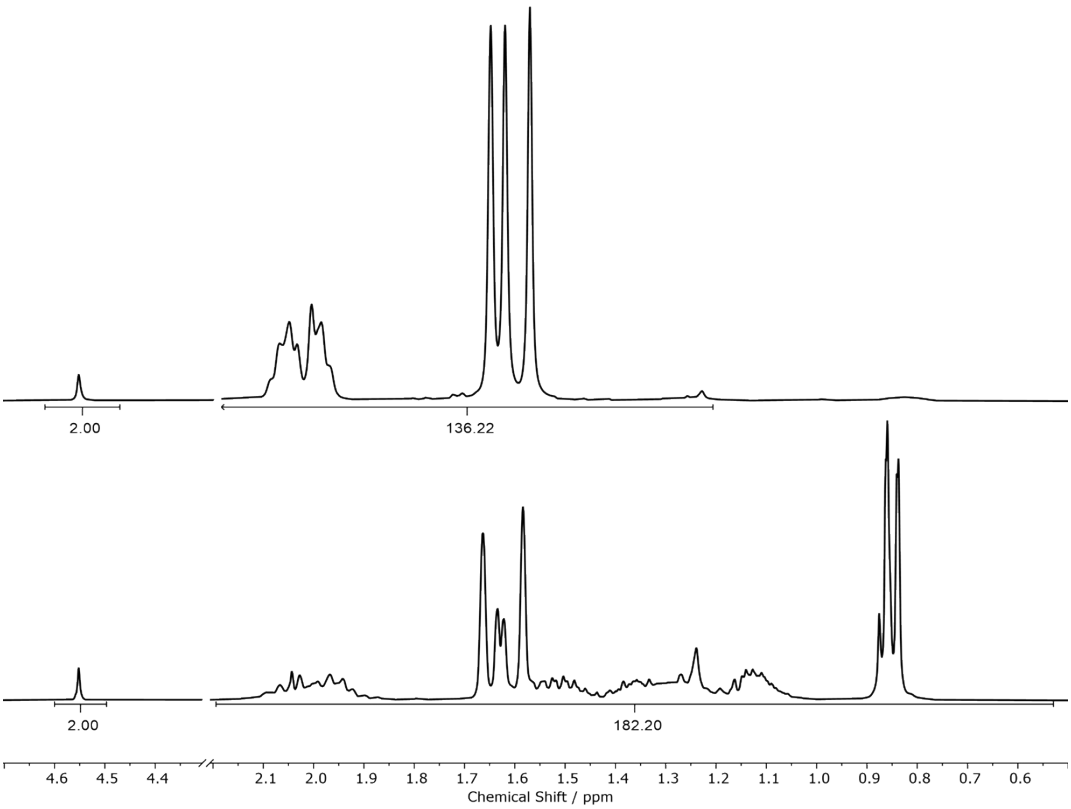

Figure S 77: Zoom of the ^{1}H NMR spectrum of P(EG$_{120}$-*co*-GeraGE$_{12}$) before (top) and after (bottom) the hydrogenation. The spectrum shows an increase of observed protons after hydrogenation.

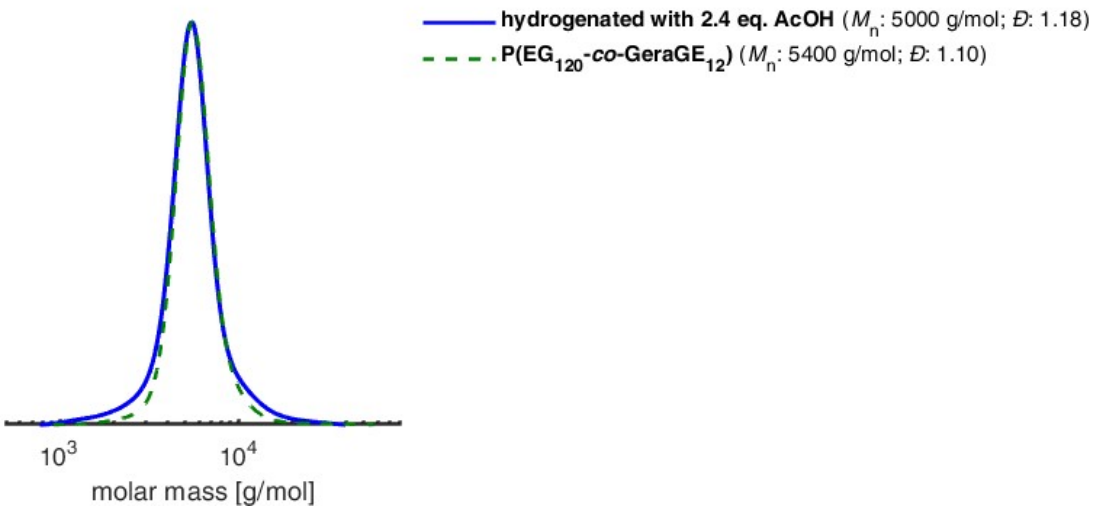

Figure S78: SEC traces of P(EG_{120}-$_{co}$-$GeraGE_{12}$) before and after hydrogenation utilizing 2.4 eq. of acetic acid (standard: 2 eq., compare Figure S75). Higher amounts of acid result in an increase in dispersity and a small lower molecular weight shoulder.

8. Thermal Characterization of Polymers

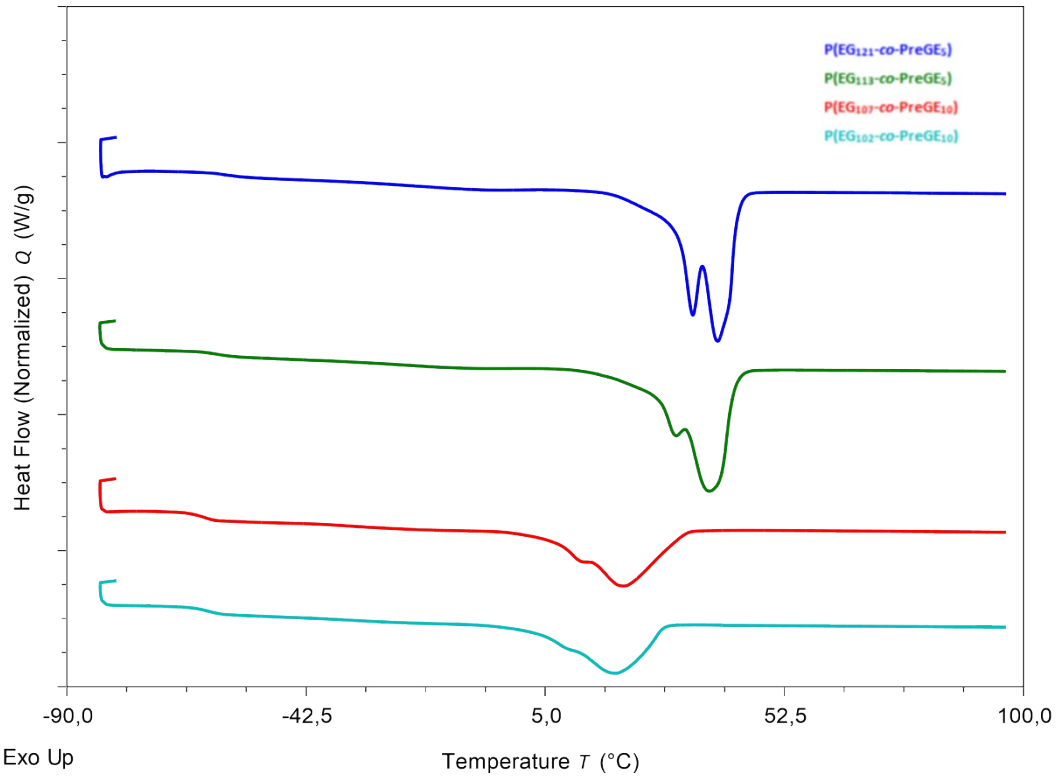

Figure S79: DSC thermograms of P(EG_n-*co*-PreGE$_m$) copolymers (second heating cycle, from -90 to 100 °C, 10 °C·min^{-1}).

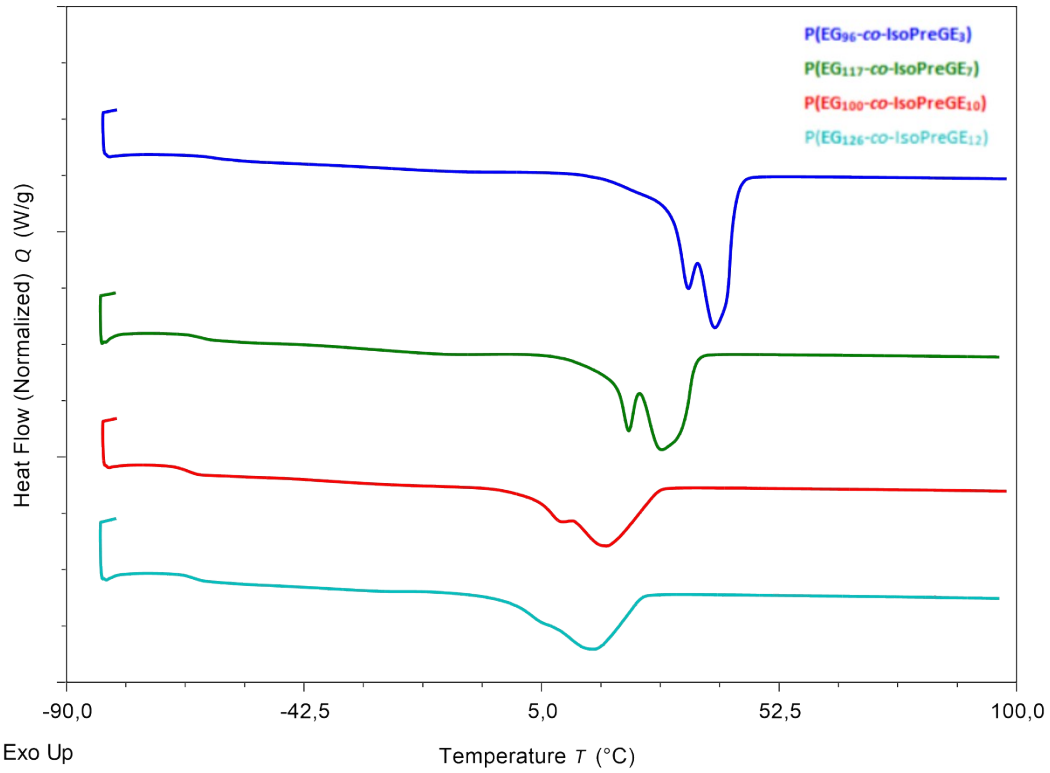

Figure S80: DSC thermograms of P(EG_n-*co*-IsoPreGE$_m$) copolymers (second heating cycle, from -90 to 100 °C, 10 °C·min^{-1}).

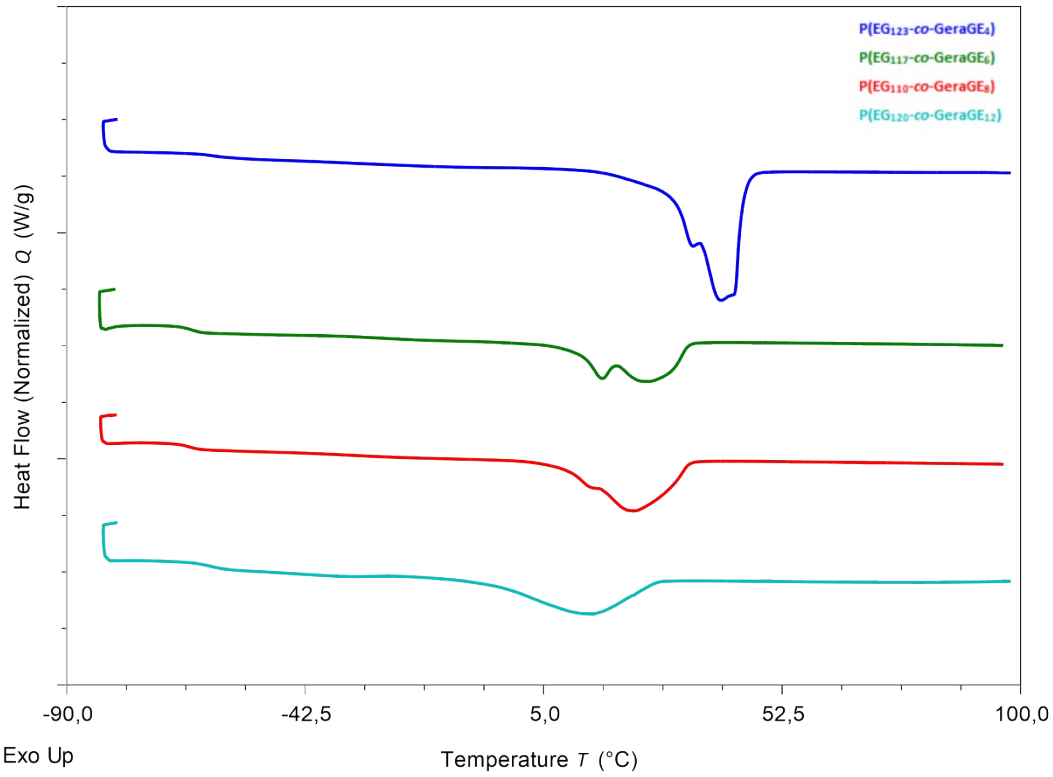

Figure S81: DSC thermograms of P(EG_n-*co*-$GeraGE_m$) copolymers (second heating cycle, from -90 to 100 °C, 10 °C·min^{-1}).

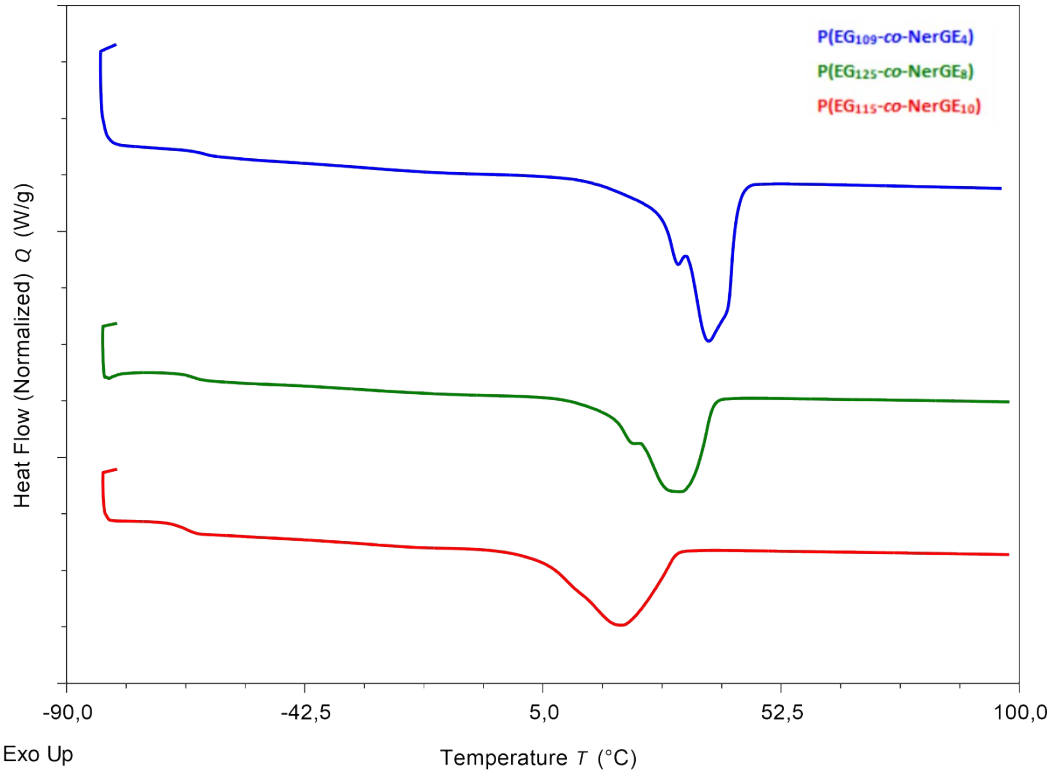

Figure S82: DSC thermograms of P(EG_n-*co*-$NerGE_m$) copolymers (second heating cycle, from -90 to 100 °C, 10 °C·min^{-1}).

9. References

1 G. Mouzin, H. Cousse, J.-P. Rieu and A. Duflos, *Synthesis*, 1983, 117–119.

2 S. Schüttner, M. Krappel, M. Koziol, L. Marquart, I. Schneider, T. Sottmann and H. Frey, *Macromolecules*, 2023, **56**, 6928–6940.

3 P. Holzmüller, C. Gardiner, J. Preis and H. Frey, *Macromolecules*, 2024, **57**, 5358–5367.

4 J. Herzberger, D. Leibig, J. C. Liermann and H. Frey, *ACS Macro Lett.*, 2016, **5**, 1206–1211.

5 M. Steube, T. Johann, M. Plank, S. Tjaberings, A. H. Gröschel, M. Gallei, H. Frey and A. H. E. Müller, *Macromolecules*, 2019, **52**, 9299–9310.

6 V. Jaacks, *Makromol. Chem.*, 1972, **161**, 161–172.

7 J. T. Groves and K. W. Ma, *J. Am. Chem. Soc.*, 1977, **99**, 4076–4082.

8 C. Schunicht, A. Biffis and G. Wulff, *Tetrahedron*, 2000, **56**, 1693–1699.

9 J. W. Hamersma and E. I. Snyder, *J. Org. Chem.*, 1965, **30**, 3985–3988.

10 F. T. Wall, *J. Am. Chem. Soc.*, 1941, **63**, 1862–1866.

11 B. S. Beckingham, G. E. Sanoja and N. A. Lynd, *Macromolecules*, 2015, **48**, 6922–6930.

12 R. Hoffmann, V. I. Minkin and B. K. Carpenter, *Bull. Soc. Chim. Fr.*, 1996, 117–130.

13 J. Blankenburg, E. Kersten, K. Maciol, M. Wagner, S. Zarbakhsh and H. Frey, *Polym. Chem.*, 2019, **10**, 2863–2871.

14 M. Hans, H. Keul and M. Moeller, *Polymer*, 2009, **50**, 1103–1108.

15 F. Guibé, *Tetrahedron*, 1997, **53**, 13509–13556.

16 J.-M. Vatèle, *Tetrahedron*, 2002, **58**, 5689–5698.

17 T. J. Prosser, *J. Am. Chem. Soc.*, 1961, **83**, 1701–1704.

18 B. F. Lee, M. J. Kade, J. A. Chute, N. Gupta, L. M. Campos, G. H. Fredrickson, E. J. Kramer, N. A. Lynd and C. J. Hawker, *J. Polym. Sci., Part A: Polym. Chem.*, 2011, **49**, 4498–4504.